Summer 8-15-2012

Effective 1D Language for Fractional Quantum Hall States

John Flavin
Washington University in St. Louis

WASHINGTON UNIVERSITY IN ST. LOUIS

Department of Physics

Dissertation Examination Committee:
Alexander Seidel, Chair
Mark Alford
Renato Feres
Zohar Nussinov
Michael Ogilvie
Jung-Tsung Shen

Effective 1D Language for Fractional Quantum Hall States

by

John Flavin

A dissertation presented to the
Graduate School of Arts and Sciences
of Washington University in
partial fulfillment of the
requirements for the degree
of Doctor of Philosophy

August 2012

Saint Louis, Missouri

Abstract

In the theory of the fractional quantum Hall effect, much attention is paid to the correspondence between fractional quantum Hall wave functions and conformal blocks in certain rational conformal field theories (CFT). This correspondence is powerful, enabling the calculation of the fractional statistics of a state that would be difficult if not impossible to calculate directly from the wave functions. But it is, in general, conjectural, remaining without microscopic justification in many cases of interest, and involves heavy mathematical machinery. We detail an alternative method to calculate Abelian and non-Abelian fractional statistics, the coherent state method. The method relies on assumptions which are independent of those underlying the CFT correspondence, so it serves as an independent check of results for the statistics where they exist, and an alternative source of results when a CFT is not known. We show how the coherent state method can be used to derive the statistics of several increasingly complicated trial wave functions: $\nu = 1/2$ Laughlin, Moore-Read, and $k = 3$ Read-Rezayi. We discuss implications of our method for a possible notion of braiding statistics of the Gaffnian state, a "nonunitary" quantum Hall state for which the ramifications of the CFT correspondence are less well understood. We go on to

derive formulas for the counting of zero modes of all these states on the torus.

Acknowledgments

This work was supported by the National Science Foundation under NSF Grant No. DMR-0907793.

There are many people who deserve thanks for making this work possible: my advisor, Alexander Seidel, whose ideas I developed, who helped me to know how much I don't know, and who gave me the tools to know more; my fellow physics graduate students, including but not limited to Benjamin Burch, Michael DeSantis, Patrick Johnson, Jerrad Martin, Brett McArthur, and Sarah Thibadeau, without whom my studying would never have had enough breaks; and my wife, Gayle Flavin, who made sure I maintained my connection to the world outside my studies by giving me someone great to come home to.

Contents

Abstract ii

Acknowledgments iv

List of Figures vii

List of Tables viii

1 Introduction 1
- 1.1 Quantum Hall effect . . . 1
- 1.2 Anyon Statistics . . . 10
- 1.3 Non-Abelian Statistics . . . 15
- 1.4 Finding statistics of FQH wave functions . . . 16

2 The Laughlin State 22
- 2.1 Landau levels on the torus . . . 23
- 2.2 Laughlin states in the thin torus limit . . . 27
- 2.3 Delocalized quasihole states . . . 33
- 2.4 Coherent states . . . 36
- 2.5 Locality . . . 41
- 2.6 Dual description . . . 44
- 2.7 Symmetries and further simplifications . . . 49
- 2.8 Braiding . . . 57

3 The Moore-Read State 62
- 3.1 Generalized coherent state ansatz . . . 62
- 3.2 Translational symmetry . . . 68
- 3.3 Global paths . . . 74
- 3.4 Braiding . . . 77
- 3.5 Braid group representation . . . 83

4 The $k = 3$ Read-Rezayi State 87
- 4.1 n quasiholes . . . 88
- 4.2 Two quasiholes . . . 97
  - 4.2.1 Global paths . . . 97

4.2.2 Mirror symmetry 102
4.2.3 Braiding 104
4.3 Three quasiholes 107
4.3.1 Mirror symmetry 111
4.3.2 Global paths 113
4.3.3 Braiding 117
4.4 Braid group representation 119

5 The Gaffnian State **128**
5.1 n quasiholes 132
5.2 Discussion 140

6 Zero Mode Counting **145**
6.1 Laughlin counting 146
6.2 Moore-Read counting 151
6.3 RR counting 159
6.4 Gaffnian counting 163

A $k = 3$ Read-Rezayi solution: Two quasiholes **170**

B $k = 3$ Read-Rezayi solution: Three quasiholes **177**

C Gaffnian solution: Two quasiholes **185**

D Gaffnian solution: Three quasiholes **190**

Bibliography **197**

List of Figures

1.1 Classical Hall effect 2
1.2 Quantum Hall effect 4
1.3 Dual lowest Landau level bases 6
1.4 Integer quantum Hall density of states 9
1.5 Worldlines of a double braiding operation 12

2.1 Landau level basis on a torus 24
2.2 Domain walls crossing frame boundaries 33
2.3 A two-quasihole dressed domain-wall state 35
2.4 Two-quasihole configurations 48
2.5 Global paths 53
2.6 Exchange path 57

3.1 Result of exchanging two Pfaffian quasiholes 85

4.1 Three-quasihole configurations 109
4.2 Result of exchanging two RR quasiholes 120
4.3 RR Bratelli diagram 123

5.1 Configuration σ_I 136
5.2 Bratteli diagrams for RR and Gaffnian 142

6.1 MR Bratteli diagram paths with $n = 4$ links 154
6.2 MR Bratteli diagram paths with $n = 6$ links 155
6.3 RR $n = 6$ paths with kinks labeled 161
6.4 Gaffnian $n = 6$ paths 167

List of Tables

3.1 Thin torus patterns for a two–domain-wall Moore-Read state 68
3.2 Transformation properties of MR states 69

4.1 Thin torus patterns for a single–domain-wall $k = 3$ Read-Rezayi state 96
4.2 Thin torus patterns for a two–domain-wall $k = 3$ Read-Rezayi state . 97
4.3 Thin torus patterns for a three–domain-wall $k = 3$ Read-Rezayi state 107
4.4 The effect of various operations on the configuration 113

5.1 Thin torus patterns for a two-quasihole Gaffnian state 133
5.2 Thin torus patterns for a three-quasihole Gaffnian state 136

6.1 Laughlin zero modes on torus and sphere 147

Chapter 1

Introduction

1.1 Quantum Hall effect

The observation of the fractional quantum Hall (FQH) effect [1] has led to waves of new insights into the nature of electronic states of matter. Among many other novel properties, excitations in the two-dimensional many-electron FQH systems can exhibit fractional charges and fractional statistics. To see how these effects arise in the quantum Hall effect, we will first introduce the classical Hall effect.

We imagine a conducting strip in the x-y plane with width w in the $\hat{x}$ direction (see Fig. 1.1). An electronic current $\mathbf{I} = -new\mathbf{v}$ flows in the $\hat{y}$ direction on the strip, where n is the electron density, $-e$ is the electric charge, and $\mathbf{v} = -v\hat{y}$ is the electron velocity. We apply a magnetic field $\mathbf{B} = B\hat{z}$ perpendicular to the strip, which causes a Lorentz force that deflects the flowing electrons in the $\hat{x}$ direction. A buildup of excess charge on one side of the conductor and a corresponding charge deficiency on

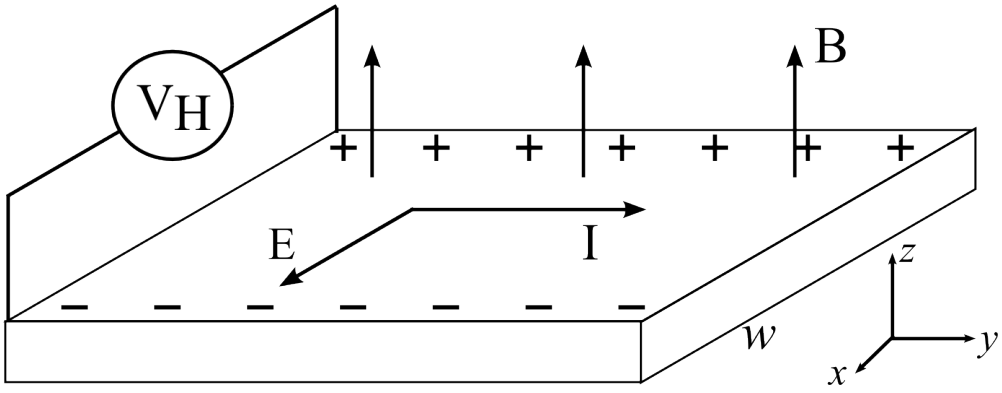

Figure 1.1: The classical Hall effect.

the other side establishes a potential difference across the transverse direction, called V_H, the Hall potential. Its gradient is E_x, the Hall field. In equilibrium the Lorentz force exactly balances the force from the Hall field,

$$\frac{vB}{c} = \frac{V_H}{w}. \tag{1.1}$$

The quantity,

$$\frac{V_H}{I} = -\frac{B}{nec}, \tag{1.2}$$

is called the Hall resistance, denoted $R_{yx} = -R_{xy}$ or R_H. Its measurement allows a determination of the sign of the charges which carry the current.

Now let us imagine that instead of a conducting strip, we have a two dimensional "electron gas", which can be realized in certain semiconductor heterostructures such as MOSFETs (metal–oxide–semiconductor field-effect transistors) and HEMTs (high electron mobility transistors). For weak magnetic fields, the classical linear relationship between R_H and B is observed. However, a quantum regime is entered for low

temperatures (~ 1 K), high magnetic fields (~ 10 T), and clean samples with electron mobilities $\sim 10^4$ cm^2/Vs (though mobilities as high as $\sim 10^6$ cm^2/Vs are possible [2]). In this regime, the relationship between the Hall resistance and magnetic field is not linear as in Eq. (1.2). The Hall resistance shows plateaux around certain ranges of magnetic field (Fig. 1.2). The value of resistance at these plateaux is universal, occurring at a fixed value regardless of the precise details of the samples used to observe the effect. These plateaux occur at

$$R_H = \frac{h}{e^2}\frac{1}{\nu}. \tag{1.3}$$

The ratio h/e^2 is the quantum of resistance, about $25.813k\Omega$. ν is a dimensionless number characterizing each plateau. Initially, plateaux were observed for integral values of ν [3]. This phenomenon, now known as the "integer quantum Hall" (IQH) effect, has a theoretical explanation in terms of filled Landau levels, which will be elaborated below. Later, plateaux were discovered at fractional values of ν with odd denominators [1], such as $1/3, 2/3, 2/5, \ldots$, and still later at even denominators, $5/2$ [4] and $3/2$ [5], which was termed the "fractional quantum Hall effect" (FQHE). These plateaux could not be readily explained in terms of filled Landau levels, or any other picture based on non-interacting electron states. Their explanation required the introduction of interactions between the many electrons within a partially filled Landau level. Over the same ranges of magnetic field giving rise to plateaux, the resistance in the direction of current flow goes to zero, meaning the current flows

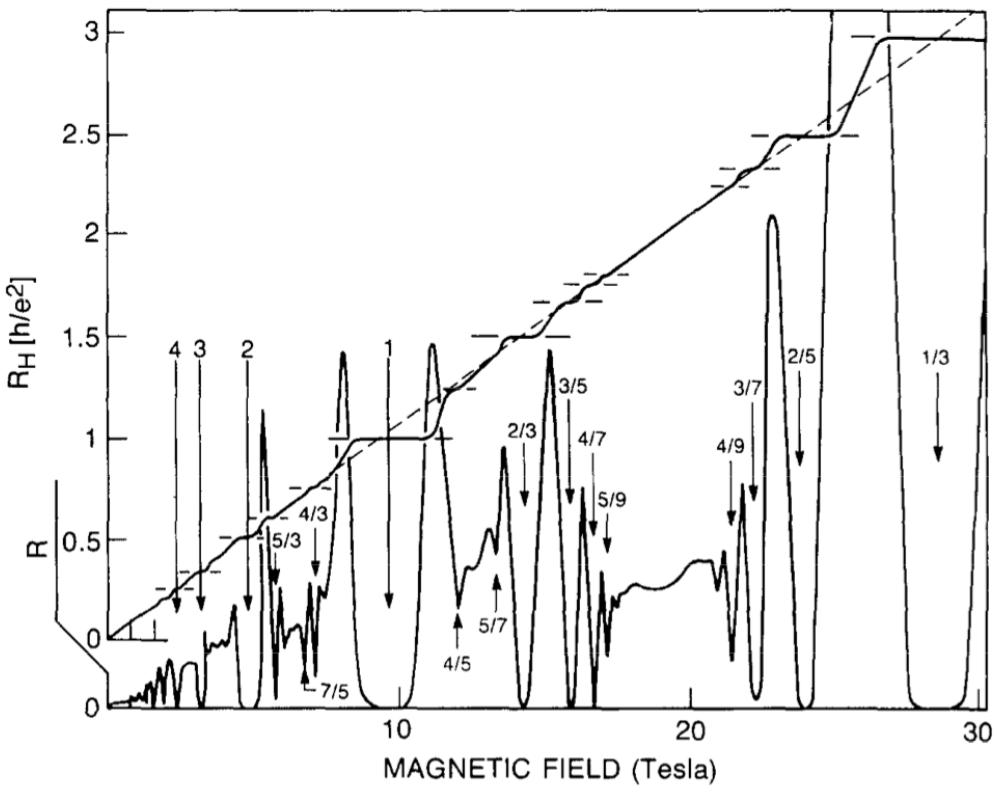

Figure 1.2: Hall resistance R_H and longitudinal resistance R. The numbers with arrows indicate the value of ν at each plateau. Reproduced from Ref. [6].

without dissipation.

The IQHE occurs when an integer number of Landau levels are filled; to review this effect, then, we will briefly review the physics of Landau levels. For now, we make the approximation that the electrons do not interact and that all their spins are polarized in the direction of the magnetic field. In this approximation, the problem of electrons in a magnetic field can be analyzed in terms of a single-electron Hamiltonian,

$$H = \frac{1}{2m}(\mathbf{p} - \frac{e}{c}\mathbf{A})^2. \tag{1.4}$$

$\mathbf{A}$ is the magnetic vector potential, defined by $\mathbf{B} = \nabla \times \mathbf{A}$. We have a gauge degree of freedom in $\mathbf{A}$, and for our purposes it is convenient to choose Landau gauge, $\mathbf{A} = (0, Bx, 0)$. Then

$$H = \frac{p_x^2}{2m} + \frac{1}{2m}\left(p_y - \frac{eBx}{c}\right)^2. \tag{1.5}$$

We will attempt to find a seperable solution of the form $\varphi_{k_y}(x, y) = \exp(ik_y y) f_{k_y}(x)$. This is an eigenstate of p_y, which commutes with the Hamiltonian, so we can replace p_y by its eigenvalue $\hbar k_y$. Now,

$$H = \frac{p_x^2}{2m} + \frac{m\omega_c^2}{2}(x - \ell^2 k_y)^2, \tag{1.6}$$

where $\omega_c = eB/mc$ is the cyclotron frequency, and $\ell = \sqrt{\hbar c/eB}$ is the magnetic length. This looks like the Hamiltonian of a 1D harmonic oscillator in x, with center shifted by $\ell^2 k_y$. Thus $f_{k_y}(x)$ is a harmonic oscillator wave function, and the (unnormalized) eigenstate φ is,

$$\varphi_{k_y,n}(x, y) = \exp(ik_y y) \exp\left(-\frac{1}{2\ell^2}(x - \ell^2 k_y)^2\right) H_n\left(\frac{1}{\ell}(x - \ell^2 k_y)\right), \tag{1.7}$$

where $H_n(x)$ is the nth Hermite polynomial. For each value of n, there is a family of degenerate orbitals, each a state of a quantum harmonic oscillator centered at a different position. Together these orbitals are called a Landau level. Each of these harmonic oscillators has energy $E_n = \hbar\omega_c(n + 1/2)$, independent of k_y. If we impose periodic boundary conditions in y, which is equivalent to working on a cylinder, k_y

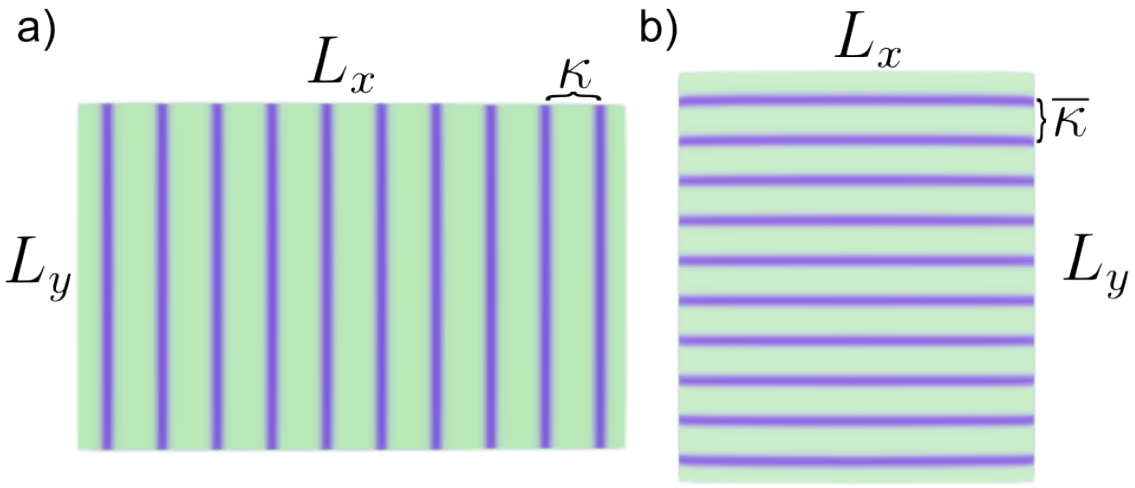

Figure 1.3: The two lowest Landau level bases on the cylinder. a) The "original" basis, $\varphi^c_{n_y,0}(x,y)$. The orbitals are localized in x, with separation by $\kappa = 2\pi/L_y$. They encircle the cylinder in y. b) The dual basis, $\overline{\varphi}^c_{n_x,0}(x,y)$. Orbitals are localized in y with separation $\bar{\kappa} = 2\pi/L_x$ and encircle the torus in x. Reproduced from Ref. [7].

becomes quantized as $k_y = \kappa n_y$ where $\kappa = 2\pi/L_y$ and $n_y = 0, 1, \ldots, L_y - 1$. Then the wave functions are

$$\varphi^c_{n_y,n}(x,y) = \exp(i\kappa y n_y) \exp\left(-\frac{1}{2}(x - \kappa n_y)^2\right) H_n(x - \kappa n_y), \tag{1.8}$$

in units where the magnetic length ℓ is set equal to 1. The wave functions in the lowest Landau level (LLL), with $n = 0$, form rings around the circumference of the cylinder at $x = \kappa n_y$ for each n_y (Fig. 1.3).

Of course, we could have made a different choice for $\mathbf{A}$, which would lead to a different set of eigenfunctions. For instance, the choice $\mathbf{A} = (-By, 0, 0)$ would, along with periodic boundary conditions in x, produce another family of harmonic oscillators in y which we call $\overline{\varphi}^c_n(x,y)$. In the LLL these wave functions form rings

at $y = \bar{\kappa} n_x$, where $\bar{\kappa} = 2\pi/L_x$ and $n_x = 0, 1, \ldots, L_x - 1$. For a boundary which is periodic in both x and y, equivalent to working on a torus, either of these Landau level descriptions (suitably generalized) could form the basis of electron wave functions. This freedom to choose a convenient Landau level basis will play a key role in the method discussed in this work. A more thorough introduction to Landau levels in the context of this method will be given in Sec. 2.1.

The dimensionless number ν, defined in Eq. (1.3) as the coefficient of the Hall resistance, can be expressed as the Landau level filling factor, or the ratio between the number of electrons, N_e, and the magnetic flux Φ,

$$\nu = N_e \frac{\Phi_0}{\Phi}, \tag{1.9}$$

where $\Phi_0 = hc/e$ is the magnetic flux quantum. The IQHE occurs when a Landau level is exactly filled, i.e., when ν is an integer. For a finite range of magnetic field values around exact integer filling, $\nu = n + \epsilon$ for n an integer and $|\epsilon| << 1$, the mismatch between number of electrons and number of flux quanta will cause electrons to occupy orbitals in the $n+1$st Landau level or holes to develop in the nth level, depending on the sign of ϵ. These can be viewed as excitations above the ground state that occurs at $\nu = n$. One might expect that the deviations from exact filling would diminish the unique properties of the quantum Hall states, the quantized Hall resistance and zero longitudinal resistance. In fact, they do not. The Hall resistance is exactly quantized at an integer or fractional unit of e^2/h to accuracy of up to one part

in 10^9 [8] over the entire range of magnetic field values giving rise to the plateau. The presence of disorder is essential to the existence of these plateaux [9, 10]. Disorder is caused by sample impurity sites, which give rise to localized electron states, in contrast to the current which is carried by nonlocal, extended states. Over the range of magnetic field values giving rise to the plateaux, the occupancy of the extended states does not change. Any change in the occupancy of states, reflected by the change in the filling factor ν, is absorbed by the impurity sites which do not affect the current. See Fig. 1.4.

The FQHE occurs at fractional ν, corresponding to partially filled Landau levels. The properties of the states at FQH plateaux can not be explained in terms of non-interacting electrons. In a remarkable insight, Laughlin [11] used a variational method to produce a wave function that captures the behavior of electrons in the $\nu = 1/3$ state,

$$\Psi_3(z_1, z_2, \ldots, z_N) = \prod_{i<j}(z_i - z_j)^3 e^{-\sum_i |z_i|^2/4}, \tag{1.10}$$

where $z_j = x_j + iy_j$ is the 2D coordinate of the jth electron, and the wave function is derived using symmetric gauge, $\mathbf{A} = B/2(-y, x, 0)$. This construction can be generalized to $\Psi_m = \prod_{i<j}(z_i - z_j)^m \exp(-\sum_i |z_i|^2/4)$, which describes the $\nu = 1/m$ plateaux for m an odd integer. As any two electrons approach each other and their separation goes to zero, the Laughin wave functions vanish as the mth power in the separation. The excitations in the wave functions away from exact $\nu = 1/m$ filling are quasiparticles/quasiholes with a charge e^* that is a fraction of the electron charge,

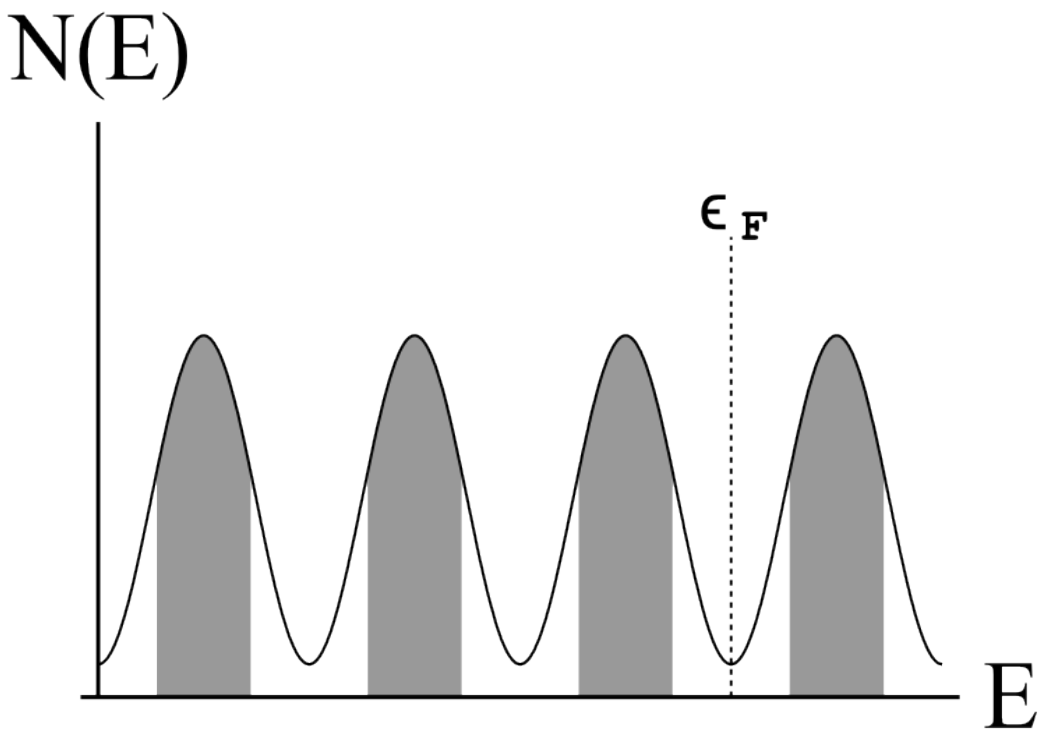

Figure 1.4: Integer quantum Hall density of states. The shaded regions are extended states, which are capable of carrying current. The dashed line is the Fermi energy, ϵ_F. When the Fermi energy is between the shaded regions, the occupied extended states are far below the Fermi level. Perturbing the Fermi energy by changing the magnetic field strength will not cause any change in the current so long as the extended states are far from the Fermi level. For these regions of magnetic field strength, the current will be exactly quantized in the Hall plateaux.

$e^* = e/m$. This fractional charge has been experimentally measured through various methods, including resonant tunneling through antidots [12], shot noise [13, 14], and local compressibility [15]. The excitations are predicted to be neither fermions nor bosons, but "anyons" [16] which obey "fractional statistics" [17].

1.2 Anyon Statistics

A wave function of identical bosons is symmetric in exchange of the positions of the particles, $\Psi_{\rm b}(x_1, x_2) = \Psi_{\rm b}(x_2, x_1)$, while a wave function of identical fermions is antisymmetric, $\Psi_{\rm f}(x_1, x_2) = -\Psi_{\rm f}(x_2, x_1)$. The properties under exchange of identical particles define the statistics of a system[1]. We can view a QH wave function as a map $\Psi : X \to \mathbb{C}$ from a configuration space of particle coordinates, X, to the complex plane. For two[2] identical bosons in d-dimensional space the naïve configuration space S is $S = \mathbb{R}^d \times \mathbb{R}^d$, and for identical fermions is $S = \mathbb{R}^d \times \mathbb{R}^d$

$\{$set of coincident points$(x, x)\}$. However, these naïve configuration spaces do not respect the indistinguishability of the particles. For any identical particles, configurations such as (x_1, x_2) should be physically indistinguishable from the interchanged configurations (x_2, x_1). We define an equivalence relation between such points, $(x_1, x_2) \sim (x_2, x_1)$. Then the configuration space for the two examples men-

[1] More specifically, the statistics defined in this way is known as the "exchange statistics". One can also define statistics through the number of distinct ways one can add additional particles to a system; this is called the "exclusion statistics" [18].

[2] We will restrict ourselves to discussion of two identical particles. The extension to N identical particles will not affect the conclusions, since any exchange involving > 2 particles can be decomposed into a sequence of two-particle exchanges.

tioned above is $S/\sim$, i.e., the naïve configuration space modulo the equivalence relation. In other words, physically indistinguishable configurations are represented by a single point in configuration space. Let us consider the homotopy class of paths which continuously connect the real-space particle coordinates (x_1, x_2) with (x_2, x_1). For $d \geq 3$, all such paths are homotopic, and the homotopy class has one element. For fermions, such a path is a monodromy, encircling the singularity in configuration space where the particles coincide. The wave function is not a single-valued in the space S, and exchanging particles along such a path results in the wave function acquiring a -1. For bosons, there is no singularity in the configuration space and the wave function is not affected by particle exchanges. These are the only two possibilities for particle statistics in $d \geq 3$ dimensional space. In this space, exchange of identical particles defines a representation of the symmetric group S_2, so exchanging particles twice (as in Fig. 1.5) must return the wave function to itself. Thus, exchanging once can only result in a change of sign of the wave function.

These same properties do not hold true for $d = 2$ dimensions. There, infinitely many homotopy classes connect (x_1, x_2) to (x_2, x_1). The particles could be exchanged one "half-turn", either clockwise or counterclockwise, three half-turns clockwise or counterclockwise, five half-turns, etc., and all of these paths are topologically distinct. Notably, exchanging the particles twice, as in Fig. 1.5, is not equivalent to the identity. The paths which exchange two particles on the plane are called "braiding paths" or "braids", which define elements of the "braid group" [19], and their action on the wave functions defines a representation of this group. The configuration space of particles

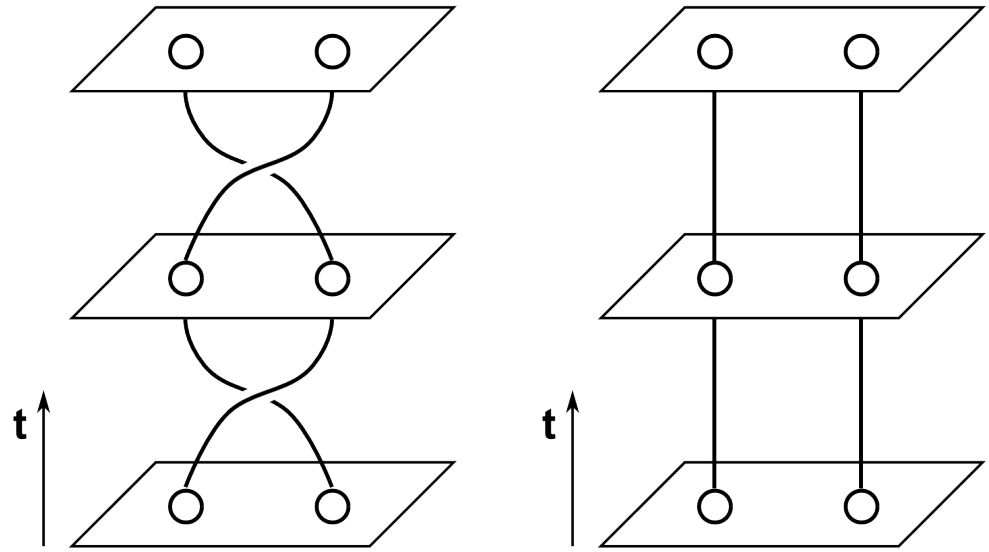

Figure 1.5: Left: The worldlines of two particles involved in a braiding operation (immediately followed by another braiding operation). Right: The worldlines of two particles undergoing the "identity" braid, i.e., remaining stationary. The space depicted in this figure is two-dimensional, with later times shown higher. If, in fact, the particles do not live in two dimensions but in $d \geq 3$ dimensions, then the two processes depicted here, the double braid and the identity braid, are equivalent. On the other hand, if the particles actually do live in two spatial dimensions as shown, then there is no guarantee that the two processes depicted here are equivalent.

which live in two dimensions thus has a richer structure than that of particles in three or more dimensions. Consequently, the wave functions of particles in two dimensional space can have statistics that are neither boson nor fermion statistics [20]. Such particles are called "anyons" [16]. Exchanging two particles by a counterclockwise half-turn, which we call the "elementary braid", can generally result in a wave function $\Psi(\dots, x_j, x_i, \dots) = e^{i\theta}\Psi(\dots, x_i, x_j, \dots)$, where θ is called the "statistical angle". Particles with $\theta = 0$ are bosons, and with $\theta = \pi$ are fermions. In two dimensions θ may take on any value. Those particles for which a finite number of exchanges in the same direction will return the wave function to itself, i.e. those particles with statistical angle $\theta = f\pi$ for some fraction f, are said to have "fractional statistics".

Defined in this way through particle monodromies, the statistical angle is not unique. If we multiply the wave functions by an arbitrary phase depending on the particle coordinates, $\psi \to \exp[i\alpha(r_1, r_2)]\psi$, this is equivalent to making a local gauge transformation, $\mathbf{A} \to \mathbf{A} + \nabla\alpha$. Introducing such a phase can shift the statistical angle defined through monodromy by an arbitrary amount. The equivalent gauge transformation may introduce long-range interaction terms into the Hamiltonian of the system. The intuitive notion of "statistics", however, is that the statistics should reflect some property of the particles and not be affected by an arbitrary gauge choice. Two general strategies for arriving at a consistent definition of statistics are the following. We could choose a preferred gauge, such as one with no long-range interaction terms in the Hamiltonian. Adopting such a gauge convention would produce a unique statistical angle from monodromy. Or, instead of fixing a certain

gauge, we can choose to define the statistics through a physical process. We can physically drag the two particles along an exchange path, using local potentials which move over time, and we imagine this process is performed infinitesimally slowly. We call such a process "adiabatic transport". If two particles are exchanged in such a way, then in addition to the phase from monodromy the wave function will accumulate a "Berry phase" [21] $e^{i\gamma}$, where

$$\gamma = i \int_{\mathcal{C}} d\mathbf{z} \langle \Psi(\mathbf{z}) | \nabla_{\mathbf{z}} \Psi(\mathbf{z}) \rangle. \tag{1.11}$$

$\mathcal{C}$ is the exchange path, and z represents all the parameters along the path. The Berry phase is, like the phase from particle monodromy, gauge dependent. However, the product of those two phases is not gauge dependent, and uniquely characterizes the statistics of particles in two dimensions.

Excitations in the Laughlin states are anyons with statistical angle $\theta = \nu\pi$. This was proved by Arovas, Schrieffer, and Wilczek [22], who calculated the Berry phase arising from exchange of two $\nu = 1/m$ Laughlin quasiholes. This result can be extended to Laughlin-type excitations in any Abelian state[3].

[3]The Laughlin-type excitations of a state may be composites of more elementary excitations. In states for which this is so, there is a certain proscription for finding the statistics of the elementary excitations from the statistics of the Laughlin-type composites.

1.3 Non-Abelian Statistics

The configuration space of the particles might not be completely described by particle position. There may be internal degrees of freedom needed to specify the state. Said differently, for given fixed particle positions there may be many states in the Hilbert space. Suppose further that these states cannot be distinguished by any local measurement. Then an exchange of particles might not result in just a phase multiplication, but can result in a matrix multiplication that acts on those internal degrees of freedom. Both the monodromy phase and Berry phase will have a matrix character. The matrices for exchange of different pairs of particles will, in general, be different and will not commute. Thus, if one braids a sequence of pairs of particles in an N particle state, the order in which the pairs are braided will affect the overall result. We say that particles of this kind, whose braids do not commute, have non-Abelian statistics. Particles for which the order of braiding operations does not matter, or for which the braiding matrix is the identity times a phase, are said to have Abelian statistics.

Non-Abelian statistics might be realized in certain QH states [23]. Recent evidence [24] suggests that the Moore-Read "Pfaffian" state [23], which has non-Abelian excitations, correctly describes the $\nu = 5/2$ quantum Hall plateau [4]. However, a direct measurement of non-Abelian statistics remains elusive. If such states are found, they have many features which would be attractive in a fault-tolerant quantum computer [25, 26]. The internal degrees of freedom of such states could form the qubits of the

quantum computer, and operations would be performed on those qubits by braiding quasiparticles. The fault-tolerance comes about automatically from the inability of local perturbations to couple to the internal degrees of freedom, thus the state of the qubits at any time is stable against dephasing and decoherence.

1.4 Finding statistics of FQH wave functions

For a large class of Abelian and non-Abelian FQH states, we have preferred trial wave functions. In the non-Abelian case there is a large gauge degree of freedom which amounts to choosing a basis for each particle configuration. If one could choose a basis for which all Berry phases are zero, then the statistics of the state could be read off from analytic properties of the wave functions. In this basis, the statistics comes purely from the particle monodromies. The conformal field theory (CFT) conjecture of Moore and Read (MR) [23] gives a proscription for choosing such a basis. MR observed that is it possible to choose basis states such that the analytic parts of the wave functions are given by conformal blocks in certain rational CFTs. It is conjectured [23, 27] that the basis thus chosen has the property that the Berry connection (the argument of the Berry phase integral in Eq. (1.11)) vanishes.

There is much support for the CFT conjecture, but no general proof. The direct calculation of the adiabatic transport of quasihole excitations has been performed for Abelian states [22], and recently for $p+ip$ wave superfluids [28, 29] and Moore-Read-type QH states [30]. For the Moore-Read "Pfaffian" state, mentioned above, a number

of non-rigorous techniques for finding the statistics have been developed earlier as alternatives to CFT. The first such technique is based on the interpretation [31, 32, 33, 34, 35] of the Pfaffian state as a $p+ip$ wave Bardeen-Cooper-Schrieffer (BCS) state of composite fermions [36]. The second technique employs the strategy of viewing a complicated, interacting, many-body state as the adiabatic descendant of a simple, non-interacting state. Using "adiabatic continuity" between the two, properties of the interacting state can be inferred from properties of the non-interacting state. These non-interacting states are given by taking the "thin torus limit", which had been considered earlier in Ref. [37]. In a series of recent works [38, 39, 40, 41, 42, 43, 44, 45, 46, 47, 48, 49, 50, 7], it has been demonstrated that FQH states and their excitations can be described in this limit through simple strings of integers, or "patterns". These same patterns arise in the study of FQH states using Jack polynomials [51, 52, 53], and are related to the "patterns of zeros" describing these states [54, 55, 56, 57]. Adiabatic continuity between the thin torus patterns and FQH states is been utilized in the so-called "coherent state method". This method has been used, in addition to the other methods mentioned above, to derive the statistics of the Pfaffian state [42]. Prior to that, it had also been used to derive the statistics of the Laughlin state [40]. However, no method for deriving the Pfaffian statistics, other than the field-theoretic approach, had thus far been generalizable to more complicated non-Abelian states. The main result of this thesis is to make the case that the coherent state method can be generalized to more complicated states. For some states, the coherent state method has provided the first independent confirmation of the CFT conjecture. In

particular, this method has been used to derive the statistics of the $k = 3$ Read-Rezayi state [58] in Ref. [7].

The bulk of this work is spent developing the formalism of the coherent state method in detail by showing how it can be applied to a series of increasingly complex trial wave functions. However, it may be useful to present a sketch of the method first, with references to those sections containing further details. We begin with a complex many-body interacting FQH wave function on the torus, or a degenerate set of such wave functions. We want to know the statistics of the excitations of the underlying state, which we find through braiding quasiholes via adiabatic transport. The problem is that, in general, calculating the result of braiding using the many-body wave functions is too difficult to perform analytically. To simplify the problem, we use adiabatic continuity. We smoothly deform the Hamiltonian of the FQH wave functions of interest to the limit where one torus dimension becomes small and the other becomes large, while keeping their product constant. This transformation takes the torus into a ring which we call the "thin torus limit", effectively mapping the 2D system onto a 1D system. In this limit, the interacting many-body FQH wave functions become non-interacting product states in the lowest Landau level (LLL) basis. The formalism for the LLL basis on the torus is developed in Sec. 2.1.

In Sec. 2.2 we construct a basis for the Laughlin states on the thin torus. The thin torus states are simple products of LLL orbitals, with each orbital having some definite electron occupation number. The list of occupation numbers of each orbital, a string of integers called the "pattern", serves as a unique label for each state. The

ground-state patterns are periodic, formed from repeating integer strings. A state with quasiholes in the 2D system maps in the thin torus limit to a pattern with domain walls between different ground state strings. These latter states are characterized by the positions of all their domain walls, and by the sequence of ground state strings between domain walls.

The thin torus states do not permit braiding, so we evolve the thin torus states into states in the 2D limit in Sec. 2.3. We can see that they do not permit braiding by imagining an exchange of two domain walls in a thin torus state. The only way to exchange them to have them pass "through" each other, which would by necessity involve nontrivial interactions between them. Only when interactions play essentially no role can the effect of braiding reasonably be assumed to be topological and yield well-defined statistics. It is clear, then, that to have a useful notion of quasihole braiding built from the simple domain wall patterns, we must use states that live on a 2D torus, not the 1D thin torus limit. We adiabatically increase the small dimension of the torus such that no transitions are induced between any states. The simple 1D product states each evolve to a 2D state that is no longer a simple LLL orbital product. The domain walls are still localized along one dimension of the torus, but are completely delocalized, wrapping around the torus, in the other.

In Sec. 2.4 we construct localized quasihole states from the delocalized states, using a coherent state ansatz. As in the thin limit, exchanging the delocalized domain wall objects through adiabatic transport is not well defined, since they still have to pass through each other to exchange positions. We need a way to localize the domain

walls in both dimensions, using them to form localized quasiholes. To accomplish this, we introduce a coherent state ansatz. However, even with the localized quasiholes in the coherent states, we still cannot find the result of braiding. Any braiding path must somewhere bring two quasiholes to the same x position, even if their absolute distance remains large, and whenever quasiholes coincide in x the coherent state ansatz is no longer a valid description of localized quasiholes.

This problem can be resolved using a dual coherent state basis which is defined for quasiholes that are well separated in y. We develop this dual basis in Sec. 2.6. In Sec. 2.7 we construct transition matrices between the two coherent state bases, and use symmetries to constrain the matrix elements. Using the two coherent state bases and the transition matrices between them, we are able to find the Berry phase from exchanging quasiholes through adiabatic transport. This calculation is performed in Sec. 2.8.

The procedure described above is presented in Chapter 2 for the Abelian $\nu = 1/2$ Laughlin state. The procedure is generalized in Chapter 3 to a non-Abelian state, the Moore-Read "Pfaffian" state. We show in Chapter 4 that the coherent state method is generalizable to more complicated non-Abelian states by deriving the statistics of the $k = 3$ Read-Rezayi state [58]. The contents of these Chapters originally appeared in Ref. [7].

The CFT conjecture gives a way to find the statistics of a FQH wave function through the monodromies of a conformal block in some CFT. Some wave functions are connected through this conjecture to "nonunitary" CFTs, so called because their

energy-momentum tensors are non-Hermitian. The conformal block monodromies are also nonunitary in such CFTs, thus quasihole monodromy would induce a nonunitary transformation on the wave functions constructed from those CFTs. However, adiabatic transport of quasiholes in a FQH wave function must always result in a unitary transformation to the state. So the implications of the QH-CFT connection for this state are not clear. What happens when quasiholes in these states are braided is an open question (and, at the least, requires great care to make well-defined). One such nonunitary state is the Gaffnian [59]. In Chapter 5 we provide insight into the braiding holonomies of this state by exchanging Gaffnian coherent state quasiholes through adiabatic transport. This Chapter has appeared as a preprint, Ref. [60].

Chapter 6 contains previously unpublished results. In Chapter 6, we use the thin torus states that underlie the coherent state method to derive formulae for the counting of the number of zero modes in all the states mentioned above. Such counting formulae have previously been derived for all of these states on the sphere [58, 61, 62, 63, 64]; in that geometry the wave functions have a polynomial structure that can aid zero-mode counting. No such polynomial structure exists in the wave functions on the torus. There, the patterns arising in the thin torus limit serve as a natural bookkeeping device. The thin torus patterns allow the development of counting formulae on the torus, but also allow the rederivation of formulae on the sphere, which serves as a useful check of the results.

Certain derivations are detailed in four Appendices.

Chapter 2

The Laughlin State

Laughlin's $\nu = 1/m$ wave functions [11] are the most elementary examples of a rich class of quantum Hall trial wave functions. These wave functions are generally characterized by a set of analytic requirements, the most basic of which enforces that the wave function is entirely contained in the lowest Landau level (LLL). Laughlin's original construction of incompressible quantum liquids in a 2D planar geometry has been generalized by Haldane to states living on a sphere [65] enclosing monopole charges and to states on a torus [66]. The torus construction has also revealed that the $\nu = 1/m$ Laughlin state is m-fold degenerate on the torus, while it is nondegenerate on the sphere. The nontrivial torus degeneracy was later understood to be the hallmark of topological order [67], and to be a necessary condition for the presence of anyonic excitations [68]. Here we focus on the torus.

We will first review the formalism of the LLL orbitals on the torus. We then find

This chapter originally appeared in Ref. [7].

a natural a basis for the Laughlin states using LLL orbitals and construct this basis in the thin torus limit. We use this basis along with adiabatic continuity to construct localized quasiholes in the non-thin limit, with both torus dimensions finite, through the coherent state ansatz. Using two mutually dual coherent state bases we can implement a braiding procedure, which allows us to find a representation of the braid group of Laughlin quasiholes.

2.1 Landau levels on the torus

We work on a torus, identified as a rectangular 2D domain of dimensions L_x and L_y subject to (magnetic) periodic boundary conditions. We take the magnetic vector potential to be in Landau gauge, $\mathbf{A} = (0, x)$. The magnetic length $\ell = \sqrt{\hbar c/eB}$ is set equal to 1. Then $L_x L_y = 2\pi L$, where L equals the number of magnetic flux quanta through the surface of the torus, which also equals the number of orbitals in the lowest Landau level (LLL). An infinite cylinder is obtained in the limit $L_x \to \infty$, with L_y kept finite. We first construct a basis of the LLL on such a cylinder. It is given by $\varphi_n^c(z) = \xi^n \exp(-\frac{1}{2}x^2 - \frac{1}{2}\kappa^2 n^2)$, where $\kappa = 2\pi/L_y$, $z = x + iy$ is the particle's complex coordinate, and $\xi = \exp(\kappa z)$. This notation differs from that of Eq. (1.8) where n labeled the Landau level (here 0) and n_y labeled the k_y eigenvalue (here n). From the LLL states φ_n^c on the infinite cylinder one can construct LLL states φ_n that satisfy proper periodic magnetic boundary conditions (cf. Ref. [66]) on a torus with finite $L_x = \kappa L$. Fixing some unimportant overall phases, these boundary conditions

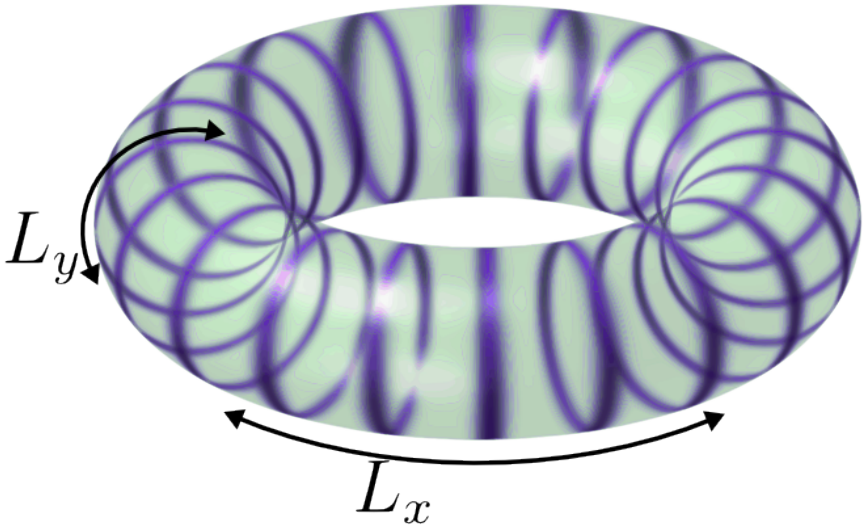

Figure 2.1: Landau level basis on the torus of dimensions $L_x \times L_y$. The orbitals $\varphi_n(z)$ form a 1D periodic "lattice" in the x direction. Each orbital $\varphi_n(z)$ localizes a particle at $x = \kappa n$ while being delocalized in the y direction, leading to a "ring shape" geometry. Consecutive orbitals are separated by a distance κ.

read

$$\begin{aligned} \varphi_n(z + L_x) &= e^{i\kappa y}\varphi_n(z) \\ \varphi_n(z + iL_y) &= \varphi_n(z) \ , \end{aligned} \tag{2.1}$$

for the present gauge, and the orbitals $\varphi_n(z)$ satisfying these conditions are then simply obtained by "repeating" the LLL orbitals of the cylinder along the x direction:

$$\varphi_n(z) = \sum_j \varphi^c_{n+jL}(z) \ . \tag{2.2}$$

For both the cylinder and the torus (with sufficiently large L_x), the n-th LLL orbital has the "ring shape" geometry shown in Fig. 2.1. The orbital $\varphi_n(z)$ localizes a particle in the x direction around $x = \kappa n$ to within one magnetic length, such that consecutive

orbitals are separated by a distance κ. At the same time, each orbital is completely delocalized in y. We can view the orbitals φ_n as forming a 1D periodic "lattice" along the x direction, with each orbital representing a lattice site. Note that we have $\varphi_{n+L}(z) = \varphi_n(z)$, and in this sense the "orbital lattice" satisfies ordinary periodic boundary conditions in n. A "thin torus limit" [69, 38, 39, 40, 41, 42, 43, 44, 45, 46, 47, 48, 49, 50, 7] can be defined as $\kappa \gg 1$. In this limit, the orbitals in the basis (2.2) are well separated and have negligible overlap.

It is clear that the choice of LLL orbital basis made above treats the x direction on the torus differently from the y direction. However, nothing prevents us from exchanging the roles of x and y. A "dual" basis of states $\overline{\varphi}_n$ localized at $y = \overline{\kappa} n$ (for $\overline{\kappa} = 2\pi/L_x$), encircling the torus in the x direction (Fig. 1.3), can be obtained by formally "rotating" the φ_n basis, followed by a gauge transformation, via

$$\overline{\varphi}_n(z) = \exp(ixy)\varphi_n(-iz)|_{\kappa\to\overline{\kappa}} \,. \tag{2.3}$$

Alternatively, it can be shown (via Poisson resummation) that the $\overline{\varphi}_n$ basis thus defined is related to the original basis (2.2) through a discrete Fourier transform, i.e

$$\overline{\varphi}_n(z) = \frac{1}{\sqrt{L}} \sum_{n'} \exp(-i\frac{2\pi}{L} nn')\varphi_{n'}(z) \,. \tag{2.4}$$

In the presence of the magnetic field, the single-particle Hamiltonian commutes

with two magnetic translation operators, whose form in the chosen gauge is given by

$$\begin{aligned} t_x &= e^{-\kappa(\partial_x - iy)} \\ t_y &= e^{-\overline{\kappa}\partial_y} \ . \end{aligned} \tag{2.5}$$

The orbital bases φ_n and $\overline{\varphi}_n$ have simple transformation properties under the action of these two non-commuting translation operators. One easily verifies that

$$t_x\varphi_n(z) = \varphi_{n+1}(z) \qquad t_x\overline{\varphi}_n(z) = e^{2\pi i n/L}\overline{\varphi}_n(z) \tag{2.6a}$$

$$t_y\varphi_n(z) = e^{-2\pi i n/L}\varphi_n(z) \qquad t_y\overline{\varphi}_n(z) = \overline{\varphi}_{n+1}(z) \ . \tag{2.6b}$$

All orbitals are thus invariant under the action of the operators ${t_x}^L$ and ${t_y}^L$, which represent magnetic translations by L_x and L_y in the respective direction. This is equivalent to the observation that both the φ_n as well as the $\overline{\varphi}_n$ orbitals satisfy the same periodic magnetic boundary conditions (2.1) appropriate to the gauge $\mathbf{A} = (0, x)$.

We finally mention some other important symmetries of the problem under consideration. Inversion symmetry acts on wave functions via $I\psi(z) = \psi(-z)$, and on the basis states defined above via

$$I\varphi_n(z) = \varphi_{-n}(z) \ , \quad I\overline{\varphi}_n(z) = \overline{\varphi}_{-n}(z) \, . \tag{2.7}$$

Similarly, while there is neither time reversal symmetry nor mirror symmetry in the

presence of the constant magnetic field, the combined symmetry does exist. We denote by τ_x the antilinear operator that acts on wave functions via $\tau_x\psi(z) = \psi(-z^*)^*$, and on basis states via

$$\tau_x\varphi_n(z) = \varphi_{-n}(z)\,, \quad \tau_x\overline{\varphi}_n(z) = \overline{\varphi}_n(z)\,, \tag{2.8}$$

where the second equation follows from the first with Eq. (2.4). The reflectional part of τ_x is obviously a reflection about the y axis. We can similarly define an antilinear operator τ_y that performs a reflection about the x axis in conjunction with time reversal, and which acts on basis states via

$$\tau_y\varphi_n(z) = \varphi_n(z)\,, \quad \tau_y\overline{\varphi}_n(z) = \overline{\varphi}_{-n}(z)\,. \tag{2.9}$$

2.2 Laughlin states in the thin torus limit

Let $|\psi^c\rangle$, where $c = 0 \ldots m-1$, denote the m incompressible Laughlin-type ground-state wave functions at filling factor $\nu = 1/m$ on the torus. We may expand the states $|\psi^c\rangle$ in the basis of the LLL Fock space that is derived from the single-particle basis φ_n:

$$|\psi^c\rangle = \sum_{\{m_n\}} C_{\{m_n\}}|m_1, m_2 \ldots m_L\rangle\,. \tag{2.10}$$

Here, m_n denotes the number of particles in the state φ_n, and we consider a system with a fixed number $L = L_xL_y/2\pi$ of flux quanta or LLL orbitals. For the time being, we will use L_y to parameterize the aspect ratio of the torus. The coefficients $C_{\{m_n\}}$

depend on the y perimeter L_y of the torus. In the thin torus limit $L_y \to 0$, the states (2.10) evolve into states dominated by a single pattern of occupancy numbers $\{m_n\}$. E.g, the state with $c = 0$ evolves into the Fock state $|100\ldots100\ldots\rangle$ (where dots indicate that 1's are separated by $m-1$ zeros), and states with $c > 0$ are obtained by repeated application of the translation operator T_x. T_x is the many-particle version of the single particle translation operator t_x discussed above, and acts on a thin torus pattern such as $100\ldots100\ldots$ as a right shift. For any value of the perimeter L_y, the Laughlin states $|\psi^c\rangle$ are ground states of a "pseudopotential" Hamiltonian [65, 70], whose action within the LLL explicitly depends on L_y. The evolution of the states $|\psi^c\rangle$ with L_y can be understood as the adiabatic evolution of the ground states of the pseudopotential Hamiltonian $H(L_y)$ as the parameter L_y is slowly changed. This has been studied in some detail for $m = 3$ in Ref. [38], where is was shown numerically that the gap above the ground states never closes as a function of L_y.

The thin torus states discussed here are formally identical to the Tau-Thouless states proposed in Ref. [71]. When considered in the "2D-limit" $L_x = L_y = \infty$, these states do not have long range charge density wave (CDW) order. In contrast, the thin torus states considered here can be characterized as 1D CDW states breaking the translational symmetry of the system. This is so since in the thin torus limit, the LLL orbitals φ_n are well separated by a distance $\kappa = 2\pi/L_y$ (Fig. 1.3), and the symmetry breaking pattern of occupancy numbers becomes visible as a CDW modulation. The findings of Ref. [38] imply that the Laughlin states retain the CDW order of the thin torus limit on any torus with at least one of the dimensions L_x, L_y finite. Related

rigorous results have been discussed in Ref. [72]. However, as long as both L_x and L_y are large compared to the magnetic length, the CDW order is exponentially small. The physics of the incompressible fluid is thus quickly approached as L_x, L_y become large, and in particular the notion of braiding statistics can be made arbitrarily well defined on a large but finite torus. This, together with the fact that the states on such a torus are adiabatically connected to simple product states sharing all their essential quantum numbers, is the foundation of the method discussed here.

For simplicity we will now focus on the case $m = 2$, the bosonic $\nu = 1/2$ Laughlin state with ground-state patterns $101010\ldots$ and $010101\ldots$, respectively. The general case was worked out in Ref. [40]. However, here we will discuss an improved variant of the method, which was used in Ref. [42] to derive the statistics of the Pfaffian state. The two degenerate $m = 2$ Laughlin states on the torus are the unique zero-energy eigenstates of the $\hat{V}_0$ Haldane pseudopotential at filling factor $\nu = 1/2$. As in other cases where parent Hamiltonians for incompressible trial states are known, further zero-energy states exist at smaller filling factors: The excitations associated with elementary quasihole-type excitations are in one-to-one correspondence with the zero modes of the parent Hamiltonian at filling factor $\nu < 1/2$. This is again true at any value of the perimeter L_y, and in particular the number of zero modes for any fixed number of constituent particles (electrons) N does not depend on L_y. We will extend the assumption of adiabatic continuity to the entire zero-mode sector. The thin torus limit of a Laughlin state with n quasiholes can easily be worked out directly from the $L_y \to 0$ limit of the Hamiltonian [38], or from the same limit of the

wave function on the torus or cylinder [69]. A state with a single Laughlin quasihole evolves into a thin torus state that has a single domain wall between the two ground-state patterns. We can distinguish domain-wall states in two "topological sectors", according to the two possible phases of the charge density wave to the left and to the right of the domain wall, i.e., 1010|0101... or 01010|010... . The 1D domain walls can be ascribed a fractional charge by means of the usual "Su-Schrieffer" counting argument [73]. This charge (here 1/2) generally agrees [38, 46] with the charge of Laughlin quasiholes, as it should by adiabatic continuity.

We introduce notation $|a, c)$ for LLL product states with a domain wall at position a in topological sector c:

$$|a, 0) = \Big| \ldots 1010101010|01010101010 \ldots \Big) \tag{2.11a}$$

$$|a, 1) = \Big| \ldots 01010101010|0101010101 \ldots \Big) \tag{2.11b}$$

The curved ket indicates that these are "bare" product states to be distinguished from states that have undergone adiabatic evolution, which we will discuss below. The number a is a half-odd integer labeling the domain-wall position relative to the LLL orbitals, such that $a \pm 1/2$ are the orbital indices of the LLL orbitals adjacent to the domain wall. The two possible values of the topological sector label c distinguish the sequence of ground-state patterns in the two states of Eq. (2.12). It is worth noting that in principle, the topological sector is already determined by the value of $\exp(i\pi a)$ and so the notation of Eq. (2.11) may seem slightly redundant. We find

it advantageous, though, to include the topological sector information explicitly into the sector label, especially with regard to more general cases discussed later.

The above observations immediately generalize to states with two quasiholes, whose thin torus limits are given by product states corresponding to patterns with two domain walls. These states are labeled $|a_1, a_2, c)$, with occupation number patterns for the values of $c = 0, 1$ given by:

$$|a_1, a_2, 0) = \Big|\ldots 1010\overset{\downarrow}{0}10101010\overset{\downarrow}{0}101010\ldots\Big) \tag{2.12a}$$

$$|a_1, a_2, 1) = \Big|\ldots 01010\overset{\downarrow}{0}10101010\overset{\downarrow}{0}10101\ldots\Big) \tag{2.12b}$$

We will always take a_1 to be less than a_2, such that a_1 and a_2 refer to the first and second domain wall, respectively. It is clear from Eq. (2.12) that the two domain-wall positions are also subject to the constraint

$$a_2 - a_1 = 1 \mod 2\,. \tag{2.13}$$

Again, the label c explicitly distinguishes the two possible sequences of ground-state patterns, even though in principle this information is also contained in the values of $\exp(i\pi a_1)$ or $\exp(i\pi a_2)$. The labels a_1, a_2, and c describing a given two–domain-wall state are unique when the condition

$$0 < a_1 < a_2 < L \tag{2.14}$$

is imposed. Whenever the domain-wall positions satisfy (2.14), we will say that they are given "in the default frame". However, since we are working on the torus and LLL orbitals satisfy the periodic boundary condition $\varphi_n \equiv \varphi_{n+L}$, it is desirable to admit domain-wall positions that refer to more general reference frames also. We thus define the states $|a_1, a_2, c)$ for all a_1, a_2 satisfying

$$a_1 < a_2 < a_1 + L \ , \tag{2.15}$$

together with the following identification:

$$|a_1, a_2, c) \equiv |a_2 - L, a_1, c') \ , \tag{2.16}$$

where $c' = 1 + c \bmod m$ (here m=2). We will say that the domain-wall positions a_1, a_2 lie in an f frame if

$$f < a_1 < a_2 < f + L \ . \tag{2.17}$$

The standard frame is the 0 frame. If necessary, repeated application of Eq. (2.16) allows one to transform domain-wall positions between different frames, where the roles of the first and second domain wall may be exchanged; whenever this happens, the topological sector label c changes also, as stated in Eq. (2.16). This fact follows from Eq. (2.13), since the value of c is determined by the value of the position of, say, the first domain wall modulo 2, as discussed above. Note that $L = 2N + 2$ is even for states with two domain walls. The topological sector label is therefore frame

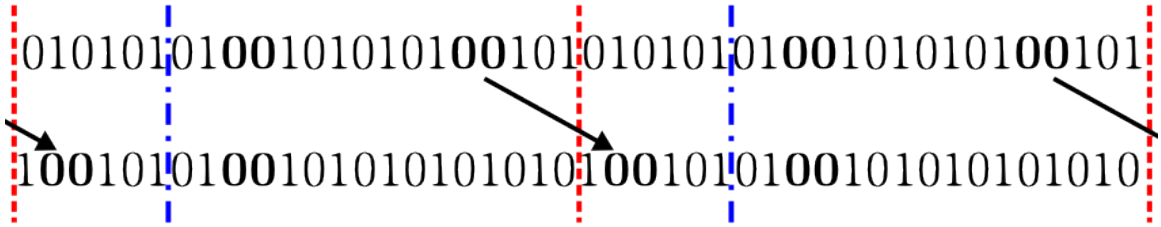

Figure 2.2: Top: A possible arrangement of two domain walls is shown in a "repeated zone scheme" with the domain-wall positions marked by the bold **00** strings. The dotted line (red) marks the boundaries of the 0 frame and the dot-dashed line (blue) marks a shifted frame, the 6 frame. Bottom: The second domain wall moves to a new position. When viewed from the 0 frame, this domain wall moves across the frame boundary where it becomes the first domain wall in a different topological sector. Viewed from the 6 frame, the domain wall does not move across the boundary and the topological sector does not change.

dependent. This is of a piece with the fact that the topological sector changes when one quasihole is transported around one of the "holes" of the torus, as we will discuss in detail below (see Fig. 2.2). The transformation properties of topological sectors under the exchange of two quasiholes along nontrivial loops (going once around the torus) are thus encoded in the thin torus patterns. This is a key ingredient of the method presented here, and sector transformation rules analogous to Eq. (2.16) will be of much importance especially in the non-Abelian states to be discussed below.

2.3 Delocalized quasihole states

The notion of braiding is not well defined in the thin torus limit. In order for a well-defined statistics to emerge from an adiabatic exchange of quasiholes, throughout the exchange the quasiholes must be spatially localized in both x and y, and at the same time must be kept away from each other at distances large compared to their

individual spatial extent. Both are not simultaneously possible in the thin torus limit. Hence, in order to "braid" quasiholes through adiabatic transport, we will need to work with states that live not on a thin torus but on a full-sized torus with L_x, L_y both large. Formally, the assumption of adiabatic continuity means the following. There exists a family of unitary operators $\hat{S}(L_y, L_y')$ that describe the adiabatic evolution of the eigenstates (in particular the zero modes) of the pseudopotential Hamiltonian at perimeter L_y' into those at L_y. In particular, we define $\hat{S}(L_y) \equiv \hat{S}(L_y, 0)$, the unitary operator that evolves thin torus states, Eqs. (2.11), (2.12), into states at finite L_y. We hence define the "dressed" or adiabatically evolved domain-wall states as the descendants of thin torus states via the operator $\hat{S}(L_y)$. In particular, for states with a single domain wall, we write

$$|a, c, L_y\rangle = \hat{S}(L_y)\,|a, c) \ , \tag{2.18}$$

where we will suppress the label L_y whenever no confusion can arise, using the regular ket to denote dressed states as opposed to bare domain-wall states. For sufficiently large L_y (and $L_x = 2\pi L/L_y$), the states in Eq. (2.18) describe a quasihole immersed into a Laughlin liquid (here with $\nu = 1/2$). The quasihole is localized in x around $x = \kappa a$. However, it is entirely delocalized in the y direction. To see this, we consider the operator T_y which is the many-body analogue of the single-particle translation operator t_y discussed above. The bare domain-wall states are T_y eigenstates by construction, with eigenvalues that are easily calculated from the pattern of occupation

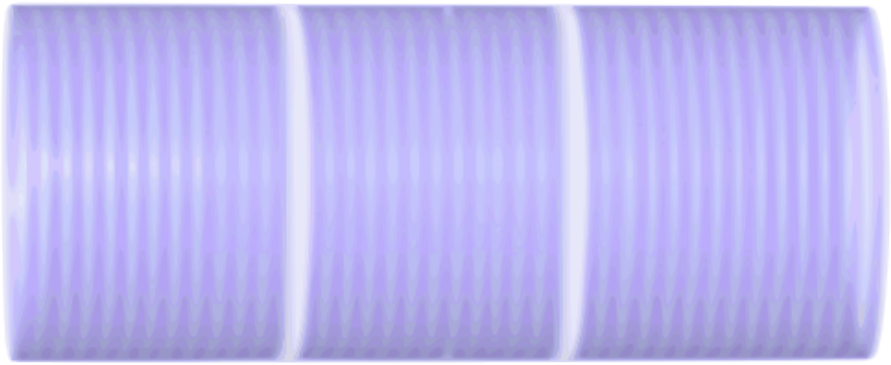

Figure 2.3: A two-quasihole dressed domain-wall state. These states are adiabatically evolved from the "bare" thin torus domain-wall states but live on the full-sized torus. The quasiholes described by this state are localized at some position in the x direction but delocalized in the y direction.

numbers. Since the pseudopotential Hamiltonian commutes with the magnetic translation operators for any value of L_y, so does the adiabatic evolution operator $\hat{S}(L_y)$. It follows that the dressed domain-wall states transform under magnetic translations in the same manner as the bare ones do. The states in Eq. (2.18) are thus still T_y eigenstates, with eigenvalues identical to those of their bare counterparts. It is clear that in such a state, the quasihole must be completely delocalized in the y direction (see Fig. 2.3). Again, these observations can be extended to states with two quasiholes,

$$|a_1, a_2, c, L_y\rangle = \hat{S}(L_y)\,|a_1, a_2, c) \ . \tag{2.19}$$

Here, two Laughlin quasiholes in the topological sector c are localized in x around $x_1 = \kappa a_1$ and $x_2 = \kappa a_2$, respectively, and are both delocalized in y. Note that the x separation between the two quasiholes depends on L_y via $\Delta x = \kappa \Delta a = 2\pi(a_2 - a_1)/L_y$.

The two delocalized quasiholes in the state $|a_1, a_2, c, L_y\rangle$ will be uncorrelated as long as Δx is much larger than a magnetic length (set equal to 1). There are certainly no such correlations in the thin torus limit, and even at finite L_y both the correlation length of the incompressible fluid and the range of the interaction remain on the order of a magnetic length. As we increase L_y, the adiabatic evolution will therefore not induce any correlations between the two quasiholes as long as $\Delta x \gg 1$ remains satisfied. In this case, the local properties of each of the quasiholes will be the same as those of the single quasihole described by Eq. (2.18).

We emphasize once more that the adiabatically continued domain-wall states in Eqs. (2.18) and (2.19) are neither simple product states, nor are they any longer "thin torus states" in any sense. Rather, the assumption of adiabatic continuity allows one to organize the zero-mode subspace into a basis labeled by 1D patterns for any value of L_y. These patterns carry information about the properties under magnetic translations not only of the thin torus states, but also of their adiabatically descended counterparts at finite L_y. Finally, it will be of some significance that, since the adiabatic evolution operator $\hat{S}(L_y)$ is unitary, the dressed states of Eqs. (2.18) and (2.19) are orthonormal, since the thin torus product states certainly are.

2.4 Coherent states

Individually, the members of the basis of zero-mode states defined above describe delocalized Laughlin quasiholes. In order to analyze the braiding statistics of these

quasiholes, we need to form states where quasiholes are localized in both x and y. Laughlin has constructed analytic wave functions for such states [11], which are also zero-energy eigenstates of the pseudopotential Hamiltonian. It must therefore be possible to write these localized quasihole states as superpositions, or coherent states, in the zero-mode basis defined in the preceding section.

We consider the single-quasihole case first. According to the above, it must be possible to write

$$|\psi_c(h)\rangle = \sum_a C(h,a)|a,c\rangle \tag{2.20}$$

for a state with a quasihole localized at complex coordinate $h = h_x + ih_y$. Here, we anticipate that to localize a quasihole, it is sufficient to include states of a single topological sector into the superposition, such that the localized quasihole state still carries a well-defined sector label. The left-hand side of Eq. (2.20) is assumed to be a Laughlin single-hole state. Interestingly, as long as we assume that a zero-mode basis $|a,c\rangle$ with the properties claimed in the preceding section exists, the coefficients $C(h,a)$ of this expansion are fully determined. To this end, we note that

$$(a',c|a,c\rangle = \text{const} \times \delta_{a,a'} \ . \tag{2.21}$$

The vanishing of Eq. (2.21) for $a \neq a'$ follows since for different domain-wall positions the bare state $|a',c)$ and the dressed state $|a,c\rangle$ have different T_y eigenvalues, as is easily seen by writing out the corresponding domain-wall patterns and calculating the action of T_y. On the other hand, the constant in Eq. (2.21) does not depend on a,

since states with different domain-wall position a are related by repeated application of T_x. From Eqs. (2.20) and (2.21), it follows that

$$C(h,a) \propto (a,c|\psi_c(h)\rangle\,. \tag{2.22}$$

We also expect only those states $|a,c\rangle$ to have any appreciable weight in the coherent state (2.20) whose domain-wall position $x = \kappa a$ is close to the x position h_x of the quasihole. We will assume that the coefficients $C(h,a)$ in this region are not affected by a change from periodic to open boundary conditions, as long as the torus is cut into a cylinder by a cut along y that is far away in x from the quasihole. In particular, it is clear from the discussion in Sec. 2.1 that such a cut would affect the local structure of the φ_n LLL basis (in terms of which the states $|a,c\rangle$ have been defined) only by negligible amounts (for large L_x). For cylindrical topology, however, it is possible to evaluate the right-hand side of Eq. (2.22) explicitly. For definiteness, we explicitly write out the wave function for the Laughlin state $|\psi_c(h)\rangle$ on a cylinder of perimeter L_y:

$$\psi_c(h; z_1 \ldots z_N) = \prod_i (\xi_i - \eta) \prod_{i<j} (\xi_i - \xi_j)^2 \times e^{-1/2 \sum_i x_i^2}\,. \tag{2.23}$$

Here, $\xi_i = \exp(\kappa z_i)$ and $\eta = \exp(\kappa h)$. Evaluating Eq. (2.22) amounts to evaluating the coefficients of "dominance patterns" in the polynomial of Eq. (2.23). This can be done using "squeezed lattice" methods discussed in Refs. [41, 44]. This shows that the above wave function does indeed lie in a definite topological sector, as defined by

the thin cylinder limit.[1] One finds:[2]

$$|\psi_c(h)\rangle = \mathcal{N} \sum_a \phi(h, \kappa a)|a, c\rangle \,, \tag{2.24}$$

where

$$\phi(h, x) = \exp\left[\frac{1}{2} i(h_y + \pi/\kappa)x - \frac{1}{4}(h_x - x)^2\right] \,, \tag{2.25}$$

and $\mathcal{N}$ is a normalization constant independent of h. The general form of the coherent state wave function Eq. (2.25) could have been guessed based on the following observations. As a function of x, $\phi(h, x)$ can be interpreted as a "minimum uncertainty" coherent state of a particle confined to one spatial dimension. This is consistent with the fact that, after projection into a single Landau level, the x and y components of the position operator do not commute, but satisfy a position-momentum–type commutation relation $[x, y] \propto i$. y position can thus be regarded as x momentum, and vice versa. It is thus natural that the y position of the quasihole enters as a momentum-like phase twist in Eqs. (2.24), (2.25). On the other hand, as a function of h, $\phi(h, x)$ looks like a lowest Landau level orbital of a charge 1/2 degree of freedom in the same magnetic field that is felt by the underlying electrons. These heuristic considerations will later allow us to generalize the coherent state form Eq. (2.24) to more complicated cases, where a direct derivation of the kind outlined here is not straightforward.

[1] The other sector can be reached by multiplication with $\prod_i \xi_i$.

[2] An h_y-dependent phase has been dropped for simplicity. As a result, note that the original Laughlin state Eq. (2.23) is single valued in h_y, whereas Eq. (2.24) is not.

The next logical step is to generalize the expression (2.24) to states with two localized quasiholes. This is not difficult, as long as the two quasiholes at complex positions h_1 and h_2 are well separated along the x axis, i.e., $h_{2,x} - h_{1,x} \gg 1$. In this case, we can argue that the presence of the one quasihole does not influence the other, and the natural generalization of the coherent state Eq. (2.24) takes on the following form:

$$|\psi_c(h_1, h_2)\rangle = \mathcal{N}^2 \sum_{a_1<a_2}{}' \phi(h_1, \kappa a_1)\phi(h_2, \kappa a_2) \, |a_1, a_2, c\rangle \ . \tag{2.26}$$

The function $\phi(h, x)$ is just as defined in Eq. (2.25). The prime in the above sum denotes the restriction of the domain-wall positions to values corresponding to the topological sector c. These are different for a_1 and a_2, as a result of Eq. (2.13). To be precise, we can define the topological sector c for two quasiholes via the following constraint on the domain-wall positions:

$$a_1 = 2n_1 - 1/2 + c\,, \qquad a_2 = 2n_2 + 1/2 + c \tag{2.27}$$

with integers $n_2 \geq n_1$. By default, the sum in Eq. (2.26) is further restricted to domain-wall positions within the default frame, Eq. (2.14). The restriction to a different frame according to (2.17) will be indicated by a subscript f, $|\psi_c(h_1, h_2)\rangle_f$.

For as long as the condition $h_{2,x} - h_{1,x} \gg 1$ holds, Eq. (2.26) can be inferred from Eq. (2.24) in a more formal way, using assumptions about the action of local operators on the adiabatically continued domain-wall basis. Locality arguments of this kind will play an important role in the following, and we will devote the next

section to the development these arguments.

2.5 Locality

It is useful to formalize the assumptions that enter the factorized two-quasihole ansatz, Eq. (2.26). This naturally leads to general assumptions about the matrix elements of local operators within the zero-mode basis of adiabatically continued domain-wall states defined above, which will be of further relevance in much of the following. Let $\hat{\rho}(\vec{r})$ be a local operator, localized at some position $\vec{r} = (r_x, r_y)$. We will later consider $\hat{\rho}(\vec{r})$ to be the operator for the local charge density at $\vec{r}$, but for now we wish to consider a generic (not necessarily single-particle) local operator. The action of this operator within the LLL Fock space depends on the aspect ratio of the torus. We first consider the action of $\hat{\rho}(\vec{r})$ on a bare domain-wall state $|a_1, a_2, a_3, \ldots, c)$ (which for finite L_y is not an eigenstate of the pseudopotential Hamiltonian). Quite obviously, the operator $\hat{\rho}(\vec{r})$ can only generate matrix elements between this state and some other domain-wall state $|b_1, b_2, b_3, \ldots, c)$ if the associated pattern of orbital occupancy numbers differs only locally between these two states, for orbitals whose location lies within a magnetic length of r_x. We will usually be interested in cases where the domain-wall positions $\kappa a_1, \kappa a_2, \kappa a_3, \ldots$ are all separated by much more than a magnetic length. In this case, for the matrix element between these two states to be finite, it is clear that either $a_i = b_i$ for all i, or there is a single j such that $a_j \neq b_j$, with both κa_j and κb_j in the vicinity of r_x. Otherwise the patterns associated

with the two states would differ even in orbitals that are far removed from r_x along the x axis, and their matrix element would be exponentially small. In particular, matrix elements between states in different topological sectors are not possible (in the thermodynamic limit). Although at large L_y, the dressed domain-wall states $|a_1, a_2, a_3 \ldots, c\rangle$ are quite different from their bare counterparts, they still describe topological defects inserted into the torus at x positions κa_i. We will assume here and in the following that if the associated patterns of two dressed domain-wall states differ by many microscopic degrees of freedom, then this is also true for dressed states themselves. In particular, if the patterns of two states differ in orbitals whose separation along the x axis is large compared to one magnetic length, we assume that their matrix element for any local operator will be negligible. For states with well separated domain walls, the observation made above for bare states then extends to their dressed counterparts. I.e., non-zero matrix elements are of the form

$$\langle \ldots a_i \ldots | \hat{\rho}(\vec{r}) | \ldots b_i \ldots \rangle = \rho(a_i, b_i) \; , \tag{2.28}$$

where the ellipses represent other domain-wall positions, which must remain fixed but otherwise do not affect the value of the matrix element, and again $\kappa a_j \approx \kappa b_j \approx r_x$ to within a magnetic length. With these assumptions, we can easily show that Eq. (2.26) describes two localized quasiholes, assuming that Eq. (2.24) describes a single localized quasihole. Let now $\hat{\rho}(\vec{r})$ be the local density operator. We consider the expectation value $\langle \psi_c(h_1, h_2) | \hat{\rho}(\vec{r}) | \psi_c(h_1, h_2) \rangle$ for $|h_{2x} - r_x| \gg 1$, and show that

this expectation value reduces exactly to that of $\langle\psi_c(h_1)|\hat{\rho}(\vec{r})|\psi_c(h_1)\rangle$, which we know to describe a single quasihole at position h_1. Using Eq. (2.28), we have

$$\begin{aligned}
&\langle\psi_c(h_1,h_2)|\hat{\rho}(\vec{r})|\psi_c(h_1,h_2)\rangle \\
&\qquad = \mathcal{N}^4 {\sum_{a_1,a_2}}' {\sum_{b_1,b_2}}' \phi(h_1,\kappa a_1)^*\phi(h_2,\kappa a_2)^*\phi(h_1,\kappa b_1)\phi(h_2,\kappa b_2)\,\langle a_1,a_2,c|\,\hat{\rho}(\vec{r})\,|b_1,b_2,c\rangle \\
&\qquad \simeq \mathcal{N}^4 {\sum_{a_1,a_2,b_1}}' \phi(h_1,\kappa a_1)^*\phi(h_2,\kappa a_2)^*\phi(h_1,\kappa b_1)\phi(h_2,\kappa a_2)\,\langle a_1,a_2,c|\,\hat{\rho}(\vec{r})\,|b_1,a_2,c\rangle \\
&\qquad = \mathcal{N}^4 {\sum_{a_1,a_2,b_1}}' \phi(h_1,\kappa a_1)^*\phi(h_1,\kappa b_1)\phi(h_2,\kappa a_2)^*\phi(h_2,\kappa a_2)\,\rho(a_1,b_1) \\
&\qquad \simeq \mathcal{N}^2 {\sum_{a_1,b_1}}' \phi(h_1,\kappa a_1)^*\phi(h_1,\kappa b_1)\,\rho(a_1,b_1)\ .
\end{aligned} \tag{2.29}$$

In the above, the primes on the sums enforce all the necessary constraints such that the bras and kets correspond to domain-wall patterns in the topological sector c, cf. Eq. (2.27). In the second line, we have used that the matrix elements are diagonal in the second domain-wall position for $|h_{2x} - r_x| \gg 1$. Furthermore, for $h_{2x} - h_{1x} \gg 1$ the constraint $a_1, b_2 < a_2$ which the domain-wall positions obey becomes irrelevant due to the Gaussian nature of the ϕ functions, and the sum over a_2 in the third line simply yields the normalization of the single-quasihole state, Eq. (2.24). The last line is, however, identical to $\langle\psi_c(h_1)|\hat{\rho}(\vec{r})|\psi_c(h_1)\rangle$. In words, this shows that when $\vec{r}$ is far away along the x axis from the second quasihole, the expectation value of $\hat{\rho}(\vec{r})$ reduces to that of a state with a single quasihole at h_1. Similar arguments show that if $\vec{r}$ is far away along the x axis from the first quasihole, $\langle\hat{\rho}(\vec{r})\rangle$ reduces to that of a

state with a single quasihole at h_2. Together, this shows that for $h_{2x} - h_{1x} \gg 1$, the state (2.26) describes two quasiholes localized at h_1 and h_2.

2.6 Dual description

The coherent state expression (2.26) is in principle suited to calculate the Berry connection governing adiabatic transport [21, 59, 16]. However, as the arguments in the preceding section have made clear, Eq. (2.26) can be expected to be accurate only in the limit of quasiholes that are well separated along the x axis. As can be seen in Fig. 2.6, the x separation of the quasiholes must vanish at some point for any exchange path, even though the absolute distances between the quasiholes remain large throughout. As a result, Eq. (2.26) is by itself not sufficient to fully calculate the result of adiabatic transport.

The resolution to this problem lies in making use of the modular S invariance of the torus. Though we have so far only used the thin torus limit $L_y \to 0$, the physics must be invariant under an exchange of x and y. In doing so, we may now define a zero-mode basis by working from the limit $L_x \to 0$. In this limit, the zero modes of the pseudopotential Hamiltonian are domain-wall states that are occupation number eigenstates in the $\overline{\varphi}_n$ basis. The corresponding ground-state and domain-wall patterns are the same as those appearing in the $L_y \to 0$ limit, except that the associated charge density waves extend along the y direction of the torus. We denote the bare domain-wall states in the $\overline{\varphi}_n$ basis with an overline, e.g. $\overline{|a_1, a_2, c)}$ for a two–domain-wall

state. We now proceed in a manner that is completely analogous to the definition of the "original" zero-mode basis on a general torus, Eq. (2.19). To this end, we define a unitary operator $\overline{S}(L_x)$ that describes the adiabatic evolution of states from the "narrow x limit" to a finite value of L_x. We then define the general zero-mode basis for two-quasihole states via

$$\overline{|a_1, a_2, c, L_x\rangle} = \overline{S}(L_x)\overline{|a_1, a_2, c)} \, , \tag{2.30}$$

where again, we will drop the label L_x on the left-hand side whenever no confusion is possible. The states in Eq. (2.30) describe quasiholes that are localized in y but delocalized around the torus along x. Similar definitions are made for states with n quasiholes. We can form localized quasihole states in a manner completely analogous to Eq. (2.26). So long as Eq. (2.26) describes two localized quasiholes at positions h_1 and h_2 for any aspect ratio of the torus, invariance of the physics under exchange of x and y implies that the following expression will do the same in terms of the dual zero-mode basis Eq. (2.30):

$$\overline{|\psi_c(h_1, h_2)\rangle} = \bar{\mathcal{N}}^2 \sum_{a_1<a_2} \overline{\phi}(h_1, \overline{\kappa} a_1)\overline{\phi}(h_2, \overline{\kappa} a_2)\overline{|a_1, a_2, c\rangle} \tag{2.31}$$

where

$$\overline{\phi}(h, y) = \phi(-ih, y)|_{\kappa\to\overline{\kappa}} = \exp\left[-\frac{i}{2}(h_x + \pi/\overline{\kappa})y - \frac{1}{4}(h_y - y)^2\right] \, , \tag{2.32}$$

and Eq. (2.31) is now applicable to the case $h_{2y} - h_{1y} \gg 1$. We thus have at least one valid coherent state expression for any configuration of the two quasiholes along the exchange path shown in Fig. 2.6. At some points along the path, however, we will be forced to translate back and forth between the two coherent state expressions (2.26) and (2.31). This task is nontrivial. To see this, it is important to note that the topological sector label c has different meanings in the original zero-mode basis Eq. (2.19) and the dual zero-mode basis Eq. (2.30): in the former, it means that the state evolves into a well defined charge density wave product state in the limit $L_y \to 0$, characterized by a certain sequence of ground-state patterns separated by domain walls; in the latter, it means the same in the opposite thin torus limit, $L_x \to 0$. It will turn out that a state that carries a definite sector label c in the original basis, Eq. (2.19), is a superposition of states carrying different topological sector labels in the dual basis Eq. (2.30), and vice versa. The same is true for the coherent state expressions Eqs. (2.26) and (2.31). While the relation between the sets of states $|\psi_c(h_1, h_2)\rangle$ and $\overline{|\psi_c(h_1, h_2)\rangle}$ is thus not diagonal in the topological sector label c, for given quasihole coordinates h_1, h_2 both sets span the same subspace, namely the space associated with having quasiholes localized at h_1, h_2. The relation between the states $|\psi_c(h_1, h_2)\rangle$ and $\overline{|\psi_c(h_1, h_2)\rangle}$ is thus diagonal in the quasihole positions, and we may write

$$|\psi_c(h_1, h_2)\rangle = \sum_{c'} u^{\sigma}_{cc'}(h_1, h_2) \overline{|\psi_{c'}(h_1, h_2)\rangle} \, . \tag{2.33}$$

Note that above, we had defined $|\psi_c(h_1, h_2)\rangle$ only for $h_{2x} > h_{1x}$, and $\overline{|\psi_{c'}(h_1, h_2)\rangle}$ only

for $h_{2y} > h_{1y}$. While we will stick to these restrictions most of the time, we will generally let $|\psi_c(h_2, h_1)\rangle \equiv |\psi_c(h_1, h_2)\rangle$ and $\overline{|\psi_{c'}(h_2, h_1)\rangle} \equiv \overline{|\psi_{c'}(h_1, h_2)\rangle}$ for convenience. This allows us to write relations such as Eq. (2.33) without distinguishing different cases. The transition functions $u^{\sigma}_{cc'}(h_1, h_2)$ are then meaningful in regions where both $|h_{1x} - h_{2x}| \gg 1$ and $|h_{1y} - h_{2y}| \gg 1$, since it is only in these regions where we have defined both $|\psi_c(h_1, h_2)\rangle$ and $\overline{|\psi_{c'}(h_1, h_2)\rangle}$ through coherent state expressions. The final technical obstacle is to sufficiently determine these transition functions from symmetries and topological considerations.

To this end, we begin by distinguishing two regions of the 2-hole configuration space. Let $\sigma = \mathrm{sgn}(h_{1x} - h_{2x})\mathrm{sgn}(h_{1y} - h_{2y})$. $\sigma = \pm 1$ then refers to first and second quasihole configuration in Fig. 2.4, respectively. We will first be interested in the "local" dependence of the transition functions on coordinates within each of these regions. Later we will use the fact that these regions are actually connected by "global" trajectories where one quasihole is taken around one of the holes of the torus (Fig. 2.5). For now we will not allow these global moves. Within each of these regions, we now show that the local dependence of the u functions on coordinates is as follows,

$$u^{\sigma}_{cc'}(h_1, h_2) = \xi^{\sigma}_{cc'}\, e^{i/2(h_{1x}h_{1y} + h_{2x}h_{2y})} \equiv \xi^{\sigma}_{cc'} u(h_1, h_2)\,, \tag{2.34}$$

where the parameters $\xi^{\sigma}_{cc'}$ are complex constants and $u(h_1, h_2)$ is the phase function $e^{i/2(h_{1x}h_{1y} + h_{2x}h_{2y})}$.

The h_1, h_2 dependence of $u^{\sigma}_{cc'}$ can be locally determined from the Berry connec-

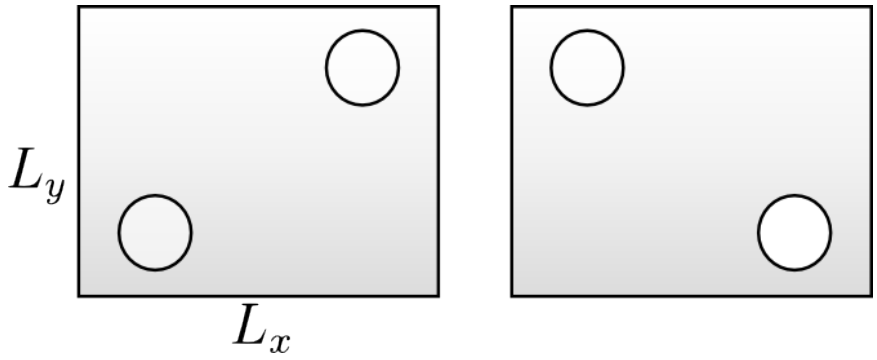

Figure 2.4: The two possible configurations of two quasiholes, which are distinguished by the value of $\sigma = \mathrm{sgn}(h_{1x} - h_{2x})\mathrm{sgn}(h_{1y} - h_{2y})$. Left: $\sigma = +$. Right: $\sigma = -$.

tions. Using the coherent state expressions in Eqs. (2.26) and (2.31) on the full-sized torus ($\kappa, \overline{\kappa} \ll 1$), the Berry connections can be calculated to be

$$\begin{aligned} i \langle \psi_c(h_1, h_2)| \boldsymbol{\nabla}_{h_{1,2}} |\psi_c(h_1, h_2)\rangle &= -\frac{1}{2}(0, h_{1x,2x}) \\ i\overline{\langle \psi_c(h_1, h_2)|} \boldsymbol{\nabla}_{h_{1,2}} \overline{|\psi_c(h_1, h_2)\rangle} &= \frac{1}{2}(h_{1y,2y}, 0). \end{aligned} \tag{2.35}$$

An essential ingredient in the above is the fact that the zero-mode basis states we have defined are orthonormal, as explained at the end of Sec. 2.3. This is where the assumption of adiabatic continuity is crucial in our approach. Obtaining Eq. (2.35) is then straightforward, since in the limit $\kappa, \overline{\kappa} \ll 1$, the remaining sums can be replaced by Gaussian integrals.

Let us consider an adiabatic process where one quasihole is fixed at h_1 and the other is dragged from h_2 to h_2' (which are both in the same region σ). This process is described by a unitary operator, which acts separately on each term on both sides

of Eq. (2.33), yielding

$$\begin{aligned} &\exp\left(i\int_{h_2}^{h_2'} \mathrm{d}\boldsymbol{h}\cdot\left[-\frac{1}{2}\left(0,h_x\right)\right]\right)|\psi_c(h_1,h_2')\rangle \\ &\quad=\sum_{c'} u^{\sigma}_{cc'}(h_1,h_2)\,\exp\left(i\int_{h_2}^{h_2'} \mathrm{d}\boldsymbol{h}\cdot\left[\frac{1}{2}\left(h_y,0\right)\right]\right)\overline{|\psi_{c'}(h_1,h_2')\rangle}\,. \end{aligned} \tag{2.36}$$

The above equation may be compared to Eq. (2.33) evaluated at (h_1, h_2') instead of (h_1, h_2). This yields a relationship between the u functions at these two locations,

$$\begin{aligned} u^{\sigma}_{cc'}(h_1,h_2') &= u^{\sigma}_{cc'}(h_1,h_2)\,\exp\left(i\int_{h_2}^{h_2'} \mathrm{d}\boldsymbol{h}\cdot\left[\frac{1}{2}\boldsymbol{\nabla}_h h_x h_y\right]\right) \\ &= u^{\sigma}_{cc'}(h_1,h_2)\,\exp\left(\frac{1}{2}i(h_{2x}'h_{2y}'-h_{2x}h_{2y})\right) \end{aligned} \tag{2.37}$$

where we used the fact that $(h_y, 0) = -(0, h_x) + \boldsymbol{\nabla}_h h_x h_y$. In order to satisfy Eq. (2.37), the dependence of u on h_2 must be proportional to $e^{i/2h_{2x}h_{2y}}$. Using a similar argument in which the quasihole at h_2 remains fixed while the quasihole at h_1 is moved, we find that the dependence of u on h_1 is proportional to $e^{i/2h_{1x}h_{1y}}$. Therefore the general form of the u functions is given by Eq. (2.34).

2.7 Symmetries and further simplifications

With the above considerations, the transition functions $u^{\sigma}_{cc'}$ have been reduced to parameters $\xi^{\sigma}_{cc'}$, of which there are eight at $\nu = 1/2$. We will now establish further relations between these parameters using symmetries and adiabatic transport along the "global" trajectories mentioned above.

First, we derive relations arising from properties under magnetic translations. The magnetic many-body translation operators T_x, T_y introduced above have the following effect on the dressed domain-wall states:

$$\begin{aligned} T_x \left|a_1, a_2, c\right\rangle &= \left|a_1+1, a_2+1, 1-c\right\rangle \\ T_x \overline{\left|a_1, a_2, c\right\rangle} &= e^{2\pi i/L \sum_j n_j} \overline{\left|a_1, a_2, c\right\rangle} \end{aligned} \tag{2.38}$$

$$\begin{aligned} T_y \left|a_1, a_2, c\right\rangle &= e^{-2\pi i/L \sum_j n_j} \left|a_1, a_2, c\right\rangle \\ T_y \overline{\left|a_1, a_2, c\right\rangle} &= \overline{\left|a_1+1, a_2+1, 1-c\right\rangle} \end{aligned} \tag{2.39}$$

where $c = 0, 1$, and n_j is the orbital index of the orbital occupied by the j-th particle in the thin torus pattern associated with the state. For the bare product states associated with these patterns, the above identities are direct consequences of Eqs. (2.6) for the single particle translation operators. However, the properties under magnetic translations remain the same for the dressed states, as explained in Sec. 2.3. Note that the basis states $\left|a_1, a_2, c\right\rangle$ are eigenstates of T_y whereas T_x changes the topological sector label, and vice versa for the basis states $\overline{\left|a_1, a_2, c\right\rangle}$.

Equations (2.38) and (2.39) allow us to work out the properties of the coherent states under magnetic translations. The fact that both sides of Eq. (2.33) must transform the same way under these translations poses severe constraints on the coefficients $\xi^{\sigma}_{cc'}$. Observing that for given domain-wall positions,

$$\sum_j n_j = \frac{1}{2} L (\frac{1}{2} L + c) - \frac{1}{2}(a_1 + a_2), \tag{2.40}$$

it is a simple thing to verify the following properties of the coherent states under magnetic translations:

$$\begin{aligned} T_x \left|\psi_c(h_1,h_2)\right\rangle &= e^{-i\kappa/2(h_{1y}+h_{2y})+i\pi} \left|\psi_{1-c}(h_1+\kappa,h_2+\kappa)\right\rangle \\ T_x \overline{\left|\psi_c(h_1,h_2)\right\rangle} &= e^{i\pi\lambda+i\pi c} \overline{\left|\psi_c(h_1+\kappa,h_2+\kappa)\right\rangle} \end{aligned} \tag{2.41}$$

$$\begin{aligned} T_y \left|\psi_c(h_1,h_2)\right\rangle &= e^{i\pi\lambda+i\pi c} \left|\psi_c(h_1+i\overline{\kappa},h_2+i\overline{\kappa})\right\rangle \\ T_y \overline{\left|\psi_c(h_1,h_2)\right\rangle} &= e^{i\overline{\kappa}/2(h_{1x}+h_{2x})+i\pi} \overline{\left|\psi_{1-c}(h_1+i\overline{\kappa},h_2+i\overline{\kappa})\right\rangle} \end{aligned} \tag{2.42}$$

where we define $\lambda = \nu L$ (which in the present case, evaluates to the integer $L/2 = N+1$).

We can use these translational properties to constrain the eight $\xi^{\sigma}_{cc'}$s. We recast Eq. (2.33) in matrix form,

$$\begin{pmatrix} \left|\psi_0(h_1,h_2)\right\rangle \\ \\ \left|\psi_1(h_1,h_2)\right\rangle \end{pmatrix} = u(h_1,h_2)\Xi^{\sigma} \begin{pmatrix} \overline{\left|\psi_0(h_1,h_2)\right\rangle} \\ \\ \overline{\left|\psi_1(h_1,h_2)\right\rangle} \end{pmatrix}, \tag{2.43}$$

where we have used Eq. (2.34), and Ξ^{σ} is the matrix with elements $\xi^{\sigma}_{cc'}$. Let us apply T_y to Eq. (2.43).

$$e^{i\pi\lambda}\,\sigma_z \begin{pmatrix} \left|\psi_0(h_1',h_2')\right\rangle \\ \\ \left|\psi_1(h_1',h_2')\right\rangle \end{pmatrix} = u(h_1',h_2')\Xi^{\sigma}(e^{i\pi})\,\sigma_x \begin{pmatrix} \overline{\left|\psi_0(h_1',h_2')\right\rangle} \\ \\ \overline{\left|\psi_1(h_1',h_2')\right\rangle} \end{pmatrix} \tag{2.44}$$

The positions $h_j' = h_j + i\overline{\kappa}$ for $j = 1, 2$, and the $u(h_1, h_2)$ function has been shifted by absorbing the spatially dependent phase in Eq. (2.42). If we compare Eq. (2.44) to

Eq. (2.43) evaluated at the shifted positions (h_1', h_2'), we find that the two equations are consistent, provided that the Ξ^σ matrix satisfies the following constraint:

$$\Xi^\sigma = e^{i\pi\lambda + i\pi}\, \sigma_z \Xi^\sigma\, \sigma_x. \tag{2.45}$$

We can derive another constraint using the same logic after translating Eq. (2.43) with T_x:

$$\Xi^\sigma = e^{i\pi\lambda + i\pi}\, \sigma_x \Xi^\sigma\, \sigma_z. \tag{2.46}$$

These two sets of equations constrain the Ξ^σ matrix to be of the following form,

$$\Xi^\sigma = \frac{\xi^\sigma}{\sqrt{2}} \begin{pmatrix} 1 & e^{i\pi\lambda + i\pi} \\ e^{i\pi\lambda + i\pi} & -1 \end{pmatrix}, \tag{2.47}$$

where ξ^σ is a pure phase, and the overall normalization factor $1/\sqrt{2}$ has been determined from the requirement that Ξ^σ is a unitary matrix. Thus, after using translations we have only two unknowns remaining: The overall phases ξ^+ and ξ^-. Only the relative phase between the two will have physical significance.

In order to fix this relative phase, we will now drag one of the quasiholes in a two quasihole state along a "global path", i.e., a path where the quasihole disappears on one end of the standard frame (see Sec. 2 and Fig. 2.2) and reappears at the other. The merit of such a path is that it connects the $\sigma = +$ and $\sigma = -$ configuration while maintaining both conditions $|h_{1x} - h_{2x}| \gg 1$, $|h_{1y} - h_{2y}| \gg 1$. Let us consider the

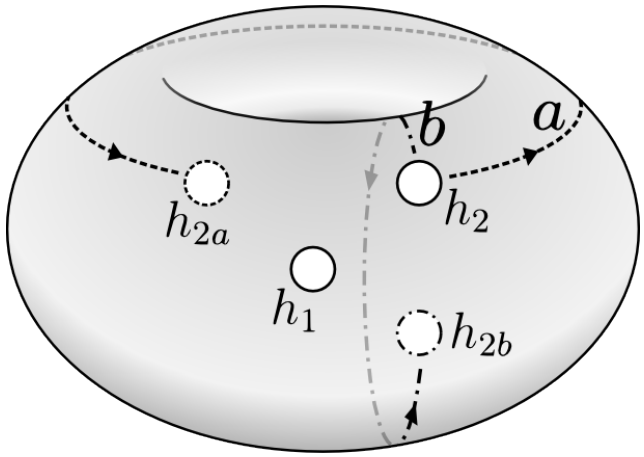

Figure 2.5: Different configurations σ can be connected by dragging one quasihole along a global path. Initially, the two quasiholes at h_1 and h_2 are in configuration $\sigma = +$. Keeping the quasihole at h_1 fixed, the quasihole at h_2 can be moved along one of two paths: path a, in which the quasihole at h_2 moves around the torus in the x direction to h_{2a}, or path b, in which the quasihole at h_2 moves around the torus in the y direction to h_{2b}. Both paths can be used to change the configuration σ while keeping quasiholes well separated in both x and y. At the same time, the topological sector also changes.

coherent state $|\psi_c(h_1, h_2)\rangle$, Eq. (2.26), with two quasiholes in the topological sector c in the $\sigma = +$ configuration. We will drag the second quasihole along path "a" as shown in Fig. 2.5. We will do so by continuously changing the position of this quasihole from a value h_2^i with h_{2x}^i well within the boundaries 0 and L_x to a value h_2^f with $L_x < h_{2x}^f < h_{1x} + L_x$. The default frame introduced in Sec. 2.2 is not suited to describe this process continuously. We thus choose an f frame as described in Secs. 2.2 and 2.4, and consider the state $|\psi_c(h_1, h_2)\rangle_f$, i.e., the coherent state (2.26) with the sum restricted to the f frame. For this we choose a parameter f such that $\kappa f < h_{1x} < h_{2x}^i < h_{2x}^f < \kappa(f+L) = \kappa f + L_x$. Note that as long as the x position h_{2x} of the second quasihole is well between h_{1x} and L_x, one has $|\psi_c(h_1, h_2)\rangle_f \doteq |\psi_c(h_1, h_2)\rangle$, where $\doteq$ denotes equality up to exponentially small terms. In this case the weight

of both Gaussians in the coherent state is well contained within both frames, and so $|\psi_c(h_1, h_2)\rangle_f$ and $|\psi_c(h_1, h_2)\rangle$ may be used interchangeably. However, as soon as h_{2x} approaches L_x, we must work with $|\psi_c(h_1, h_2)\rangle_f$. In this regime, we will see that the coherent state $|\psi_c(h_1, h_2)\rangle_f$ is identical up to a phase to the (default frame) state $|\psi_{c'}(h_2 - L_x, h_1)\rangle$. That is, the second quasihole reappears on the left end of the standard frame, thus becoming the new 'first' quasihole (Figs. 2.2 and 2.5). However, in the default frame the final state will be in a different topological sector with $c' = 1 - c$. At the same time, the quasiholes are now in the $\sigma = -$ configuration. This allows us to obtain one more relation between the transition functions $u^{\sigma}_{cc'}$ and their defining parameters $\xi^{\sigma}_{cc'}$.

We first establish the precise relationship between $|\psi_c(h_1, h_2)\rangle_f$ and $|\psi_{c'}(h_2 - L_x, h_1)\rangle$, where h_{2x} exceeds L_x by more than a magnetic length. One finds:

$$\begin{aligned} |\psi_c(h_1, h_2)\rangle_f &= e^{i/2h_{2y}L_x + i\pi\eta + i\pi} |\psi_{1-c}(h_2 - L_x, h_1)\rangle_{f-L} \\ &\doteq e^{i/2h_{2y}L_x + i\pi\eta + i\pi} |\psi_{1-c}(h_2 - L_x, h_1)\rangle \end{aligned} \tag{2.48}$$

where in the first identity we have passed to the $f - L$ frame by straightforwardly plugging the identification (2.16) into the coherent state (2.26). The second identity follows from the fact that for h_{2x} well exceeding L_x, the states $|\psi_{c'}(h_2 - L_x, h_1)\rangle_{f-L}$ and $|\psi_{c'}(h_2 - L_x, h_1)\rangle$ are again identical up to exponentially small terms, as discussed above.

Next we look at the comparatively trivial issue of how the dual state $\overline{|\psi_{c'}(h_1, h_2)\rangle}$

transforms along the same path, where h_2 is again taken from h_2^i to h_2^f. Since the motion is chiefly along the x direction, there is no need for a change of the frame for the $\overline{|a_1, a_2, c'\rangle}$ basis states. By inspection of Eq. (2.31), it is easy to see that we have

$$\overline{|\psi_{c'}(h_1, h_2)\rangle} = e^{-i\pi(1/2+c')}\overline{|\psi_{c'}(h_1, h_2 - L_x)\rangle}\,. \tag{2.49}$$

While the states $\overline{|\psi_{c'}(h_1, h_2)\rangle}$ are not single valued under a shift of quasihole positions by L_x, path a in Fig. 2.5 can be described continuously without leaving the default frame. Since we have established that both $|\psi_c(h_1, h_2)\rangle_f$ and $\overline{|\psi_{c'}(h_1, h_2)\rangle}$ describe states with quasiholes in the same position for h_1 fixed and h_2 along the path a in Fig. 2.5, a relation of the form

$$|\psi_c(h_1, h_2)\rangle_f = \sum_{c'} u^+_{cc'}(h_1, h_2)\overline{|\psi_{c'}(h_1, h_2)\rangle}\,. \tag{2.50}$$

must again hold for (some neighborhood of) this path. It is clear that the coefficient functions $u^+_{cc'}(h_1, h_2)$ appearing in there must be the analytic continuation (for $h_{2x} > L_x$) of those already defined, since 1) the arguments leading to the functional dependence Eq. (2.34) can be extended to the regime $h_{2x} > L_x$ and 2) for $h_{2x} < L_x$ the functions in Eq. (2.50) must be identical to those in Eq. (2.33). At the same time, for $h_{2x} > L_x$ we have by definition

$$|\psi_c(h_2 - L_x, h_1)\rangle = \sum_{c'} u^-_{cc'}(h_1, h_2)\overline{|\psi_{c'}(h_1, h_2 - L_x)\rangle}\,. \tag{2.51}$$

After plugging Eqs. (2.48) and (2.49) into Eq. (2.50), and further Eqs. (2.34) and (2.47) into both Eqs. (2.50) and (2.51), comparing coefficients leads to the following additional relation between the ξ parameters:

$$\xi^- = \xi^+ \, e^{-i\pi/2} \tag{2.52}$$

All ξ parameters are thus defined up to some overall phase ξ. We have

$$\begin{aligned} \Xi^+ &= \frac{\xi}{\sqrt{2}} \begin{pmatrix} 1 & e^{i\pi\lambda+i\pi} \\ e^{i\pi\lambda+i\pi} & -1 \end{pmatrix} \\ \Xi^- &= \frac{\xi}{\sqrt{2}} e^{-i\pi/2} \begin{pmatrix} 1 & e^{i\pi\lambda+i\pi} \\ e^{i\pi\lambda+i\pi} & -1 \end{pmatrix} . \end{aligned} \tag{2.53}$$

We note that processes similar to our moves along global paths play a fundamental role in all studies of anyonic statistics on the torus (see, e.g., Ref. [68]). Unlike in the present case, it is usually assumed from the beginning that these anyons are entities carrying a representation of the braid group. Typically, complete monodromies are considered, where the particle moves back into its original position after following a path associated with one of the generators of the fundamental group of the torus. In the present case, it is of some importance that these global moves end before the quasihole crosses over back into a configuration labeled by the initial σ value, thus changing the value of σ.

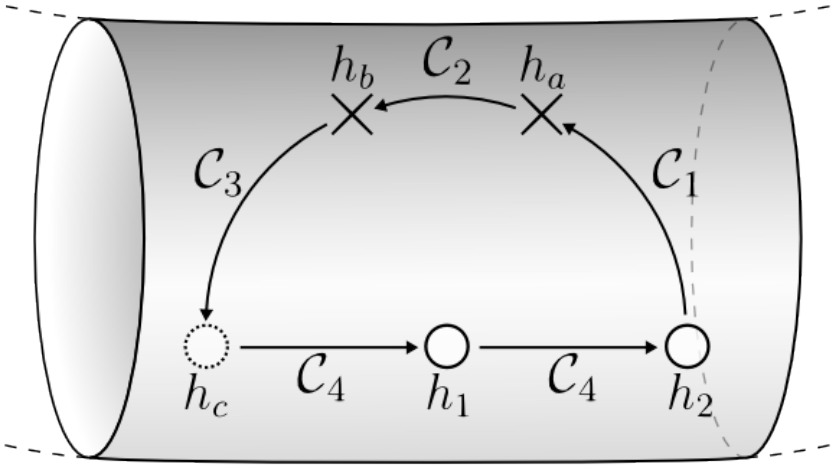

Figure 2.6: Exchange path for two quasiholes. First, the quasihole at h_2 is dragged along path $\mathcal{C}_1$ to h_a. There the coherent state representation is changed from the original basis to the dual basis using Eq. (2.33). The quasihole at h_a is then dragged along $\mathcal{C}_2$ to h_b, and the representation is changed back to the original basis. The quasihole at h_b is moved along $\mathcal{C}_3$ to h_c. At this point both quasiholes are moved to their final positions: the quasihole at h_1 goes to h_2 and the quasihole at h_c goes to h_1.

2.8 Braiding

With the transition functions Eq. (2.33) now fully defined via Eqs. (2.34) and (2.53), the result of adiabatic transport along an exchange path as shown in Fig. 2.6 can be calculated without difficulty. We assume that in the beginning, the quasiholes are arranged at positions h_1 and h_2 as shown, with $h_{2x} - h_{1x} \gg 1$. The quasihole initially at h_2 is then dragged into the position h_c directly opposite the other quasihole, via path segments $\mathcal{C}_1$, $\mathcal{C}_2$, $\mathcal{C}_3$ which are separated by points h_a, h_b. Finally, the quasihole at h_1 is moved into position h_2, and the other quasihole is moved from h_c into h_1, completing the exchange. When the one quasihole reaches the point h_a, we pass from the coherent state expression (2.26) to the dual expression (2.31) via

the transition functions, and use the dual coherent state expression to calculate the adiabatic transport along the path segment $\mathcal{C}_2$. At the point h_b, the state is again re-expressed in terms of the original coherent state expression (2.26), which may be used to describe the completion of the exchange.

Let the initial state be $|\psi_c(h_1, h_2)\rangle$, the state that lies in the topological sector c as defined by the $L_y \to 0$ limit. Adiabatic transport along the path $\mathcal{C}_1$ will change the coherent state according to

$$|\psi_c(h_1, h_2)\rangle \to e^{i\gamma_1} |\psi_c(h_1, h_a)\rangle \tag{2.54}$$

where, using Eq. (2.35),

$$\begin{aligned} \gamma_1 &= i \int_{\mathcal{C}_1} d\boldsymbol{h}_2' \cdot \langle \psi_c(h_1, h_2')| \boldsymbol{\nabla}_{h_2'} |\psi_c(h_1, h_2')\rangle \\ &= \int_{\mathcal{C}_1} d\boldsymbol{h} \cdot \left[-\frac{1}{2}(0, h_x) \right] . \end{aligned} \tag{2.55}$$

At h_a we reexpress the state in the dual basis, using Eqs. (2.33) and (2.34):

$$e^{i\gamma_1} |\psi_c(h_1, h_a)\rangle = e^{i\gamma_1} u(h_1, h_a) \sum_{c'} \xi^+_{cc'} \overline{|\psi_{c'}(h_1, h_a)\rangle} . \tag{2.56}$$

We proceed by moving the same quasihole along the path segment $\mathcal{C}_2$. This process is easily described in terms of the dual basis states $\overline{|\psi_{c'}(h_1, h_2')\rangle}$, which appear on the right-hand side of Eq. (2.56). In this basis the adiabatic process is simply described

by the acquisition of a phase $e^{i\gamma_2}$, where, using again Eq. (2.35),

$$\begin{aligned}\gamma_2 &= i\int_{\mathcal{C}_2} d\boldsymbol{h}_2' \cdot \overline{\langle\psi_{c'}(h_1,h_2')|}\boldsymbol{\nabla}_{h_2'}\overline{|\psi_{c'}(h_1,h_2')\rangle} \\ &= \int_{\mathcal{C}_2} d\boldsymbol{h}\cdot\left[\frac{1}{2}(h_y,0)\right] \ , \end{aligned} \tag{2.57}$$

which does not depend on the "dual" sector label c'. At the endpoint h_b of $\mathcal{C}_2$ we have thus transitioned into the state

$$e^{i\gamma_1+i\gamma_2}u(h_1,h_a)\sum_{c'}\xi^+_{cc'}\,\overline{|\psi_{c'}(h_1,h_b)\rangle}\,. \tag{2.58}$$

The key observation is that this state is still in the topological sector c as defined in the original coherent state basis, i.e., is of the form $|\psi_c(h_b,h_1)\rangle$ times a phase. To see this, note that the quasiholes are now in the $\sigma=-1$ configuration, and we have from Eq. (2.53)

$$\xi^+_{cc'} = e^{i\pi/2}\xi^-_{cc'}\,. \tag{2.59}$$

The state (2.58) can thus be rewritten as

$$\begin{aligned} &e^{i\pi/2}e^{i\gamma_1+i\gamma_2}u(h_1,h_a)u(h_b,h_1)^{-1}\sum_{c'}u(h_b,h_1)\xi^-_{cc'}\,\overline{|\psi_{c'}(h_1,h_b)\rangle} \\ &= e^{i\pi/2}e^{i\gamma_1+i\gamma_2}u(h_1,h_a)u(h_b,h_1)^{-1}|\psi_c(h_b,h_1)\rangle \end{aligned} \tag{2.60}$$

The rest of the exchange path is trivially described using the coherent states $|\psi_c(h_1',h_2')\rangle$. The phase γ_3 associated with the path segment $\mathcal{C}_3$ is again given by an integral over

a Berry connection of the form Eq. (2.55). The final move along the "baseline" $\mathcal{C}_4$ is carried out by moving both quasiholes, one from h_c into h_1, and the other from h_1 into h_2. The components of the Berry connection associated with each complex coordinate are, however, both of the same form, Eq. (2.35). For the remaining phases we thus get

$$\gamma_{3,4} = \int_{\mathcal{C}_3+\mathcal{C}_4} d\boldsymbol{h} \cdot \left[-\frac{1}{2}(0, h_x) \right] . \tag{2.61}$$

The entire exchange process thus results in the following transformation of the state:

$$|\psi_c(h_1, h_2)\rangle \to e^{i\pi/2} e^{i\sum_{i=1}^{4}\gamma_i} u(h_1, h_a) u(h_b, h_1)^{-1} |\psi_c(h_1, h_2)\rangle \tag{2.62}$$

As apparent from Eq. (2.34), the u factors in the above equation equal $i(h_{ax}h_{ay} - h_{bx}h_{by})/2 = -i/2 \int_{\mathcal{C}_2} d\boldsymbol{h} \cdot (h_y, h_x)$. When combined with the expression for γ_2, all contour integrals can be combined into a single integral equal to the Aharonov-Bohm phase $\Phi_{AB} = \int_{\mathcal{C}} d\boldsymbol{h} \cdot [-1/2(0, h_x)]$, corresponding to a charge $-1/2$ particle moving in a unit magnetic field. We thus recover the well-known result [22] that the exchange of two Laughlin quasiparticles results in the acquisition of a phase, which is equal to the sum of the Aharonov-Bohm phase and a purely topological, statistical part:

$$|\psi_c(h_1, h_2)\rangle \to e^{i\Phi_{AB}} e^{i\pi/2} |\psi_c(h_1, h_2)\rangle . \tag{2.63}$$

We emphasize once more that we did not assume *a priori* that any aspect of this phase is topological. Rather, this result followed naturally from the coherent state

ansatz Eqs. (2.26), (2.31), and the constraints we have derived. Note that one can read the statistical phase of $\pi/2$ directly off Eq. (2.59), which relates the transition functions for different quasihole configurations. While we have focused on the simplest case of $\nu = 1/2$ for clarity, the case $\nu = 1/m$ can be treated by the same method through straightforward generalization[3] [40].

[3]Some care must be given to fermion negative signs at odd denominator filling factors, in equations such as (2.38), (2.39), and (2.16). See Ref. [40].

Chapter 3

The Moore-Read State

3.1 Generalized coherent state ansatz

An appealing aspect of the method developed above, thus far for Laughlin states, is that the Berry connections Eq. (2.35) are trivial, i.e., essentially contributing only to the AB-phase. In contrast, all aspects relating to the statistics are manifest in the transition functions (cf. Eq. (2.59)), which need to be evaluated only at two isolated points. This fact might suggest that the same method may be amenable to discuss non-Abelian states in relatively simple terms as well, if suitably generalized. That this is so has been shown in Ref. [42] for the special case of the Moore-Read (Pfaffian) state. In the following, we will review this method, emphasizing aspects that need nontrivial generalization when compared to the Laughlin case. We will later show that the same method may then, with little or no further modification, be applied to

This chapter originally appeared in Ref. [7].

more complicated non-Abelian states also.

The $\nu = 1$ (bosonic) Moore-Read, in planar geometry, is the state described by the following wave function:

$$\psi_{\rm Pf}(z_1, \ldots, z_N) = {\rm Pfaff}\left[\frac{1}{z_i - z_j}\right] \prod_{i<j} (z_i - z_j)^2 e^{-\sum_i |z_i|^2/4} \tag{3.1}$$

The torus degeneracy of this state is 3, and torus wave functions for the three ground states have been worked out in Ref. [74]. A program similar to the one described for Laughlin states can now be implemented. A study [42] of the special Hamiltonian [74] associated with the Pfaffian state has demonstrated that again, the three ground states are adiabatically connected to a thin torus limit, in which the ground-state patterns 111111..., 020202..., and 202020... emerge.

The elementary quasihole-type excitations, which are again zero modes of the special Hamiltonian, turn out to evolve into charge 1/2 domain walls between 1111 ... and 2020 ... ground-state patterns. Periodic boundary conditions on the torus then require such domain walls to occur in even numbers. This observation is the thin torus statement of the well-known fact that the elementary Pfaffian quasiholes may only be created in pairs [23]. For the minimum number of two quasiholes, one thus has four topological sectors corresponding to the sequences of thin torus ground-state patterns shown in Table 3.1.

As in the Laughlin case, we denote these two–domain-wall states $|a_1, a_2, c)$, and their adiabatically continued counterparts by $|a_1, a_2, c\rangle$. We assume that a coherent

ansatz of a form similar to Eq. (2.26) and its dual version Eq. (2.31) also describe localized quasiholes in this non-Abelian state. In particular, we assume a Gaussian form for the coherent state form factors $\phi(h,x)$ in the expression

$$|\psi_c(h_1,h_2)\rangle = \mathcal{N}\sum_{a_1<a_2}\phi(h_1,\kappa a_1)\phi(h_2,\kappa a_2)\,|a_1,a_2,c\rangle \tag{3.2}$$

for quasiholes well separated along the x axis. A Gaussian form for $\phi(h,x)$ is essentially dictated by the fact that x and y are conjugate variables, as argued in Sec. 2.4. Unlike in the case of Laughlin quasiholes, however, we cannot extract all the parameters entering this expression from the analytic wave functions. Instead, we will have to rely more on symmetries and other consistency requirements to do this. We will thus initially assume $\phi(h,x)$ to be of the following generic form:

$$\phi(h,x) = \exp\left[i\beta(h_y+\delta/\kappa)x - \gamma(h_x-x)^2\right]. \tag{3.3}$$

Unlike in the case of the Laughlin state, we cannot derive Eq. (3.3) analytically from the Pfaffian 2-hole wave functions [23, 74]. We observe, however, that these wave functions are holomorphic in the quasihole positions h_1, h_2. We thus require the same for the coherent state (3.2), except for an overall normalization factor that depends on the quasihole positions only (and in particular does not depend on the parameters a_1, a_2 in Eq. (3.2)). Equation (3.3) is certainly the simplest expression that satisfies all these requirements, and is consistent with the fact that x and y

are conjugate variables, the latter implying that y position enters as x momentum. The discussion of Sec. 2.4 then makes it natural to expect that, as a function of h, Eq. (3.3) should have the form of a LLL orbital for a charge 1/2 degree of freedom in a unit magnetic field (for some choice of vector potential, and where boundary conditions in h_y may be twisted). This implies $\beta = 1/2$, $\gamma = 1/4$, as for the $\nu = 1/2$ Laughlin state. We will show shortly that $\beta = 1/2$ also follows more rigorously from duality requirements. The parameter γ merely controls the shape of the quasiholes. Its precise value will not be needed in the following.

Naively, it appears that the parameter δ can be formally absorbed into a shift of the coordinate origin. This is, however, not quite right. We will again require that there is a formally equivalent way to write two-hole states in the dual basis, defined as before via adiabatic evolution of domain-wall states:

$$\overline{|\psi_c(h_i, h_j)\rangle} = \mathcal{N}' \sum_{a_1<a_2} \overline{\phi}(h_i, \overline{\kappa} a_1)\overline{\phi}(h_j, \overline{\kappa} a_2)\overline{|a_1, a_2, c\rangle} \tag{3.4}$$

where

$$\begin{aligned} \overline{\phi}(h, y) &= \phi(-ih, y)|_{\kappa\to\overline{\kappa}} \\ &= (\text{const}) \exp\left[-i\beta(h_x + \delta/\overline{\kappa})y - \gamma(h_y - y)^2\right] \ . \end{aligned} \tag{3.5}$$

It is clear that the formal equivalence between Eq. (3.2) and Eq. (3.4) does not survive arbitrary shifts of the origin for the quasihole coordinates h_1, h_2. It is also clear that the coherent state expressions (3.2)–(3.5) assume definite relations between the orbital

indices in the LLL bases φ_n and $\bar{\varphi}_n$, respectively, which define the properties of these orbitals under magnetic translations, Eq. (2.6), and determine the positions of these orbitals in space[1]. The choice of coordinate system, and its relation to the orbital indices, is also encoded in the definition of the symmetry operators I, τ_x, τ_y, Eqs. (2.7)-(2.9), together with their geometric interpretation given above. We may use this to severely constrain the possible values of δ. Indeed, these symmetries fix δ to be a multiple of π. Since the same conclusion will also emerge from duality arguments below, we will not pause here to show this in detail[2]. The final result for the braid matrix will depend on δ only via $e^{2i\delta}$, which is fully determined and equals unity.

There is one more parameter entering the generalized coherent state ansatz that is not yet explicit in Eqs. (3.2) and (3.4). This parameter enters when generalizing Eq. (2.27), which fixes the relation between the domain-wall positions $a_{1,2}$ entering the coherent states and an adjacent LLL orbital with index, e.g., $2n_{1,2}$. In the case of Laughlin states, a single domain wall has inversion symmetry, and this symmetry clearly demands that the position a of this domain wall is defined as shown in Eq. (2.12), i.e., as the position halfway in between the adjacent ground-state patterns.

[1]Note that a coordinate shift in particular changes both the magnetic vector potential and the quasiperiodic boundary condition in x on wave functions. The constant Δ in $A = (0, x + \Delta)$ determines the locations of the LLL orbitals φ_n. An additional phase twist in the magnetic boundary condition in x does the same for the orbitals $\overline{\varphi}_n$. In this sense, fixing Δ and the magnetic boundary conditions leads to a preferred set of coordinate systems on the torus, which up to scaling ($\kappa \to \bar{\kappa}$) is symmetric with respect to the LLL bases ϕ_n and $\bar{\phi}_n$. Here, the index n is always defined via properties under magnetic translations, Eq. (2.6).

[2]One may consider a generalized version of the coherent state (3.2), with δ replaced by δ_1 in the first ϕ-factor, and by δ_2 in the second. Consistent behavior of this expression under τ_y requires $\delta_1 = \delta_2 \mod \pi/\beta$. Consistent behavior under I requires $\delta_1 = -\delta_2 \mod \pi/\beta$. This yields that either $\delta_{1,2} = 0 \mod \pi/\beta$, or $\delta_{1,2} = \pi/(2\beta) \mod \pi/\beta$. We can then take $\delta_1 = \delta_2 \equiv \delta$ without loss of generality, since shifting δ_i by π/β only results in an overall change of phase. Cf. Sec. 3.2, where furthermore $\beta = 1/2$ is derived.

More precisely, it must be the distance $h_x - a$ between this domain-wall position and the x position of a quasihole that suppresses the amplitude in the coherent states (2.20) or (2.26). There is no similar symmetry argument for the Pfaffian domain-wall patterns. Here, quasiholes must always come in pairs, as mentioned above. Consider a 2-hole coherent state, Eq. (3.2), in the topological sector $c = 1$, Table 3.1. It is clear that the domain-wall position a_1 entering the coherent state must be of the form $a_1 = 2n_1 - s$, where $2n_1$ is the position of the first 0 of the string, and s is a shift parameter that defines the position of the domain wall relative to this leading 0. For suitably chosen quasihole positions, an inversion symmetry leaving the coherent state invariant will map one quasihole onto the other. This does not fix the parameter s, but merely implies that the second domain wall must be assigned the position $a_2 = 2n_2 + s$, where $2n_2$ is the position of the last 0. In the topological sector c, we can thus write

$$a_i = 2n_i + f_i(c)\,, \tag{3.6}$$

where $f_1(1) = -s$, $f_2(1) = +s$ as discussed above, and the values for $f_i(c)$ for $c > 1$ can be related to those for $c = 1$ by magnetic translations in x as shown in Table 3.1. Here, we have defined $\eta = 0$ for even particle number N, $\eta = 1$ for N odd. Note that the even- or oddness of the particle number N is just determined by the length of the $1111\ldots$ string in the patterns of Table 3.1.

Equations (3.2)-(3.5), together with the shifts in the domain-wall positions given by Eq. (3.6) and Table 3.1, define the generalized coherent state ansatz. We will now

c	Thin torus pattern	$f_1(c)$	$f_2(c)$
1	111111**1**$\underline{\mathbf{0}}$2020202$\underline{\mathbf{0}}$**1**1111111	$-s$	s
2	1111111$\underline{\mathbf{1}}$**0**2020**2**$\underline{\mathbf{0}}$**1**1111111	$-s+1$	$s+1$
3	02020**2**$\underline{\mathbf{0}}$**1**1111111$\underline{\mathbf{1}}$**0**2020202	$s-1$	$-s+\eta$
4	2020202$\underline{\mathbf{0}}$**1**1111111$\underline{\mathbf{1}}$**0**202020	s	$-s+\eta+1$

Table 3.1: Thin torus patterns for a two–domain-wall Moore-Read state, and the offset functions of those domain walls. The latter are defined in terms of the shift parameter s, and relate domain-wall positions a_i to orbital positions $2n_i$ (underlined) via $a_i = 2n_i + f_i(c)$. Some offset functions depend on the particle number parity η, with $\eta = 0$ ($\eta = 1$) when N is even (odd).

show that this ansatz can be used to make precise statements about the statistics of the Pfaffian, and other non-Abelian states.

3.2 Constraints from translational symmetry

With the generalized coherent state ansatz in place, we continue by carrying out steps similar to those described in Secs. 2.6 and 2.7 for Laughlin states. Equation (2.33), the general relation between the coherent state in the two mutually dual bases, can be carried over unchanged. Again, the transition matrices appearing in these relations are strongly constrained by translational symmetry. To utilize this, we first state some of the analogues of Eqs. (2.41), (2.42):

$$T_x \left|\psi_c(h_1,h_2)\right\rangle = e^{-i\beta\kappa(h_{1y}+h_{2y})-2i\beta\delta} \left|\psi_{T(c)}(h_1+\kappa,h_2+\kappa)\right\rangle \tag{3.7a}$$

$$T_y \overline{\left|\psi_c(h_1,h_2)\right\rangle} = e^{i\beta\overline{\kappa}(h_{1x}+h_{2x})+2i\beta\delta} \overline{\left|\psi_{T(c)}(h_1+i\overline{\kappa},h_2+i\overline{\kappa})\right\rangle}\,. \tag{3.7b}$$

These properties again follow straightforwardly from the associated transformation

c	$T(c)$	$F(c)$
1	2	$3+\eta$
2	1	$4-\eta$
3	4	2
4	3	1

Table 3.2: Transformation properties of the states shown in Table 3.1. Here, it is assumed that the sector c refers to the original zero-mode basis, defined through the $L_y \to 0$ limit. Translating the state with T_x would transition the state into sector $T(c)$. After dragging a quasihole along the path a in Fig. 2.5 the state would transition from sector c into sector $F(c)$, which is dependent on the particle number parity η.

properties of the dressed domain-wall states, Eqs. (2.38) and (2.39). However, the relation of the shifted sector $T(c)$ to the original sector c is different in the present case. These relations can easily be read off the patterns in Table 3.1 and are summarized in Table 3.2. The remaining two transformation laws depend more critically on the value of β, and allow us to determine its value. We focus on the action of T_y on $|\psi_c(h_1,h_2)\rangle$ first. Since by duality, $|\psi_c(h_1,h_2)\rangle$ is a superposition of the states $\overline{|\psi_{c'}(h_1,h_2)\rangle}$, Eq. (3.7b) implies that

$$T_y\,|\psi_c(h_1,h_2)\rangle = |\psi_c(h_1+i\overline{\kappa},h_2+i\overline{\kappa})\rangle \times \text{ phase factor}\,. \tag{3.8}$$

Here, we have also used that T_y does not change the topological sector c when acting on $|a_1,a_2,c\rangle$, Eq. (2.39). The left-hand side of the last equation is easily evaluated using Eq. (2.39) inside the coherent state expression. For $c=1$ domain-wall states, e.g., one finds $\sum n_i = L^2/2-(a_1+a_2)/2$ for the sum in Eq. (2.39). With this one

finds that Eq. (3.8) indeed holds, provided that

$$\beta = 1/2\,, \tag{3.9}$$

as anticipated earlier in the preceding section. With this, one then finds

$$T_y|\psi_c(h_1,h_2)\rangle = e^{i\pi N}|\psi_c(h_1+i\overline{\kappa},h_2+i\overline{\kappa})\rangle \times \begin{cases} 1 & \text{for } c=1,2 \\ -1 & \text{for } c=3,4 \end{cases}\,, \tag{3.10a}$$

and similarly

$$\begin{aligned} T_x\overline{|\psi_c(h_1,h_2)\rangle} = e^{i\pi N}\overline{|\psi_c(h_1+i\overline{\kappa},h_2+i\overline{\kappa})\rangle} \\ \times \begin{cases} 1 & \text{for } c=1,2 \\ -1 & \text{for } c=3,4 \end{cases}\,. \end{aligned} \tag{3.10b}$$

The relations worked out above impose strong constraints on the transition matrices $u_{cc'}(h_1,h_2)$ defined in Eq. (2.33). We apply T_y to Eq. (2.33) using Eqs. (3.7b) (with $\beta = 1/2$) and (3.10a). On the resulting equation, we use Eq. (2.33) again, obtaining a relation between the coherent states $\overline{|\psi_c(h_1,h_2)\rangle}$:

$$\begin{aligned} \chi(c)e^{i\pi N}\sum_{c'} u_{cc'}(h_1+i\overline{\kappa},h_2+i\overline{\kappa})\overline{|\psi_{c'}(h_1+i\overline{\kappa},h_2+i\overline{\kappa})\rangle} = \\ \sum_{c'} u_{cc'}(h_1,h_2)e^{i\overline{\kappa}(h_{1x}+h_{2x})/2+i\delta}\overline{\left|\psi_{T(c')}(h_1+i\overline{\kappa},h_2+i\overline{\kappa})\right\rangle}\,, \end{aligned} \tag{3.11}$$

where $\chi(c) = 1$ ($\chi(c) = -1$) for $c = 1, 2$ ($c = 3, 4$). For the local dependence of functions $u_{cc'}(h_1, h_2)$ on coordinates, Eq. (2.34) can again be derived, using the same method as in Sec. 2.6, assuming again $|h_{1x} - h_{2y}| \gg 1$, $|h_{1y} - h_{2y}| \gg 1$. When plugged into Eq. (3.11), the dependence on quasihole coordinates drops out, except for the dependence on the quasihole configurations shown in Fig. 2.4, which is again denoted by $\sigma = \pm 1$. This gives the following equation for the coefficients $\xi^{\sigma}_{cc'}$, Eq. (2.34),

$$\chi(c) e^{i\pi N - i\delta} \xi^{\sigma}_{cc'} = \sum_{c''} \delta_{T(c'),c''} \xi^{\sigma}_{cc''} \ , \tag{3.12}$$

where the linear independence of the kets in Eq. (3.11) was used. For fixed c, σ, this can be looked at as an eigenvalue problem for the quantities $\xi^{\sigma}_{cc'}$, $c' = 1 \ldots 4$. Obviously, solutions only exist if $\pm e^{i\pi N - i\delta}$ is an eigenvalue of the matrix $\delta_{T(c'),c''}$ on the right-hand side. This is only the case for

$$\exp(2i\delta) = 1 \ . \tag{3.13}$$

The coherent states are invariant, up to an unimportant phase, under $\delta \to \delta + 2\pi$. Hence Eq. (3.13) narrows possible values of δ down to two inequivalent possibilities. Our result for the statistics, however, will be the same for $\delta = 0$ and $\delta = \pi$. We will thus keep δ as a parameter, but use Eq. (3.13) wherever convenient.

Since the eigenvalues of $\delta_{T(c'),c''}$ are doubly degenerate, Eq. (3.11) does not completely determine the coefficients $\xi^{\sigma}_{cc'}$. To this end, we must also consider the equation

that is obtained by acting with T_x on Eq. (2.33). In an analogous manner, this gives rise to the equation

$$\sum_{c''} \delta_{T(c),c''} \xi^{\sigma}_{c''c'} = \chi(c') e^{i\pi N - i\delta} \xi^{\sigma}_{cc'} \ , \tag{3.14}$$

which differs from Eq. (3.12) only by a replacement of the ξ matrix by its transpose.

To explicitly solve the constraints (3.12), (3.14), the following transformation is useful. We define new topological sector labels $(\mu\nu)$, $\mu, \nu = \pm 1$ via the following superposition of states carrying c labels:

$$\begin{aligned} |\psi_{\mu\nu}\rangle &= \frac{1}{\sqrt{2}} \left[|\psi_{c=2-\nu}\rangle + \mu e^{i\pi\eta - i\delta} |\psi_{c=3-\nu}\rangle \right] \\ \overline{|\psi_{\mu\nu}\rangle} &= \frac{1}{\sqrt{2}} \left[\overline{|\psi_{c=2-\mu}\rangle} + \nu e^{i\pi\eta - i\delta} \overline{|\psi_{c=3-\mu}\rangle} \right] \ , \end{aligned} \tag{3.15}$$

where the dependence on h_1 and h_2 has been suppressed. The significance of the states $|\psi_{\mu\nu}\rangle$ is that under translations in both T_x and T_y, they are now diagonal in the $\mu\nu$ label. Transition matrices $\tilde{u}_{\mu\nu,\mu'\nu'}$ and coefficients $\tilde{\xi}^{\sigma}_{\mu\nu,\mu'\nu'}$ can be defined analogous to Eqs. (2.33) and (2.34), and are related to the quantities $u_{cc'}$ and $\xi^{\sigma}_{cc'}$ via the transformation Eq. (3.15). In terms of the matrices $\tilde{\boldsymbol{\xi}}^{\sigma}$, the constraints (3.12), (3.14) read

$$\tilde{\boldsymbol{\xi}}^{\sigma} = \mathbf{D} \tilde{\boldsymbol{\xi}}^{\sigma} \mathbf{D} = \mathbf{D}' \tilde{\boldsymbol{\xi}}^{\sigma} \mathbf{D}' \ , \tag{3.16}$$

where $\mathbf{D} = \mathrm{diag}(1, 1, -1, -1)$ and $\mathbf{D}' = \mathrm{diag}(1, -1, 1, -1)$ are diagonal matrices. It is clear from Eq. (3.16) that only the diagonal elements of $\tilde{\boldsymbol{\xi}}^{\sigma}$ are unconstrained, whereas the remaining ones must vanish. The transition matrix is thus diagonal in the $\mu\nu$

basis. We write:

$$\tilde{\xi}^{\sigma}_{\mu\nu,\mu'\nu'} = \delta_{\mu,\mu'}\delta_{\nu,\nu'}\,\xi^{\sigma}_{\mu\nu}\ , \tag{3.17}$$

$$\begin{aligned} |\psi_{\mu\nu}(h_1,h_2)\rangle &= u_{\mu\nu}(h_1,h_2)\overline{|\psi_{\mu\nu}(h_1,h_2)\rangle} \\ &= \xi^{\sigma}_{\mu\nu}u(h_1,h_2)\overline{|\psi_{\mu\nu}(h_1,h_2)\rangle}\ , \end{aligned} \tag{3.18}$$

where $u(h_1,h_2)$ is as defined below Eq. (2.34), and no summation over indices is implied. We drop the tilde from now on, since there should be no confusion between the coefficient $\xi^{\sigma}_{\mu\nu}$ above and the coefficient $\xi^{\sigma}_{cc'}$ defined earlier. (Note again that $\mu\nu$ should be viewed as the single index of a diagonal matrix element). By unitarity of the transition matrixes, the $\xi^{\sigma}_{\mu\nu}$'s are pure phases.

The subscript $\mu\nu$ carries direct information about the properties of the states $|\psi_{\mu\nu}(h_1,h_2)\rangle$, $\overline{|\psi_{\mu\nu}(h_1,h_2)\rangle}$ under translation. From the definitions (3.15), it is easily verified directly that

$$\begin{aligned} &\langle\psi_{\mu\nu}(h_1,h_2)|\,T_y\,|\psi_{\mu\nu}(h_1,h_2)\rangle \approx \nu\, e^{-i\overline{\kappa}/2(h_{1y}+h_{2y})+i\pi\eta} \approx \overline{\langle\psi_{\mu\nu}(h_1,h_2)|}T_y\overline{|\psi_{\mu\nu}(h_1,h_2)\rangle}\ , \\ &\langle\psi_{\mu\nu}(h_1,h_2)|\,T_x\,|\psi_{\mu\nu}(h_1,h_2)\rangle \approx \mu\, e^{i\kappa/2(h_{1x}+h_{2x})+i\pi\eta} \approx \overline{\langle\psi_{\mu\nu}(h_1,h_2)|}T_x\overline{|\psi_{\mu\nu}(h_1,h_2)\rangle}\ . \end{aligned} \tag{3.19}$$

Since T_x, T_y are unitary operators, an expectation value of almost unit modulus implies that the states $|\psi_{\mu\nu}(h_1,h_2)\rangle$, $\overline{|\psi_{\mu\nu}(h_1,h_2)\rangle}$ are, to good approximation, eigenstates of these operators, with the approximate eigenvalue given by the expectation value. Even though the $|\psi_{\mu\nu}(h_1,h_2)\rangle$, $\overline{|\psi_{\mu\nu}(h_1,h_2)\rangle}$ describe states of localized quasiholes, this is possible since T_x and T_y translate by distances κ and $\overline{\kappa}$, respectively,

which are small compared to the size of the quasiholes (on the order of a magnetic length). To the extent that we can regard these states as T_x, T_y eigenstates, the different associated eigenvalues already imply that the transition functions must be diagonal in the $\mu\nu$ basis, Eq. (3.18). This argument has been used in Ref. [42]. Naively, however, in treating the states $|\psi_{\mu\nu}(h_1, h_2)\rangle$, $\overline{|\psi_{\mu\nu}(h_1, h_2)\rangle}$ as T_x, T_y eigenstates one neglects terms that scale as $1/\sqrt{L}$. The present treatment shows that no such approximation is necessary in deriving Eq. (3.18).

3.3 Constraints from global paths

The transition functions are thus far described by eight unknown phase parameters $\xi^{\sigma}_{\mu\nu}$, Eq. (3.18). Each of these parameters describes the relation between the pair of coherent states $|\psi_{\mu\nu}(h_1, h_2)\rangle$ and $\overline{|\psi_{\mu\nu}(h_1, h_2)\rangle}$ within various patches of the two-hole configuration space. As already discussed in Sec. 2.7, these patches may be connected through paths where one quasihole is dragged across a frame boundary, Fig. 2.5. This then leads to relations between the ξ parameters on different patches. In the case of the Laughlin state, all patches have been so connected, and there was only one independent parameter. It turns out that in the present case, the configuration space comes in two disjoint segments, which cannot be linked through paths as shown in Fig. 2.5, or any paths that maintain the conditions that the two quasiholes remain well separated in both x and y.

Equation (2.48) is straightforwardly generalized to the present case, following the

same reasoning:

$$|\psi_c(h_1,h_2)\rangle_f \doteq e^{ih_{2y}L_x/2+iL\delta/2}\,|\psi_{F(c)}(h_2-L_x,h_1)\rangle\,. \tag{3.20}$$

Here again, f denotes a frame that will allow us to extend h_{2x} beyond L_x, which has been assumed in the above equation. Equation (2.48) is just a special case of Eq. (3.20) for $L = 2N + 2$, $\delta = \pi$, as befits the $\nu = 1/2$ Laughlin 2-hole state. For the $\nu = 1$ Moore-Read state, however, one has $L = N + 1$ in the presence of two quasiholes. Also, the function $F(c)$ assigns to c the new sector that one enters when the second quasihole is dragged across the frame boundary along the path shown in Fig. 2.5. The value of $F(c)$ can easily be read off the patterns that define the 2-hole sectors in Table 3.1. Note however, that the patterns shown in the table correspond to the case of even particle number N, as the 1111 strings are even in length. As a new feature, $F(c)$ depends on the particle number parity as shown in Table 3.2.

Likewise, Eq. (2.49) may be generalized to

$$\overline{|\psi_{c'}(h_1,h_2)\rangle} = e^{-i\pi f_2(c')}\overline{|\psi_{c'}(h_1,h_2-L_x)\rangle}\,. \tag{3.21}$$

When analyzed in the $\mu\nu$ basis, Eq. (3.15), both the above equations imply that the sector labeled $\mu\nu$ transitions into the sector labeled $\mu,-\nu$ when the quasihole with coordinate h_2 is dragged along path a shown in Fig. 2.5. Specifically, Eq. (3.20)

implies

$$|\psi_{\mu\nu}(h_1,h_2)\rangle_f \doteq e^{i/2h_{2y}L_x+iL\delta/2}\,|\psi_{\mu,-\nu}(h_2-L_x,h_1)\rangle \times \begin{cases} 1 & \text{for } N \text{ even}, \nu=1, \\ \mu e^{i\delta+i\pi N} & \text{otherwise}, \end{cases} \tag{3.22}$$

while Eq. (3.21) gives

$$\overline{|\psi_{\mu\nu}(h_1,h_2)\rangle} = e^{-i\pi f_2(2-\mu)}\overline{|\psi_{\mu,-\nu}(h_1,h_2-L_x)\rangle}\,. \tag{3.23}$$

Using the same arguments given below Eq. (2.50), we may apply Eq. (3.18) to an f-frame state $|\psi_{\mu\nu}(h_1,h_2)\rangle_f$ with two quasiholes in the $\sigma=+$ configuration:

$$|\psi_{\mu\nu}(h_1,h_2)\rangle_f = \xi^+_{\mu\nu}u(h_1,h_2)\overline{|\psi_{\mu\nu}(h_1,h_2)\rangle}\,. \tag{3.24}$$

Here again $h_{2x} > L_x$, such that (h_1,h_2) can be taken to be the final configuration of the path a shown in Fig. 2.5. Plugging in Eqs. (3.22) and (3.23) gives a relation between the states $|\psi_{\mu,-\nu}(h_2-L_x,h_1)\rangle$ and $\overline{|\psi_{\mu,-\nu}(h_1,h_2-L_x)\rangle}$. On the other hand, these equations are, by definition, related via

$$|\psi_{\mu,-\nu}(h_2-L_x,h_1)\rangle_f = \xi^-_{\mu,-\nu}u(h_2-L_x,h_1)\overline{|\psi_{\mu,-\nu}(h_1,h_2-L_x)\rangle}\,. \tag{3.25}$$

Comparing these two relations, recalling $u(h_1,h_2) = e^{i/2(h_{1x}h_{1y}+h_{2x}h_{2y})}$, gives the fol-

lowing relation between $\xi^{+}_{\mu\nu}$ and $\xi^{-}_{\mu,-\nu}$.

$$\xi^{-}_{\mu,-\nu} = \xi^{+}_{\mu\nu}\, e^{-iL\delta/2 - i\pi f_2(2-\mu)} \times \begin{cases} 1 & \text{for } N \text{ even}, \nu = 1, \\ \mu e^{-i\delta + i\pi N} & \text{otherwise}, \end{cases} \tag{3.26}$$

We may also link patches of configuration space labeled by different μ, ν, and σ by dragging one of the quasiholes along path b shown in Fig. 2.5. This is obviously a dual version of the process just considered, and by following completely analogous reasoning, we find the following relation complementing Eq. (3.26):

$$\xi^{-}_{-\mu,\nu} = \xi^{+}_{\mu\nu}\, e^{-iL\delta/2 - i\pi f_2(2-\nu)} \times \begin{cases} 1 & \text{for } N \text{ even}, \mu = 1, \\ \nu e^{-i\delta + i\pi N} & \text{otherwise}, \end{cases} \tag{3.27}$$

The above two equations allow us to relate any of the parameters $\xi^{\sigma}_{\mu\nu}$ with the same value of $\sigma\mu\nu = \pm 1$. The transition functions have thus been reduced to two unknown phases, where only the relative phase will be of interest. Together with the shift parameter s, this phase will be determined in the final step by using the locality considerations of Sec. 2.5.

3.4 Pfaffian braiding

Given that the transition functions are diagonal in the $\mu\nu$ basis (Eq. (3.18)), the result of adiabatic exchange of the two quasiholes in the state $|\psi_{\mu\nu}(h_1, h_2)\rangle$ is necessarily diagonal in this basis as well. Even in a non-Abelian state, it is of course

possible to diagonalize any given generator of the braid group, which describes the (counter-clockwise) exchange of any two quasiholes. The phase picked up during the exchange will, however, depend on the index $\mu\nu$. Given the parameters $\xi^{\sigma}_{\mu\nu}$ defining the transition functions, we can calculate this phase in a manner that is completely analogous to that discussed in Sec. 2.8. In particular, the expressions (2.35) for the Berry connections carry over to the present case. The calculation is thus the same within each $\mu\nu$ sector. In particular, we recall that the statistical part of the Berry phase could be directly read off Eq. (2.59). Equation (2.63) can therefore be generalized to read

$$|\psi_{\mu\nu}(h_1, h_2)\rangle \to e^{i\Phi_{AB}} \frac{\xi^{+}_{\mu\nu}}{\xi^{-}_{\mu\nu}} |\psi_{\mu\nu}(h_1, h_2)\rangle \ . \tag{3.28}$$

We denote by $\gamma_{\mu\nu}$ the topological part of this phase:

$$e^{i\gamma_{\mu\nu}} = \frac{\xi^{+}_{\mu\nu}}{\xi^{-}_{\mu\nu}} \ . \tag{3.29}$$

By means of the relations (3.26) and (3.27) derived in the preceding section, it is clear that all phases $\gamma_{\mu\nu}$ can be related to γ_{++}. These relations depend both on the parameter s, as well as the particle number parity η. We must, therefore, distinguish the case of even ($\eta = 0$) and odd ($\eta = 1$) particle number N. In each case, using $L = N + 1$ we find that only even multiples of δ enter, which are zero modulo 2π. Hence the parameter δ does not enter the result, as anticipated earlier. For N even

(superscript e), we find:

$$\gamma^e_{+-} = \gamma^e_{-+} = -\gamma^e_{++} + 2\pi s, \quad \gamma^e_{--} = \gamma^e_{++} + \pi - 4\pi s \; . \tag{3.30}$$

Likewise, for N odd (superscript o), we find:

$$\gamma^o_{+-} = \gamma^o_{-+} = -\gamma^o_{++} + 2\pi s, \quad \gamma^o_{--} = \gamma^o_{++} - 4\pi s \; . \tag{3.31}$$

There are thus three remaining parameters in the theory, which can be taken to be the phases γ^e_{++} and γ^o_{++}, and the shift parameter s. It turns out that these parameters are highly constrained by locality considerations of the kind discussed in Sec. 2.5.

The adiabatic transport of the quasiholes is facilitated by local potentials that pin the quasiholes to a certain location that gradually changes with time. The matrix elements of these local potentials in the dressed domain-wall basis are subject to the general considerations for local operators made in Sec. 2.5. From these considerations it follows that the patterns contributing to the coherent states before and after the quasihole exchange can only change for orbitals whose x position (κn, where n is the orbital index) is within a magnetic length (plus the range of the local potentials) of the exchange path. Regions far to the left or right of the initial quasihole positions do not participate in the exchange process, i.e., orbitals in this region are far away from any point on the exchange path. According to the above, this implies that in this region, the pattern associated with dressed domain-wall states entering the coherent

state is unaffected during the exchange process.

Let us consider the implications of this for the case where the initial state is in the sector labeled $c = 3$, Table 3.1. Since for a state initially in the $c = 3$ sector, all patterns form one of the two possible 2020 strings far to the left and far to the right of the quasiholes, this must also be true after the exchange process, with the 2020 patterns unchanged. This, however, implies that the state is still in the $c = 3$ sector after the exchange. Identical observations can be made for the $c = 4$ sector.

It is easy to translate these statements into the $\mu\nu$ basis. In order for the exchange process to be diagonal in the sectors $c = 3$ and $c = 4$, the phases $\gamma_{\mu\nu}$ must be independent of μ when $\nu = -1$. This is true for both even and odd particle number. We thus have:

$$e^{i\gamma^e_{+-}} = e^{i\gamma^e_{--}} \ , \quad e^{i\gamma^o_{+-}} = e^{i\gamma^o_{--}} \ . \tag{3.32}$$

Note that in the case of even or odd particle number, the 1111 strings linking domain walls in the sectors $c = 3$, $c = 4$ are even/odd in length, respectively. The locality assumptions made in Sec. 2.5 further imply that the matrix elements of local operators cannot depend on the length of the 1111 string as long as the domain walls are well separated, since in this case such matrix elements do not depend on the separation of the quasiholes. In particular, this implies that the Berry connection is insensitive to particle number parity (which is solely encoded in the length of 1111 strings) for well separated quasiholes. This is manifest in equations (2.35) which hold independent of particle number. However, this reasoning breaks down for dressed domain-wall states

whose domain walls are not well separated. Referring to the original basis $|a_1, a_2, c\rangle$, this happens when two quasiholes are not well separated in x. In this regime, it is reasonable to expect that matrix elements between dressed domain-wall states do depend on whether the (short) 1111 strings of patterns entering the coherent states are even or odd in length. This is not manifest in our formulation, since in this regime, we always work with the dual $\overline{|a_1, a_2, c\rangle}$ basis. However, the transition functions that we calculated can be expected to "know" of these parity effects. Hence, we expect that the phases in Eq. (3.32), which describe braiding in the $c = 3, 4$ sectors, will depend on particle number parity.

The situation is quite the opposite for the sectors $c = 1$ and $c = 2$. Here, locality requires that the string pattern to the far left and right of the dressed domain-wall states forming the coherent states remain of the 1111 form before and after the exchange. This only forbids transitions from the sectors $c = 1, 2$ into the sectors $c = 3, 4$. This we already know from the fact that exchange processes are diagonal in the $\mu\nu$ basis, which followed from properties under translation. However, this does not forbid transitions between the sectors $c = 1$ and $c = 2$.

On the other hand, the 2020 strings forming the links between domain walls in these sectors, and which become short during the exchange process, carry no information about the particle number parity. This information remains hidden in the 1111 strings, which remain arbitrarily long during the exchange, in the limit of large L. We thus conclude that within the $c = 1, 2$ subspace, the braid matrix describing the result of the adiabatic exchange of the quasiholes is independent of particle number

parity. In the $\mu\nu$ basis, this leads to the following requirements:

$$e^{i\gamma^e_{++}} = e^{i\gamma^o_{-+}} \,, \quad e^{i\gamma^e_{-+}} = e^{i\gamma^o_{++}} \,. \tag{3.33}$$

Using Eqs. (3.30) and (3.31), the latter reduce to the same equation, $\gamma^e_{++}+\gamma^o_{++} = 2\pi s \mod 2\pi$. Equations (3.32) give two more, $2\gamma^e_{++} = 6\pi s - \pi \mod 2\pi$, and $2\gamma^o_{++} = 6\pi s \mod 2\pi$. The solutions to these equations are of the form

$$s = \frac{3}{8} - \frac{r}{4} \tag{3.34a}$$

$$\gamma^e_{++} = \gamma^o_{+-} = \gamma^o_{-+} = \gamma^o_{--} = \frac{5}{8}\pi - \frac{3}{4}\pi r \tag{3.34b}$$

$$\gamma^o_{++} = \gamma^e_{+-} = \gamma^e_{-+} = \gamma^e_{--} = \frac{1}{8}\pi + \frac{1}{4}\pi r \,, \tag{3.34c}$$

where $r \in \mathbb{Z}$. This amounts to eight inequivalent possible solutions for the statistics. To discuss the relation between these different solutions, we first generalize our result to the case of $2n$ quasiholes on the torus. This will show that up to unitary transformations (taking on the form of simple phase conventions), all solutions are related by overall Abelian phases. We will further obtain a useful pictorial representation of Pfaffian statistics, and relate it to more standard ones.

3.5 Representation of the braid group of $2n$ MR quasiholes

The locality arguments used above immediately allow one to generalize the results obtained thus far for two quasiholes to the general case of $2n$ quasiholes. Consider the result of exchanging two quasiholes in a topological sector as defined by taking in the $L_y \to 0$ limit, e.g. Fig. 3.1. Such states are the analogue of the states $|\psi_c(h_1, h_2)\rangle$ defined above, generalized to $2n$ quasiholes. Locality then implies that the result of exchanging two quasiholes can at most affect the string linking the associated domain walls in the sector label. Furthermore, the presence of other quasiholes, which are assumed to be well away along the x axis, cannot affect the result of the exchange. One can therefore infer the result of exchanging any two quasiholes in a state of $2n$ quasiholes from the results established above for states of two quasiholes.

These results can be generally stated as follows:

- If the two quasiholes to be exchanged are linked by a 1111 string in the topological sector label, the state merely picks up a phase as a result of the exchange. This phase is given by Eq. (3.34b) when the linking 1111 string is odd in length (Fig. 3.1b), and by Eq. (3.34c) when the linking 1111 string is even in length.

- If the two quasiholes are linked by a 2020 string, then upon exchange, the state will remain in the same topological sector with an amplitude $e^{i\theta}/\sqrt{2}$, where $\theta = \pi(1/8 + r/4 + (-1)^r/4)$. It will transition with an amplitude $(-1)^r i e^{i\theta}/\sqrt{2}$

into the sector with the linking 2020 string shifted.[3]

These rules are represented graphically in Fig. 3.1. To make connection with the standard way to represent these statistics [27, 32, 33, 35], we introduce a Majorana fermion degree of freedom η_i associated with the i-th domain wall in the string patterns associated with our topological sectors. Let the pair η_{2j}, η_{2j+1} be associated with the left and right domain wall of a 1111 string. We then introduce fermion operators $c_j = (\eta_{2j} + i\eta_{2j+1})/2$. Each c_j is now associated to a 1111 string. The topological Hilbert space can be constructed by acting with the operators $c_j^\dagger$ on the vacuum of the c_j operators, where states have the j-th fermion occupied if the j-th 1111 string in the associated topological sector label is odd in length, and unoccupied otherwise. It is easy to check that according to the above rules, the exchange of the i-th and $(i+1)$-th quasihole is then represented by the operator

$$e^{i\theta} \exp\left((-1)^r \frac{\pi}{4} \eta_i \eta_{i+1}\right) \tag{3.35}$$

within this fermionic space, as expected for the Pfaffian state. The sign of $\eta_i\eta_{i+1}$ in the above can be absorbed by a unitary transformation, facilitated by the operator $\prod_j \eta_{2j}$. With this, the non-Abelian part of the statistics is thus determined unambiguously by the present formalism, whereas for the overall Abelian phase $e^{i\theta}$, there are eight possible values. In the present case, these are all the values that are consistent with the

[3]Here, an additional phase factor $e^{i\delta}$ that was present in Eq. (3.15), which would arise in the off-diagonal matrix element with the conventions of the preceding sections, has been absorbed into a sign convention for the adiabatically continued domain-wall state basis.

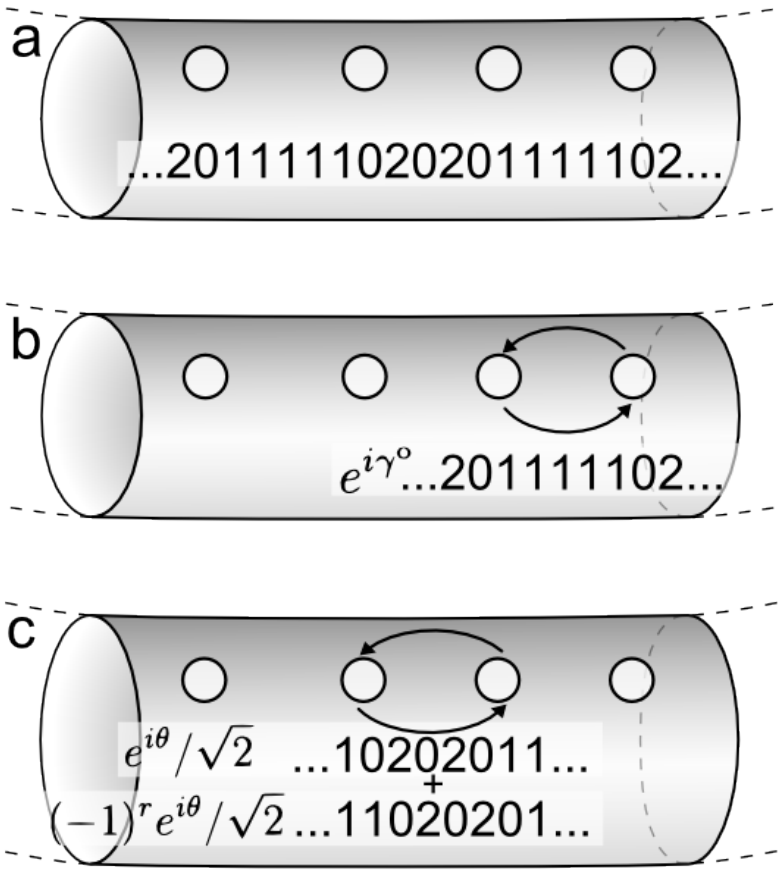

Figure 3.1: Graphical representation of the result of exchanging two Pfaffian quasiholes for two representative pairs. a) A possible state in which four quasiholes could be prepared, labeled by its associated thin torus pattern. The state shown could be a four-quasihole state, in which the 20 strings at either end would continue around the torus, or could be a $2n$-quasihole state for $n > 2$, in which the ellipses mask additional domain walls in the thin torus pattern. The results of braiding any pair of quasiholes will be the same in either case. In the following we show only the section of the pattern relevant to the exchange; locality implies that only the segment of the pattern within a magnetic length of the exchange path may be affected by the exchange and the rest remains fixed. b) Upon exchange of the indicated quasiholes, the state picks up the phase γ^o, given by Eq. (3.34b). Had the 11 string separating the quasiholes been even in length, the phase would have been γ^e, Eq. (3.34c). In either case the thin torus pattern, and thus the topological sector of the state, remains unchanged, which is shown. c) When the two indicated quasiholes are exchanged the state remains in the same topological sector or transitions into a sector with the linking 20 string shifted. The amplitudes for these two possibilities are shown next to the thin torus patterns for the sectors, where $\theta = \pi(1/8 + r/4 + (-1)^r/4)$. r is an integer labeling the eight possible values for the overall Abelian phase, where $r = 0$ reproduces the representation given by conformal block monodromies.

$SU(2)_2$ fusion rules [75, 76]. For $r = 0$ one obtains the value that agrees [27] with the transformation properties of the conformal blocks from which the Pfaffian many-body wave functions are constructed [23]. The approach discussed here is thus consistent with the CFT approach. For the Pfaffian case, the CFT approach was recently backed more rigorously through plasma analogy methods [30]. Similar results can also be obtained from the $p + ip$-wave superconductor analogy [32, 33, 31], although the present approach yields more information about the overall Abelian phase.

Chapter 4

The $k = 3$ Read-Rezayi State

We have seen that the method developed above is sufficiently general to obtain the statistics of Abelian FQH states and, with some adaptations, the non-Abelian Moore-Read state. Here we will show that the techniques developed in the preceding sections are indeed general enough to allow us to obtain, essentially without modification, the statistics of a more complicated non-Abelian state as well. We will demonstrate this for the $k = 3$ Read-Rezayi (RR) state [58].

We focus on the bosonic "root" (highest filling factor, or $M = 0$) state of the $k = 3$ sequence. This state has $\nu = 3/2$ and a torus degeneracy of 4. In taking the thin torus limit, the ground states are adiabatically evolved into the patterns $0303\ldots$, $3030\ldots$, $1212\ldots$ and $2121\ldots$ [51, 77]. Elementary excitations evolve into charge 1/2 domain walls between the 3030 and 2121 ground-state patterns, or into charge 1/2 domain walls between 2121 and 1212 (see Table 4.2). Periodic boundary

This chapter originally appeared in Ref. [7].

conditions require that the former type of domain wall must come in pairs, but allow the latter type to exist singly.

In the examples above, we found that to work out the braid group for n quasiholes with general n, one needs to consider only braiding for pairs of quasiholes associated with all possible pairs of domain walls, as given by all possible combinations of three ground state patterns. Locality then implies that all the other ground state patterns appearing in the topological sector label will not affect the result of braiding. To this end, we will solve for the reduced braid matrix in the simple cases of $n = 2$ (Sec. 4.2 and App. A) and $n = 3$ (Sec. 4.3 and App. B). Together, these results can be used to construct braid matrices for n-quasihole states, since these cases exhaust all possible sequences of three ground state patterns separated by domain walls. However, the solution of the $n = 2$ and $n = 3$ cases can be simplified if we first consider translational properties of states with general n.

4.1 RR states with n quasiholes

In the Moore-Read case, we introduced sector labels (μ, ν) that encoded the properties of states under translations. The conventions there made use of the fact that at filling factor $\nu = 1$, T_x and T_y commute. For the $k = 3$ RR state at $\nu = 3/2$, we have to proceed somewhat differently in exploiting translational properties.

To this end, we denote a thin torus state with n domain walls by $|a_1, \ldots, a_n; c, \alpha)$, and the adiabatically evolved state by $|a_1, \ldots, a_n; c, \alpha\rangle$. We introduce two labels c,

α to denote topological sectors, where α labels classes of sectors that are not related by translation (see Tables 4.1, 4.2), and $c = 0, 1$ labels the two members of each class that are related by translation. The meaning of c is thus very much the same as in our discussion of Laughlin states. The utility of this labeling will become apparent shortly; the dependence of various quantities on the c label will be constrained by translational symmetries, and c is conserved during braiding, in much the same way as for the Laughlin states. In contrast, the interesting non-Abelian behavior will be associated with the α label.

We use the same mutually dual coherent state expressions as before (see Eqns. (2.26) and (3.2)),

$$|\psi_{c,\alpha}(\{h\})\rangle = \mathcal{N} \sum_{a_1<\ldots<a_n} \prod_{j=1}^{n} \phi_{\alpha,j}(h_j, \kappa a_j)\, |a_1, \ldots, a_n; c, \alpha\rangle \tag{4.1}$$

$$\overline{|\psi_{c,\alpha}(\{h\})\rangle} = \mathcal{N}' \sum_{a_1<\ldots<a_n} \prod_{j=1}^{n} \overline{\phi}_{\alpha,j}(h_j, \overline{\kappa} a_j) \overline{|a_1, \ldots, a_n; c, \alpha\rangle} \tag{4.2}$$

where the first is defined for n quasiholes that are well separated along the x axis, and the second for n quasiholes that are well separated along the y axis. We have used $\{h\}$ for the set of quasihole positions $h_1, \ldots, h_n$. For the same reasons that we discussed in Sec. 3 originally for the Pfaffian, we will assume the generic Gaussian form of $\phi_{\alpha,j}(h, x)$ given in Eq. (3.3):

$$\phi_{\alpha,j}(h_j, x) = \exp\left[i\left(h_{jy} + \delta(\alpha, j)/\kappa\right) x/2 - \gamma(h_{jx} - x)^2\right] \tag{4.3}$$

and

$$\overline{\phi}_{\alpha,j}(h_j, y) = \phi_{\alpha,j}(-ih_j, y)|_{\kappa\to\overline{\kappa}} = \exp\left[-i(h_{jx} + \delta(\alpha, j)/\overline{\kappa})y/2 - \gamma(h_{jy} - y)^2\right] \ . \quad (4.4)$$

In the above, we have already set $\beta = 1/2$, which follows in exactly the same way as for the Pfaffian. We have written ϕ as a function of the sector α, to allow for the possibility that the momentum shift δ may take on different values for quasiholes associated with different types of domain walls. However, ϕ is independent of c since the type of the j-th domain wall is invariant under translation.

Again, the two bases (4.1) and (4.2) are related to each other by a transition matrix. In general, the elements of this matrix depend on both c and α.

$$|\psi_{c,\alpha}(\{h\})\rangle = \sum_{c',\alpha'} u^{\sigma}_{c,c',\alpha,\alpha'}(\{h\})\overline{|\psi_{c',\alpha'}(\{h\})\rangle} \quad (4.5)$$

In complete analogy with Eq. (2.34), we can derive the local dependence of the transition matrix within each of the regions labeled by σ, which are components of the quasihole configuration space with quasihole coordinates well separated in both x and y (cf. Fig. 2.4 as well as Fig. 4.1 below),

$$u^{\sigma}_{c,c',\alpha,\alpha'}(\{h\}) = \xi^{\sigma}_{c,c',\alpha,\alpha'}\, u(\{h\}), \quad (4.6)$$

again with $u(\{h\}) = e^{i/2\sum_j h_{jx}h_{jy}}$. For $n = 2$, there are 72 of these parameters $\xi^{\sigma}_{c,c',\alpha,\alpha'}$: we distinguish two configurations σ (Fig. 2.4), and for each there is a 6×6 matrix in

the sector labels.

We first state the translational properties of the n–domain-wall states, which are the same as in Eqs. (2.38) and (2.39), since α is a spectator under translations. We now adopt a natural definition for the c labels. Recall that the action of T_y is given as follows,

$$T_y \left| a_1, \ldots, a_n; c, \alpha \right\rangle = \exp\left(-\frac{2\pi i}{L} \sum_j n_j \right) \left| a_1, \ldots, a_n; c, \alpha \right\rangle \tag{4.7}$$

where the n_j are the orbitals occupied in the pattern labeling the state. We find that the sum over the n_j takes on the following form,

$$\sum_j n_j = \frac{1}{2} L \left(\nu L - c \right) - \frac{1}{2} \sum_j a_j \mod L \tag{4.8}$$

where $c = 0, 1$, and the domain-wall positions are defined via $a_i = 2n_i + f_i(c, \alpha)$ as before, with the orbital position $2n_i$ defined in relation to the domain wall as shown in Table 4.2. Equation (4.8) then defines c modulo 2, and α labels the three "supersectors" formed by the translational pairs of states.

The translational properties of the n–domain-wall states are

$$\begin{aligned} T_x \left|a_1, \ldots, a_n; c, \alpha\right\rangle &= \left|a_1 + 1, \ldots, a_n + 1; 1 - c, \alpha\right\rangle \\ T_x \overline{\left|a_1, \ldots, a_n; c, \alpha\right\rangle} &= e^{-i\pi\lambda + i\pi c + \kappa\overline{\kappa}/2 \sum_j a_j} \overline{\left|a_1, \ldots, a_n; c, \alpha\right\rangle} \end{aligned} \tag{4.9}$$

$$\begin{aligned} T_y \left|a_1, \ldots, a_n; c, \alpha\right\rangle &= e^{i\pi\lambda - i\pi c - \kappa\overline{\kappa}/2 \sum_j a_j} \left|a_1, \ldots, a_n; c, \alpha\right\rangle \\ T_y \overline{\left|a_1, \ldots, a_n; c, \alpha\right\rangle} &= \overline{\left|a_1 + 1, \ldots, a_n + 1; 1 - c, \alpha\right\rangle} \end{aligned} \tag{4.10}$$

where again we write $\lambda = \nu L$, this time with $\nu = 3/2$.

As in the preceding cases, the translational properties of the coherent states follow directly from Eqs. (4.9) and (4.10):

$$\begin{aligned} T_x \left|\psi_{c,\alpha}(\{h\})\right\rangle &= e^{-i\kappa/2 \sum_j h_{jy} - i/2 \sum_j \delta(\alpha, j)} \left|\psi_{1-c,\alpha}(\{h + \kappa\})\right\rangle \\ T_x \overline{\left|\psi_{c,\alpha}(\{h\})\right\rangle} &= e^{i\pi\lambda - i\pi c} \overline{\left|\psi_{c,\alpha}(\{h + \kappa\})\right\rangle} \end{aligned} \tag{4.11}$$

$$\begin{aligned} T_y \left|\psi_{c,\alpha}(\{h\})\right\rangle &= e^{-i\pi\lambda + i\pi c} \left|\psi_{c,\alpha}(\{h + i\overline{\kappa}\})\right\rangle \\ T_y \overline{\left|\psi_{c,\alpha}(\{h\})\right\rangle} &= e^{i\overline{\kappa}/2 \sum_j h_{jx} + i/2 \sum_j \delta(\alpha, j)} \overline{\left|\psi_{1-c,\alpha}(\{h + i\overline{\kappa}\})\right\rangle}, \end{aligned} \tag{4.12}$$

where we have used the notation $\{h + \kappa\} = h_1 + \kappa, \ldots, h_n + \kappa$, and similarly used $\{h + i\overline{\kappa}\}$. We can use these translational properties to completely determine the dependence of the transition matrices on c. To make this decoupling more explicit,

we introduce two-component objects, denoted by a Ψ:

$$|\Psi_\alpha(\{h\})\rangle = \begin{pmatrix} |\psi_{0,\alpha}(\{h\})\rangle \\ e^{i/2\sum_j \delta(\alpha,j)}\,|\psi_{1,\alpha}(\{h\})\rangle \end{pmatrix}$$
$$\overline{|\Psi_\alpha(\{h\})\rangle} = \begin{pmatrix} \overline{|\psi_{0,\alpha}(\{h\})\rangle} \\ e^{i/2\sum_j \delta(\alpha,j)}\overline{|\psi_{1,\alpha}(\{h\})\rangle} \end{pmatrix}, \tag{4.13}$$

where the phase splitting between the $c = 0$ and $c = 1$ states has been introduced with foresight to keep later phases in check. Correspondingly, we may view the full transition matrix as a "supermatrix" Ξ^σ, i.e., an $\alpha_{\max} \times \alpha_{\max}$ matrix, the elements of which are each 2×2 matrices denoted $\Xi^\sigma_{\alpha,\alpha'}$. So we write the equation between the original and dual bases as

$$|\Psi_\alpha(\{h\})\rangle = \sum_{\alpha'} u(\{h\})\Xi^\sigma_{\alpha,\alpha'}\overline{|\Psi_{\alpha'}(\{h\})\rangle}\,. \tag{4.14}$$

Note the similarity of Eq. (4.14) to the Laughlin transition matrix Eq. (2.43), to which Eq. (4.14) reduces for $\alpha_{\max} = 1$.

We rewrite Eqs. (4.11) and (4.12) in terms of the two-component basis.

$$
\begin{aligned}
T_x \left|\Psi_\alpha(\{h\})\right\rangle &= e^{-i\kappa/2\sum_j h_{jy}} \begin{pmatrix} 0 & e^{-i\sum_j \delta(\alpha,j)} \\ 1 & 0 \end{pmatrix} \left|\Psi_\alpha(\{h+\kappa\})\right\rangle \\
T_x \overline{\left|\Psi_\alpha(\{h\})\right\rangle} &= e^{i\pi\lambda} \begin{pmatrix} 1 & 0 \\ 0 & -1 \end{pmatrix} \overline{\left|\Psi_\alpha(\{h+\kappa\})\right\rangle} \,,
\end{aligned}
\tag{4.15}
$$

$$
\begin{aligned}
T_y \left|\Psi_\alpha(\{h\})\right\rangle &= e^{-i\pi\lambda} \begin{pmatrix} 1 & 0 \\ 0 & -1 \end{pmatrix} \left|\Psi_\alpha(\{h+i\overline{\kappa}\})\right\rangle \\
T_y \overline{\left|\Psi_\alpha(\{h\})\right\rangle} &= e^{i\overline{\kappa}/2\sum_j h_{jx}} \begin{pmatrix} 0 & 1 \\ e^{i\sum_j \delta(\alpha,j)} & 0 \end{pmatrix} \overline{\left|\Psi_\alpha(\{h+i\overline{\kappa}\})\right\rangle} \,.
\end{aligned}
\tag{4.16}
$$

As before, (cf. Eqs. (3.12), (3.14)), when applied to Eq. (4.14), Eqs. (4.15) and (4.16) each give a consistency equation that must be satisfied by every $\Xi^\sigma_{\alpha,\alpha'}$:

$$
\Xi^\sigma_{\alpha,\alpha'} = e^{i\pi\lambda} \begin{pmatrix} 0 & 1 \\ e^{i\sum_j \delta(\alpha,j)} & 0 \end{pmatrix} \Xi^\sigma_{\alpha,\alpha'} \begin{pmatrix} 1 & 0 \\ 0 & -1 \end{pmatrix}
\tag{4.17}
$$

$$
\Xi^\sigma_{\alpha,\alpha'} = e^{i\pi\lambda} \begin{pmatrix} 1 & 0 \\ 0 & -1 \end{pmatrix} \Xi^\sigma_{\alpha,\alpha'} \begin{pmatrix} 0 & 1 \\ e^{i\sum_j \delta(\alpha,j)} & 0 \end{pmatrix},
\tag{4.18}
$$

which imply

$$
\Xi^\sigma_{\alpha,\alpha'} = \frac{\xi^\sigma_{\alpha,\alpha'}}{\sqrt{2}} \begin{pmatrix} 1 & e^{i\pi\lambda} \\ e^{-i\pi\lambda} & -1 \end{pmatrix},
\tag{4.19}
$$

together with the constraint

$$\exp\left(2\pi i\lambda + i\sum_j \delta(\alpha, j)\right) = 1\ . \tag{4.20}$$

In the above, $\xi^{\sigma}_{\alpha,\alpha'}$ is an overall coefficient, and $\sqrt{2}$ is a normalization factor.

The phase choice we made in Eq. (4.13) has allowed us to decouple the α and c indices within the transition function. We can write the matrix Ξ^{σ} defining the transition function Eq. (4.14) as

$$\Xi^{\sigma} = \xi^{\sigma} \otimes M\ , \tag{4.21}$$

where ξ^{σ} is the $\alpha_{\max} \times \alpha_{\max}$ matrix of coefficients $\xi^{\sigma}_{\alpha,\alpha'}$ and M is the 2×2 matrix

$$M = \frac{1}{\sqrt{2}} \begin{pmatrix} 1 & e^{-i\pi\lambda} \\ e^{i\pi\lambda} & -1 \end{pmatrix} \tag{4.22}$$

The α dependence of Ξ^{σ} is completely contained in the corresponding coefficient matrix ξ^{σ}, and the c dependence is completely contained in the M matrix.

If we consider the translational properties of the states in the case of a single quasihole, we can constrain some of the $\delta(\alpha, j)$ parameters appearing above. For a single quasihole on a torus, the only topological sectors respecting periodic boundary conditions are those with domain walls between 2121 patterns, as shown in Table 4.1. There are two such sectors, related by translation, so for a single quasihole $\alpha_{\max} = 1$.

Sector c, α	Thin torus pattern	$f_1(c, \alpha)$
0,1	21212121121212121	1/2
1,1	12121211212121212	−1/2

Table 4.1: Thin torus patterns for a single–domain-wall $k = 3$ Read-Rezayi state, and the offset functions of the associated domain walls. The latter are fully determined by inversion symmetry of the state. The orbital positions, $2n_i$, are underlined. Since the sectors are all related by translation, α takes on a single value.

There is then only a single $\delta(\alpha, j)$ parameter, which we call d. When we consider Eq. (4.20) and note that in this case $\lambda = \nu L = 3/2((2N + 1)/3)$ is half-odd integral, we find $d = \pi$.

In general, the $\delta(\alpha, j)$s are each associated with a certain type of domain wall, so by fixing d in the single-quasihole case we also fix any $\delta(\alpha, j)$ associated with a 2121¦1212-type domain wall in an n-quasihole state. We can constrain the other $\delta(\alpha, j)$s to be either 0 or π by considering Eq. (4.20) in the case $n = 2$. For two quasiholes there are only two independent $\delta(\alpha, j)$ parameters: $\delta(3, j)$, which is associated with 2121¦1212-type domain walls and is thus known to be π from the one-quasihole argument; and $\delta(1, j)$ and $\delta(2, j)$, which are associated variously with domain walls between 1212 and 0303 strings, and which must be equal by the argument in Footnote 2, page 66. For $n = 2$, we have $\lambda = \nu L = 3/2((2N + 2)/3)$, which is an integer, and Eq. (4.20) reduces to $\exp[i \sum_j \delta(\alpha, j)] = 1$. This is already satisfied for $\delta(3, j) = \pi$, and can be satisfied for $\alpha = 2, 3$ only if $\delta(1, j) = \delta(2, j) = 0, \pi$.

In the end, we want to find explicit expressions for the elements of the transition matrices Ξ^σ, which we have reduced to the problem of finding the elements of the ξ^σ coefficient matrices. This will be our task in the following sections.

α	Thin torus pattern	$f_1(\alpha)$	$f_2(\alpha)$	$F(\alpha)$
1	3030303**0**$\underline{\mathbf{2}}$12121**2**$\underline{\mathbf{0}}$30303030	s	$-s$	2
2	1212121**2**$\underline{\mathbf{0}}$30303**0**$\underline{\mathbf{2}}$12121212	$1-s$	$1+s$	1
3	121212**1**$\underline{\mathbf{1}}$2121212$\underline{\mathbf{1}}$12121212	$-1/2$	$1/2$	3

Table 4.2: $c = 0$ thin torus patterns for a two–domain-wall $k = 3$ Read-Rezayi state, and the offset functions of the associated domain walls. The orbital positions, $2n_i$, are underlined. Patterns for $c = 1$ can be obtained by shifting each occupancy number one orbital to the right, and $c = 1$ offset functions by adding or subtracting 1 to each offset function above, whichever is more convenient.

4.2 RR states of $n = 2$ quasiholes

The thin torus patterns for two-quasihole states with $c = 0$ are given in Table 4.2. To find the statistics of these quasiholes we must constrain the transition matrices Ξ^+ and Ξ^-. Both Ξ^σs have nine complex unknowns, the entries of the ξ^σ matrices. To constrain these we will move the quasiholes around global paths, which we defined in Sec. 2.7. We will then make further use of the mirror symmetry operation, which has thus far only been discussed in Sec. 2.1 and very briefly in Sec. 3.2. As in the Moore-Read case, we gain further constraints by imposing locality and unitarity. In the general solution to these equations some unknown parameters still remain. We will be able to constrain the latter by subsequently studying the case of three quasiholes in Sec. 4.3.

4.2.1 Constraints from global paths

As discussed in sections 2.7 and 3.2, the transition matrices for different configurations can be connected by dragging the quasiholes through the global paths in Fig. 2.5. We first consider two quasiholes in the $\sigma = +$ configuration, and imagine the right

quasihole moving around the x direction of the torus along the path a in Fig. 2.5. Using the reasoning of Sec. 3.3 we find the following effects on the coherent states:

$$\begin{aligned} |\psi_{c,\alpha}(h_1,h_2)\rangle_f &\doteq e^{iL_x h_{2y}/2 + iL\delta(\alpha,2)/2}\,|\psi_{1-c,F(\alpha)}(h_2-L_x,h_1)\rangle \\ \overline{|\psi_{c,\alpha}(h_1,h_2)\rangle} &= e^{-i\pi f_2(c,\alpha)}\overline{|\psi_{c,\alpha}(h_1,h_2-L_x)\rangle}\,. \end{aligned} \tag{4.23}$$

Moving the quasihole along this path changes the sector label α for the original basis into $F(\alpha)$, the values of which can be read off the patterns and are summarized in Table 4.2.

To find a constraint on the ξ^σs, we write Eq. (4.23) in the two-component basis.

$$\begin{aligned} |\Psi_\alpha(h_1,h_2)\rangle_f &\doteq e^{iL_x h_{2y}/2 + iL\delta(\alpha,2)/2} \begin{pmatrix} 0 & e^{-i/2\sum_j \delta(\alpha,j)} \\ e^{i/2\sum_j \delta(\alpha,j)} & 0 \end{pmatrix} \big|\Psi_{F(\alpha)}(h_2-L_x,h_1)\big\rangle \\ \overline{|\Psi_\alpha(h_1,h_2)\rangle} &= e^{-i\pi f_2(\alpha)} \begin{pmatrix} 1 & 0 \\ 0 & -1 \end{pmatrix} \overline{|\Psi_\alpha(h_1,h_2-L_x)\rangle}\,, \end{aligned} \tag{4.24}$$

where we have used that $f_j(\alpha) \equiv f_j(0,\alpha) = f_j(c,\alpha) - c \bmod 2$. Applying Eq. (4.24)

to Eq. (4.14) gives

$$\begin{aligned}\left|\Psi_{F(\alpha)}(h_2 - L_x, h_1)\right\rangle = &\sum_{\alpha'} u(h_2 - L_x, h_1) e^{-iL\delta(\alpha,2)/2 - i/2\sum_j \delta(\alpha,j)} \\ &\times \begin{pmatrix} 0 & 1 \\ e^{i\sum_j \delta(\alpha,j)} & 0 \end{pmatrix} \Xi^{+}_{\alpha,\alpha'} \begin{pmatrix} 1 & 0 \\ 0 & -1 \end{pmatrix} \\ &\times e^{-i\pi f_2(\alpha')} \overline{\left|\Psi_\alpha(h_1, h_2 - L_x)\right\rangle}\end{aligned} \tag{4.25}$$

We can simplify Eq. (4.25) using Eq. (4.17).

$$\begin{aligned}\left|\Psi_{F(\alpha)}(h_2 - L_x, h_1)\right\rangle = &\sum_{\alpha'} u(h_2 - L_x, h_1) e^{-i\pi\lambda - iL\delta(\alpha,2)/2 - i/2\sum_j \delta(\alpha,j)} \\ &\times \Xi^{+}_{\alpha,\alpha'} e^{-i\pi f_2(\alpha')} \overline{\left|\Psi_\alpha(h_1, h_2 - L_x)\right\rangle}\end{aligned} \tag{4.26}$$

We want to write this as an equation between ξ^- and ξ^+, which we can do by noting the equivalence between Eq. (4.26) as written and Eq. (4.14) evaluated at quasihole positions $(h_2 - L_x, h_1)$. To make this equivalence manifest we can write the action of the function F in matrix form as:

$$(B)_{\alpha,\alpha'} = \delta_{\alpha,F(\alpha')} \tag{4.27}$$

or

$$B = \begin{pmatrix} 0 & 1 & 0 \\ 1 & 0 & 0 \\ 0 & 0 & 1 \end{pmatrix} . \tag{4.28}$$

Since the transition matrix in Eq. (4.14) evaluated at positions $(h_2 - L_x, h_1)$ involves Ξ^-, and the transition matrix in Eq. (4.26) is a product involving Ξ^+, the equivalence of Eqs. (4.14) and (4.26) implies:

$$\xi^- = B^{-1}\mathrm{diag}\left[e^{-i\pi\lambda - iL\delta(\alpha,2)/2 - i/2\sum_j \delta(\alpha,j)}\right]\xi^+\mathrm{diag}\left[e^{-i\pi f_2(\alpha)}\right] , \tag{4.29}$$

where we canceled the matrix M common to both Ξ^σs, and the argument of diag[...] specifies the α-th diagonal entry of a diagonal matrix. If we use the values of $f_2(\alpha)$ from Table 4.2, Eq. (4.29) becomes

$$\xi^- = \begin{pmatrix} 0 & \Delta & 0 \\ \Delta & 0 & 0 \\ 0 & 0 & 1 \end{pmatrix} \xi^+ \begin{pmatrix} p & 0 & 0 \\ 0 & p^{-1} & 0 \\ 0 & 0 & -1 \end{pmatrix} e^{-i\pi/2} . \tag{4.30}$$

We have defined two phases: $p = -\exp\left[i\pi(s + 1/2)\right]$ and $\Delta = \exp\left[i(L/2 + 1)(\pi - \delta)\right]$. Note that for two quasiholes L is even and $\Delta^2 = 1$.

We can perform the same process in the y direction and drag the quasihole around the global path marked b in Fig. 2.5. After an argument similar to that above we find

another equation between ξ^- and ξ^+, which we invert to yield,

$$\xi^+ = \begin{pmatrix} p^{-1} & 0 & 0 \\ 0 & p & 0 \\ 0 & 0 & -1 \end{pmatrix} \xi^- \begin{pmatrix} 0 & \Delta & 0 \\ \Delta & 0 & 0 \\ 0 & 0 & 1 \end{pmatrix} e^{i\pi/2} \tag{4.31}$$

Combining Eqs. (4.30) and (4.31) gives us a nontrivial consistency relation for ξ^+.

$$\xi^+ = \begin{pmatrix} 0 & \Delta p^{-1} & 0 \\ \Delta p & 0 & 0 \\ 0 & 0 & -1 \end{pmatrix} \xi^+ \begin{pmatrix} 0 & \Delta p & 0 \\ \Delta p^{-1} & 0 & 0 \\ 0 & 0 & -1 \end{pmatrix} \tag{4.32}$$

Equation (4.32) gives us several equations between the matrix elements of ξ^+, the coefficients $\xi^+_{\alpha,\alpha'}$. Equation (4.30) reduces the number of unknown $\xi^\sigma_{\alpha,\alpha'}$s from eighteen to nine. The consistency relationship Eq. (4.32) further reduces the number of unknown elements from nine down to five. A particular choice for the five independent $\xi^+_{\alpha,\alpha'}$s is the following:

$$\xi^+ = \begin{pmatrix} \xi_{11} & \xi_{12} & \xi_{13} \\ \xi_{12} & p^2\xi_{11} & -\Delta p\xi_{13} \\ \xi_{31} & -\Delta p\xi_{31} & \xi_{33} \end{pmatrix} \tag{4.33}$$

Note that any time the configuration index σ is omitted as in the above equation, we take it to be $\sigma = +$.

4.2.2 Constraints from mirror symmetry

We now make use of the antilinear symmetry operator τ_x defined in Sec. 2.1, i.e., the combination of time reversal and mirror symmetry. Applying τ_x will exchange the x positions of the quasiholes across the y axis. This operation changes the configuration σ, which will allow us to derive another equation between ξ^+ and ξ^-. First, we describe how this symmetry acts on an n-quasihole state.

From the definition Eq. (2.8), the effect of τ_x on bare LL product states is clear: it reflects the original basis states across the y axis, and it has no effect on the dual states. For bare product states with domain walls, the domain-wall positions will be similarly reflected. τ_x commutes with the adiabatic evolution operators (as constructed, e.g., in Ref. [40]) that define the delocalized quasihole states, thus its action on those states is:

$$\tau_x \left|a_1, \ldots, a_n; c, \alpha\right\rangle = \left|L - a_n, \ldots, L - a_1; c, F_{\tau_x}(\alpha)\right\rangle \tag{4.34a}$$

$$\tau_x \overline{\left|a_1, \ldots, a_n; c, \alpha\right\rangle} = \overline{\left|a_1, \ldots, a_n; c, \alpha\right\rangle}\,. \tag{4.34b}$$

We write that the position of the j-th dual-basis quasihole a_j goes to $L - a_j$ in Eq. (4.34a) so as to stay within the default frame. Also note that in general τ_x might or might not change α, and we describe this change by some function F_{τ_x}, the values of which can be found from the patterns. It turns out that for the case of two quasiholes, $F_{\tau_x}(\alpha) = \alpha$. Later when we analyze the case of three quasiholes, F_{τ_x} will be a nontrivial mapping.

Equation (4.34) allows us to derive how τ_x acts on coherent states of n quasiholes. In terms of two-component states:

$$\tau_x \left|\Psi_\alpha(\{h\})\right\rangle = e^{-iL_x/2\sum_j h_{jy} - iL/2\sum_j \delta(\alpha,j)} \left|\Psi_{F_{\tau_x}(\alpha)}(\{-h^* + L_x\})\right\rangle \tag{4.35a}$$

$$\tau_x \overline{|\Psi_\alpha(\{h\})\rangle} = e^{i\pi\sum_j f_j(\alpha) + i\sum_j \delta(\alpha,j) f_j(\alpha)} \overline{|\Psi_\alpha(\{-h^* + L_x\})\rangle}\,. \tag{4.35b}$$

For now, we will restrict ourselves to the case of two quasiholes. In this case, Eq. (4.35) simplifies to:

$$\tau_x \left|\Psi_\alpha(h_1, h_2)\right\rangle = e^{-iL_x/2\sum_j h_{jy}} \left|\Psi_\alpha(h_1', h_2')\right\rangle \tag{4.36a}$$

$$\tau_x \overline{|\Psi_\alpha(h_1, h_2)\rangle} = \overline{|\Psi_\alpha(h_2', h_1')\rangle}\,, \tag{4.36b}$$

where for all indices j, $h_j' = -h_j^* + L_x$. To arrive at Eq. (4.36) we have used that for two quasiholes the phase factors on Eq. (4.35a) and Eq. (4.35b) are both 1—the former because L is even, and the latter can be seen by inserting the values of $f_j(\alpha)$ from Table 4.2—and $F_{\tau_x}(\alpha) = \alpha$ as noted above. Equation (4.36) allows us to apply τ_x to Eq. (4.14). Let us begin with the two quasiholes in the $\sigma = +$ configuration; when we apply τ_x to Eq. (4.14) and compare the resulting equation to Eq. (4.14) evaluated at the changed spatial coordinates, we find the simple relationship $\xi^-_{\alpha,\alpha'} = (\xi^+_{\alpha,\alpha'})^*$, or

$$\xi^- = (\xi^+)^*\,. \tag{4.37}$$

For the moment, we leave the relation (4.37) implicit, and use it in Appendix A to

further reduce the number of independent parameters.

4.2.3 RR braiding for $n = 2$

We can perform the adiabatic exchange of two quasiholes using again the method of Secs. 2.8 and 3.4 with minor generalizations. The details formally carry over from Sec. 2.8 because all the Berry connections along the path segments considered above are independent of the sector (see Eq. (2.55) for example). I.e., for the exchange of two quasiholes as in Fig. 2.6, dragging the second quasihole along the path segment $\mathcal{C}_1$ causes the wave functions in each sector to pick up the same phase $\exp[i\gamma_1]$ defined in Eq. (2.54).

$$\begin{pmatrix} |\Psi_1(h_1,h_2)\rangle \\ |\Psi_2(h_1,h_2)\rangle \\ |\Psi_3(h_1,h_2)\rangle \end{pmatrix} \to e^{i\gamma_1} \begin{pmatrix} |\Psi_1(h_1,h_a)\rangle \\ |\Psi_2(h_1,h_a)\rangle \\ |\Psi_3(h_1,h_a)\rangle \end{pmatrix} \tag{4.38}$$

Reiterating the remaining steps described in Sec. 2.8, the result of the adiabatic exchange is the following:

$$\begin{pmatrix} |\Psi_1(h_1,h_2)\rangle \\ |\Psi_2(h_1,h_2)\rangle \\ |\Psi_3(h_1,h_2)\rangle \end{pmatrix} \to e^{i\Phi_{AB}} \Xi^+ (\Xi^-)^{-1} \begin{pmatrix} |\Psi_1(h_1,h_2)\rangle \\ |\Psi_2(h_1,h_2)\rangle \\ |\Psi_3(h_1,h_2)\rangle \end{pmatrix} . \tag{4.39}$$

Once again we see that adiabatic exchange results in a path-dependent Aharonov-Bohm phase and a topological, statistical part made of a product of the transition

functions, which we call the braid matrix. The structure of this matrix is

$$\Xi^{+}(\Xi^{-})^{\dagger} = \chi \otimes \mathbb{I}_{2\times 2} \ , \tag{4.40}$$

where the translational, c-dependent part of the braid matrix is the product $MM^{\dagger} = \mathbb{I}_{2\times 2}$, and we have defined the "reduced" braid matrix as the α-dependent part,

$$\chi = \xi^{+}(\xi^{-})^{\dagger} \ . \tag{4.41}$$

We can constrain the form of the matrix χ by making an argument about the locality of the exchange process, analogous to the argument made in Sec. 3.4. Recall that according to the latter, only the string of the pattern that is between the domain walls taking part in the exchange can be changed as a result of this process. Any regions of the pattern far to the left or right of the initial positions must remain unchanged after the exchange. For one, this requires the exchange processes to be diagonal in c. This is already manifest by the structure of the braid matrix derived thus far, Eq. (4.40). However, certain transitions of the α label are allowed. To see this, we again refer to Table 4.2. One observes that transitions into and out of the $\alpha = 1$ sector are forbidden, since this is the only sector with 3030-type patterns far to the left and far to the right of the domain walls. The other two sectors have 2121-type patterns at the left and right end. Therefore, transitions between these sectors are allowed.

These considerations imply that the reduced braid matrix Eq. (4.41) must be of the form:

$$\chi = \xi^{+}(\xi^{-})^{\dagger} = \begin{pmatrix} \cdot & 0 & 0 \\ 0 & \cdot & \cdot \\ 0 & \cdot & \cdot \end{pmatrix} \tag{4.42}$$

where dots indicate (potentially) non-zero matrix elements. Equation (4.42) gives two independent constraint equations for the matrix elements $\xi_{\alpha,\alpha'}$. We will also use constraints for the $\xi_{\alpha,\alpha'}$s gained from the fact that ξ^{+} must be unitary:

$$\xi^{+}(\xi^{+})^{\dagger} = \mathbb{I}_{3\times 3}\ . \tag{4.43}$$

Together, Eq. (4.42) and Eq. (4.43) provide enough constraint equations to fix the $\xi_{\alpha,\alpha'}$ up to the parameter p, introduced after Eq. (4.30), which is in turn defined by the shift parameter s defined in Table 4.2. These constraints allow us to write explicit expressions for the elements of the braid matrix in terms of only the parameter p:

$$\chi = e^{i\pi/2} \begin{pmatrix} p^{-1} & 0 & 0 \\ 0 & p(p+p^{-1}-1) & \pm\sqrt{p+p^{-1}}(1-p) \\ 0 & \pm\sqrt{p+p^{-1}}(1-p) & p+p^{-1}-1 \end{pmatrix} \tag{4.44}$$

The details are presented in Appendix A. While p is still unknown at this stage, it is no longer completely unconstrained. To further constrain the value of p and fully determine the statistics, we must study the case of three quasiholes.

α	Thin torus pattern	f_1	f_2	f_3	F	F_{τ_x}
1	30303$\underline{\mathbf{0}}$**2**12121$\underline{\mathbf{1}}$**1**21212$\underline{\mathbf{2}}$**0**3030	s	$1/2$	$1-s$	3	1
2	1212**1**$\underline{\mathbf{1}}$2121**2**$\underline{\mathbf{0}}$30303$\underline{\mathbf{0}}$**2**1212	$-1/2$	$-s$	s	1	3
3	12121**2**$\underline{\mathbf{0}}$3030$\underline{\mathbf{2}}$**2**1212**1**$\underline{\mathbf{1}}$21212	$1-s$	$-1+s$	$-1/2$	2	2
4	1212**1**$\underline{\mathbf{1}}$21212$\underline{\mathbf{1}}$**1**21212**1**$\underline{\mathbf{1}}$21212	$-1/2$	$1/2$	$-1/2$	4	4

Table 4.3: $c = 0$ thin torus patterns for a three–domain-wall $k = 3$ Read-Rezayi state, and the offset functions of those domain walls. The orbital positions, $2n_i$, are underlined. Patterns and offset functions for $c = 1$ can be obtained by, respectively, shifting each pattern one orbital to the right and adding 1 to each offset function.

4.3 RR states of $n = 3$ quasiholes

We expect that we can gain new information about the statistics by braiding two quasiholes among a system of three. To see this, note that as long as there are only two quasiholes, boundary conditions require that both are associated with the same "domain-wall type". I.e., both domain walls must either occur between a 3030 string and a 2121 string, or between two 2121 strings. Hence, we were not yet able to study what happens when a quasihole associated with the former type is exchanged with one associated with the latter type. To study such processes, we must consider systems with three quasiholes. The relevant topological sectors are displayed in Table 4.3. It will suffice to exchange the first two quasiholes (along x). The "new" situation described above will then occur in the sectors $\alpha = 1$ and $\alpha = 2$. Using locality arguments analogous to the preceding section, we conclude that exchanging the first two quasiholes in these sectors is a diagonal process, since it is not possible to reach a different sector by replacing the string linking the associated domain walls. On the other hand, by complete analogy with the preceding section, the same exchange processes may lead to transitions between the $\alpha = 3$ and $\alpha = 4$ sectors. These

processes are locally the same as those discussed for the $\alpha = 2$ and $\alpha = 3$ sectors in the preceding section. Invoking again locality, within the $\alpha = 3, 4$ subspace the (reduced) braid matrix must be given by the same 2×2 block displayed in Eq. (4.44). We used exactly the same argument before in Sec. 3.5, where we constructed the $2n$-quasiparticle representation of the braid group from the two-quasiparticle braid matrix for the Moore-Read state. These arguments constrain the form of the reduced braid matrix associated with the first two quasiholes to be:

$$\chi = e^{i\pi/2} \begin{pmatrix} . & & & \\ & . & & \\ & & p(p+p^{-1}-1) & \pm\sqrt{p+p^{-1}}(1-p) \\ & & \pm\sqrt{p+p^{-1}}(1-p) & p+p^{-1}-1 \end{pmatrix} \tag{4.45}$$

where the dots indicate some matrix element we do not yet know, and blank spaces represent zeros. In the above, p is the same parameter appearing in Eq. (4.44), but we leave it understood that the quantities χ, ξ and Ξ in this section refer to the three-quasihole case, and are different from their two-quasihole counterparts. In the above, we have anticipated that braiding will again be diagonal in the c label, and χ is again defined through the action of braiding on the α label, which will follow below.

We may again proceed by expressing χ through the transition matrix coefficients $\xi^{\sigma}_{\alpha,\alpha'}$ and deriving various constraints on the latter, where now additional constraints come from the 2×2 block in (4.45). The procedure is analogous to the preceding

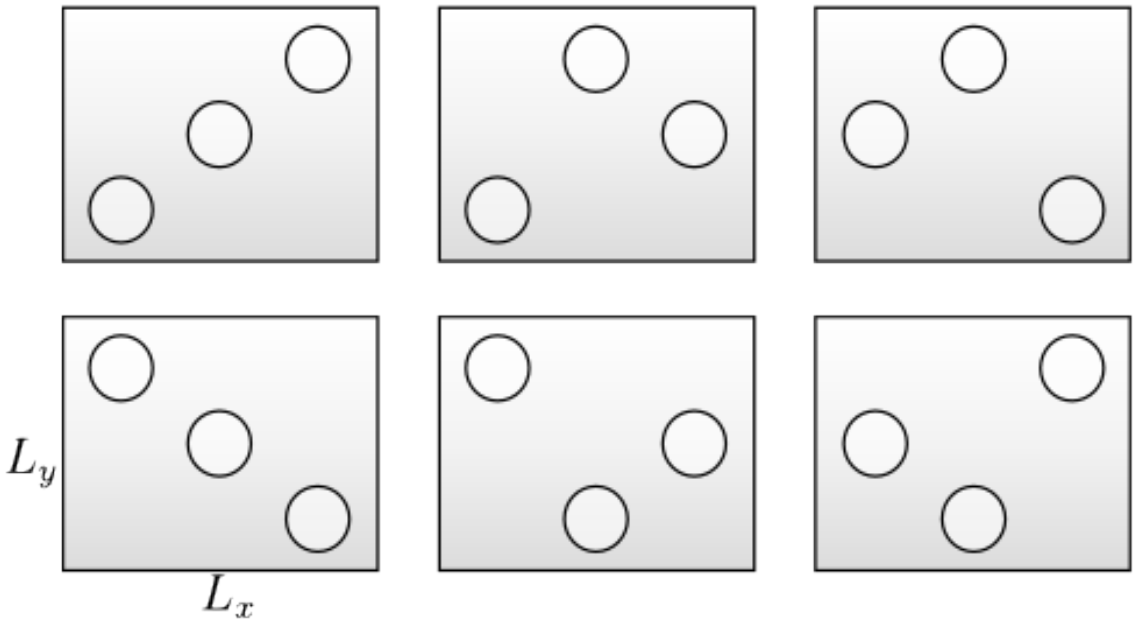

Figure 4.1: Configurations $\sigma = (\sigma_1, \sigma_2)$. σ_1 indicates the relative position of the leftmost two quasiholes, σ_2 indicates the position of the third quasihole relative to the first two. Top (left to right): $++$, $+0$, and $+-$. Bottom (left to right): $--$, -0, and $-+$.

section, where only one aspect requires nontrivial generalization: in the two-quasihole section there were only two transition matrices, Ξ^+ and Ξ^-, one for each configuration. For n quasiholes, we must distinguish $n!$ configurations and define a transition matrix for each. We choose the following notation to label these configurations. For an n-quasihole system, we let $\sigma = (\sigma_1, \ldots, \sigma_{n-1})$. σ_1 takes a value $+$ or $-$, indicating the relative position of the two leftmost quasiholes, in the same manner as in the preceding section. σ_2 takes a value $+$, $-$, or 0 and indicates the position of the third quasihole relative to the first two, as shown in Fig. 4.1 for three quasiholes. We could proceed further in the same way for $n > 3$ quasiholes, but $n \leq 3$ suffices for our purposes.

With these conventions, we can find the result of exchange of two quasiholes in

terms of the transition matrices. As pointed out, we choose to braid the two leftmost quasiholes and leave the third fixed. Further, let us say it is fixed "above" the other two, so $\sigma_2 = +^1$. The exchange can be broken down into segments in complete analogy with the two-quasihole case, yielding an equation analogous to Eq. (4.39):

$$\begin{pmatrix} |\Psi_1(\{h\})\rangle \\ |\Psi_2(\{h\})\rangle \\ |\Psi_3(\{h\})\rangle \\ |\Psi_4(\{h\})\rangle \end{pmatrix} \to e^{i\Phi_{AB}} \Xi^{++} (\Xi^{-+})^{-1} \begin{pmatrix} |\Psi_1(\{h\})\rangle \\ |\Psi_2(\{h\})\rangle \\ |\Psi_3(\{h\})\rangle \\ |\Psi_4(\{h\})\rangle \end{pmatrix} . \tag{4.46}$$

As anticipated above, using Eqs. (4.21), (4.22), we find

$$\Xi^{++} (\Xi^{-+})^\dagger = \chi \otimes \mathbb{I}_{2\times 2} \ , \tag{4.47}$$

which again defines the reduced braid matrix χ in terms of the coefficient matrices,

$$\chi = \xi^{++} (\xi^{-+})^\dagger \ . \tag{4.48}$$

As in previous examples, we will use symmetries and global paths to constrain the ξ^σ matrices, then use the implications of locality, Eq. (4.45), to find explicit expressions for the elements of χ.

[1] Other choices for the configurations of the quasiholes will result in the same braiding matrices, as it should be.

4.3.1 Constraints from mirror symmetry

In Sec. 4.2.2, the action of τ_x on n quasihole states has been discussed, Eq. (4.35). The three–domain-wall patterns are shown in Table 4.3, along with the values of $F_{\tau_x}(\alpha)$, which follow directly from these patterns. We can represent the map $F_{\tau_x}(\alpha)$ in matrix form:

$$B_\tau = \begin{pmatrix} 1 & & & \\ & 0 & 1 & \\ & 1 & 0 & \\ & & & 1 \end{pmatrix} . \tag{4.49}$$

If we apply τ_x to Eq. (4.14), proceeding as in the derivation of Eq. (4.37) and using information from Table 4.3, we find

$$\xi^{g_{\tau_x}(\sigma)} = \begin{pmatrix} \tilde{\Delta}^2 & & & \\ & 0 & \tilde{\Delta}^2 & \\ & \tilde{\Delta}^2 & 0 & \\ & & & 1 \end{pmatrix} (\xi^\sigma)^* \begin{pmatrix} \tilde{\Delta}^2 & & & \\ & 1 & & \\ & & 1 & \\ & & & 1 \end{pmatrix} e^{i\pi\lambda + i\pi} , \tag{4.50}$$

where the phase $\tilde{\Delta} = \exp[-iL(\pi - \delta)/2]$. Note that L is odd, so $\tilde{\Delta}^2 = \exp[i(\pi - \delta)]$ and $\tilde{\Delta}^4 = 1$. The function $g_{\tau_x}(\sigma)$ gives the new configuration after reflection of the quasiholes in configuration σ across the y axis, and its values are given in Table 4.4.

The matrix structure of the last equation is somewhat more complicated than Eq. (4.37). Unlike the latter, Eq. (4.50) is not "self-dual", i.e., we may obtain an

analogous but different equation by using the "dual" mirror symmetry operator τ_y instead (Sec. 2.1). It reads

$$\xi^{g_{\tau_y}(\sigma)} = \begin{pmatrix} \tilde{\Delta}^2 & & & \\ & 1 & & \\ & & 1 & \\ & & & 1 \end{pmatrix} (\xi^{\sigma})^* \begin{pmatrix} \tilde{\Delta}^2 & & & \\ & 0 & \tilde{\Delta}^2 & \\ & \tilde{\Delta}^2 & 0 & \\ & & & 1 \end{pmatrix} e^{i\pi\lambda + i\pi} \,. \tag{4.51}$$

The function $g_{\tau_y}(\sigma)$ captures the change in configuration under τ_y. Its values are given in Table 4.4.

We now evaluate Eq. (4.50) for $\sigma = (-,-)$, $g_{\tau_x}(-,-) = (+,+)$, and Eq. (4.51) for $\sigma = (+,+)$, $g_{\tau_y}(+,+) = (-,-)$, and plug one into the other. This gives the following consistency equation for ξ^{++}:

$$\xi^{++} = \begin{pmatrix} 1 & & & \\ & 0 & \tilde{\Delta}^2 & \\ & \tilde{\Delta}^2 & 0 & \\ & & & 1 \end{pmatrix} \xi^{++} \begin{pmatrix} 1 & & & \\ & 0 & \tilde{\Delta}^2 & \\ & \tilde{\Delta}^2 & 0 & \\ & & & 1 \end{pmatrix} , \tag{4.52}$$

σ	$g_x(\sigma)$	$g_y(\sigma)$	$g_{\tau_x}(\sigma)$	$g_{\tau_y}(\sigma)$
$++$	-0	$+-$	$--$	$--$
$+-$	$++$	-0	$-+$	$+0$
-0	$+-$	$++$	$+0$	$-+$
$--$	$+0$	$+0$	$++$	$++$
$+0$	$-+$	$-+$	-0	$+-$
$-+$	$--$	$--$	$+-$	-0

Table 4.4: The effect of various operations on the configuration of three quasiholes. For a state in configuration σ, when the rightmost quasihole is dragged around the torus along an a-type path (as shown in Fig. 2.5 for two quasiholes), the resulting configuration is $g_x(\sigma)$. Similarly, $g_y(\sigma)$ is the resulting configuration when the topmost quasihole is dragged along a b-type path. If a state in configuration σ is operated upon by the mirror reflection τ_x, $g_{\tau_x}(\sigma)$ is the resultant configuration. $g_{\tau_y}(\sigma)$ is similarly defined for the mirror reflection τ_y.

which constrains ξ^{++} to be of the form

$$\xi^{++} = \begin{pmatrix} \xi_{11} & \tilde{\Delta}^2\xi_{13} & \xi_{13} & \xi_{14} \\ \tilde{\Delta}^2\xi_{31} & \xi_{22} & \xi_{23} & \tilde{\Delta}^2\xi_{34} \\ \xi_{31} & \xi_{23} & \xi_{22} & \xi_{34} \\ \xi_{41} & \tilde{\Delta}^2\xi_{43} & \xi_{43} & \xi_{44} \end{pmatrix}. \tag{4.53}$$

As before, when the configuration σ is omitted, we take it to be $++$.

4.3.2 Constraints from global paths

We continue with our program by deriving constraints from "global paths", as done for the two-quasihole case in Sec. 4.2.1. We begin by generalizing Eq. (4.24) (cf. Fig. 2.5) to the case of three quasiholes. In the two-quasihole case we assumed the two quasiholes to be in a $\sigma = +$ configuration, then moved the top right quasihole around the x direction of the torus to the top left. In this section we will need to

derive more general behavior, allowing that the rightmost quasihole can be at the top, middle, or bottom relative to the other two quasiholes. The analogue of Eq. (4.23), for a path similar to path a in Fig. 2.5, then becomes:

$$\begin{aligned} |\psi_{c,\alpha}(\{h\})\rangle_f &\doteq e^{iL_x h_{3y}/2 + iL\delta(\alpha,3)/2} \left|\psi_{c+1,F(\alpha)}(\{h'\})\right\rangle \\ \overline{|\psi_{c,\alpha}(\{h\})\rangle} &= e^{-i\pi f_j(c,\alpha)} \overline{|\psi_{c,\alpha}(\{h'\})\rangle}\,. \end{aligned} \tag{4.54}$$

Here $f_j(c,\alpha)$ can be inferred from Table 4.3, and j equals 1, 2, or 3 if the quasihole encircling the torus is respectively the first, second or third when viewed from the y direction. The position $\{h'\} = h_3 - L_x, h_1, h_2$. As before, the change in α after moving the quasihole along the path is described by the function $F(\alpha)$. Its values directly follow from the associated patterns, as discussed in Sec. 4.2.1, and they are given in Table 4.3. We recast Eq. (4.54) in the two-component basis:

$$\begin{aligned} |\Psi_\alpha(\{h\})\rangle_f &\doteq e^{iL_x h_{3y}/2 + iL\delta(\alpha,3)/2 + i/2\sum_j \delta(\alpha,j)} \begin{pmatrix} 0 & e^{-i\sum_j \delta(\alpha,j)} \\ 1 & 0 \end{pmatrix} \left|\Psi_{F(\alpha)}(\{h'\})\right\rangle \\ \overline{|\Psi_\alpha(\{h\})\rangle} &= e^{-i\pi f_j(\alpha)} \begin{pmatrix} 1 & 0 \\ 0 & -1 \end{pmatrix} \overline{|\Psi_\alpha(\{h'\})\rangle}\,. \end{aligned} \tag{4.55}$$

Just as in the two-quasihole case, Eq. (4.55) allows us to derive an equation between the transition matrix in the configuration σ with the matrix in the configuration $g_x(\sigma)$.

$$\xi^{g_x(\sigma)} = B^{-1}\mathrm{diag}[e^{-i\pi\lambda - iL\delta(\alpha,3)/2 - i/2\sum_j \delta(\alpha,j)}]\xi^\sigma \mathrm{diag}\left[e^{-i\pi f_j(\alpha)}\right]. \tag{4.56}$$

The pairs $(\sigma, g_x(\sigma))$ are summarized in Table 4.4. The matrix B is defined as in Eq. (4.27), and for three quasiholes it has the form

$$B = \begin{pmatrix} & & 1 & \\ 1 & 0 & & \\ & 1 & & \\ & & & 1 \end{pmatrix} . \tag{4.57}$$

In any specific instance of Eq. (4.56), one first chooses a starting configuration σ, and identifies the corresponding y-direction index j of the quasihole that will encircle the torus. j is in one-to-one correspondence with σ_2: for σ_2 is $+$, 0, or $-$, j is respectively 3, 2, or 1. For instance, were we to begin in configuration $++$, then $j = 3$ and after the encircling the system would be in configuration -0. Thus we find the relation

$$\xi^{-0} = \begin{pmatrix} & \tilde{\Delta} & & \\ & 0 & \tilde{\Delta}^2 & \\ \tilde{\Delta} & & & \\ & & & 1 \end{pmatrix} \xi^{++} \begin{pmatrix} p & & & \\ & p^{-1} & & \\ & & -1 & \\ & & & -1 \end{pmatrix} , \tag{4.58}$$

where p is defined as before, $p = -e^{i\pi(s+1/2)}$.

We can go through the same derivation for a path similar to path b in Fig. 2.5, in which the top quasihole moves around the y direction of the torus and ends at the

bottom. We find

$$\xi^{g_y(\sigma)} = \mathrm{diag}\left[e^{-i\pi f_j(\alpha)}\right] \xi^{\sigma} \mathrm{diag}[e^{-i\pi\lambda - iL\delta(\alpha,3)/2 - i/2\sum_j \delta(\alpha,j)}] B \tag{4.59}$$

It is very important to note that for this path, the meaning of the index j is different from the previous path. In the previous case, the quasihole encircled the torus in the x direction, so the moving quasihole was the rightmost in horizontal (x) order but was the j-th quasihole in vertical (y) order; in this case, the quasihole encircles the torus in the y direction, so the moving quasihole is the topmost in vertical order but is the j-th in horizontal order. As an example, if we begin in configuration -0, the topmost quasihole is that on the left, so $j = 1$. Plugging in the appropriate values from the tables,

$$\xi^{++} = \begin{pmatrix} p^{-1} & & & \\ & -1 & & \\ & & p & \\ & & & -1 \end{pmatrix} \xi^{-0} \begin{pmatrix} & & \tilde{\Delta} & \\ \tilde{\Delta} & 0 & & \\ & \tilde{\Delta}^2 & & \\ & & & 1 \end{pmatrix} \tag{4.60}$$

Combining Eqs. (4.60) and (4.58) gives us a consistency relation for ξ^{++},

$$\xi^{++} = \begin{pmatrix} & \tilde{\Delta}p^{-1} & & \\ & 0 & -\tilde{\Delta}^2 & \\ \tilde{\Delta}p & & & \\ & & & -1 \end{pmatrix} \xi^{++} \begin{pmatrix} & & \tilde{\Delta}p & \\ \tilde{\Delta}p^{-1} & 0 & & \\ & -\tilde{\Delta}^2 & & \\ & & & -1 \end{pmatrix}, \tag{4.61}$$

which further constrains ξ^{++} in addition to Eq. (4.53).

$$\xi^{++} = \begin{pmatrix} \xi_{11} & \tilde{\Delta}^2\xi_{13} & \xi_{13} & \xi_{14} \\ \tilde{\Delta}^2\xi_{13} & \tilde{\Delta}^2p^2\xi_{11} & -\tilde{\Delta}^{-1}p\xi_{13} & -\tilde{\Delta}^{-1}p\xi_{14} \\ \xi_{13} & -\tilde{\Delta}^{-1}p\xi_{13} & \tilde{\Delta}^2p^2\xi_{11} & -\tilde{\Delta}p\xi_{14} \\ \xi_{41} & -\tilde{\Delta}^{-1}p\xi_{41} & -\tilde{\Delta}p\xi_{41} & \xi_{44} \end{pmatrix} \tag{4.62}$$

4.3.3 RR braiding for $n = 3$

As in the two-quasihole section, we will further determine the structure of the reduced braid matrix using constraint equations from unitarity and from locality. Enforcing locality means that we equate the matrix product for χ in Eq. (4.46) with the form in Eq. (4.45), which is implied by locality, as we argued above. The details are given in Appendix B, resulting in the following form for χ:

$$\chi = e^{i\theta} \begin{pmatrix} p & & & \\ & p & & \\ & & p^2(1-p) & e^{i\theta_2} p^2 \sqrt{p+p^{-1}-1} \\ & & e^{i\theta_2} p^2 \sqrt{p+p^{-1}-1} & e^{2i\theta_2} p(1-p) \end{pmatrix} \tag{4.63}$$

where θ and θ_2 are as yet undetermined phases.

In deriving the above equation, only the zero-valued matrix elements of Eq. (4.45) have been used. To enforce consistency between the two- and three-quasihole braiding matrices, as dictated by locality, we must equate the 2×2 block of Eq. (4.63) to that of Eq. (4.45). Equating the expressions for the element χ_{33} gives us a consistency relation that we can use to constrain p:

$$e^{i\theta} p^2 (1-p) = e^{i\pi/2} p (p + p^{-1} - 1) \; . \tag{4.64}$$

If we define $x = p + p^{-1}$ for convenience and take the absolute square of Eq. (4.64), we find

$$2 - x = (x-1)^2 \; , \tag{4.65}$$

which is solved when x is the golden ratio,

$$x = \varphi \equiv \frac{1+\sqrt{5}}{2} \; . \tag{4.66}$$

We have chosen the positive root because Eq. (B.9b) implies $x \geq 1$. If we define the

angle a by $p = \exp(i\pi a)$ then $x = 2\cos(\pi a)$ and Eq. (4.66) implies

$$a = \pm\frac{1}{5}\,. \tag{4.67}$$

a is also related to the shift parameter $s = a + 1/2$, and so Eq. (4.67) tells us[2]

$$s = \frac{1}{2} \pm \frac{1}{5}\,. \tag{4.68}$$

The phase information in Eq. (4.64) fixes the overall phase θ,

$$e^{i\theta} = e^{i\pi s}\,. \tag{4.69}$$

There are two more consistency equations found from equating Eqs. (4.45) and (4.63). One yields $\exp(i\theta_2) = \pm 1$, and the other is trivially satisfied when $x = \varphi$. Up to some signs, the braid matrices for two- and three-quasihole systems have thus been completely solved for. We will discuss our solution(s) in the following section.

4.4 Representation of the braid group of n RR quasiholes

In Sec. 4, we have found solutions for the braid matrices describing exchange processes between two and three quasiholes that are consistent with the coherent state ansatz

[2]We leave it understood that this relation holds modulo 2.

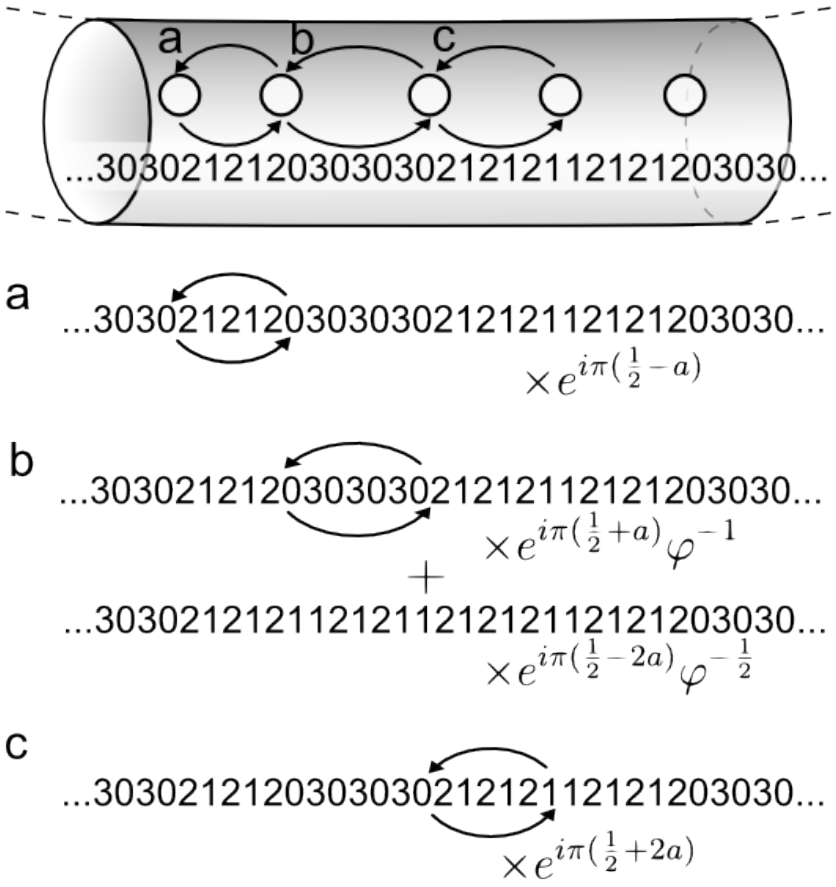

Figure 4.2: Graphical representation of the result of exchanging two $k = 3$ Read-Rezayi quasiholes for three example pairs. Top) A possible state in which five quasiholes could be prepared, labeled by its associated thin torus pattern. The state shown could be a five-quasihole state, in which the 30 strings at either end would continue around the torus, or could be an n-quasihole state for $n > 5$, in which the ellipses mask additional domain walls in the thin torus pattern. The results of braiding any pair of quasiholes shown here will be the same in either case. a) Upon exchange of the indicated quasiholes, the state picks up the phase $e^{i\pi(1/2-a)}$, where a is given by Eq. (4.67) (with the lower sign correctly describing the conformal block monodromies of the RR trial states). The thin torus pattern, and thus the topological sector of the state, remains unchanged after the exchange, as shown. b) When the two indicated quasiholes are exchanged the state remains in the same topological sector or transitions into a sector with the linking 30 string changed to a 21 string. The amplitudes for these two possibilities are shown beneath the thin torus patterns for the sectors, where φ is the golden ratio, Eq. (4.66). c) Upon exchange of the indicated quasiholes, the state picks up the phase $e^{i\pi(1/2+2a)}$. The thin torus pattern, and thus the topological sector of the state, remains unchanged after the exchange, as shown.

for the $k = 3$, $\nu = 3/2$ Read-Rezayi state. In the following, we discuss how many independent solutions we have found, how they lead to general rules for the braiding of n quasiholes, and how these solutions compare to those obtained by other methods.

By means of Eq. (4.66), we may now express the braid matrices for two quasiholes, Eq. (4.44), and three quasiholes, Eq. (4.63), in terms of only the golden ratio φ and the parameter $a = \pm 1/5$. The two-quasihole matrix is then

$$\chi = e^{i\pi/2} \begin{pmatrix} e^{-i\pi a} & & \\ & e^{i\pi a}\varphi^{-1} & e^{-2i\pi a}\varphi^{-1/2} \\ & e^{-2i\pi a}\varphi^{-1/2} & \varphi^{-1} \end{pmatrix}, \tag{4.70}$$

and the three-quasihole matrix is

$$\chi = e^{i\pi/2} \begin{pmatrix} e^{2i\pi a} & & & & \\ & e^{2i\pi a} & & & \\ & & & e^{i\pi a}\varphi^{-1} & e^{-2i\pi a}\varphi^{-1/2} \\ & & & e^{-2i\pi a}\varphi^{-1/2} & \varphi^{-1} \end{pmatrix}. \tag{4.71}$$

In writing these matrices, we have removed the $\pm$ from the off-diagonal elements, choosing the $+$ sign. Choosing the negative sign instead leads to a unitarily equivalent solution, where the transformation is facilitated through multiplication of each state by $(-1)^{\#30}$, where #30 is the number of $3030\ldots$ strings in the thin torus pattern associated with that state. The arguments given below will make it obvious that this

equivalence also carries over to general n-quasihole sectors. We have thus obtained only two unitarily inequivalent solutions. It is clear from the above that these two solutions are closely related, namely by complex conjugation and an overall Abelian phase -1. Thus, the non-Abelian content of the $k = 3$ state has been determined uniquely by our method.

We will now use the locality arguments already made in Sec. 4.2.3 for states of three quasiholes, and applied earlier in Sec. 3.5 to the Pfaffian case, to generalize these solutions to the case of n quasiholes. In essence, these arguments implied that the result of exchanging two neighboring quasiholes can only affect the ground-state pattern linking the associated domain walls in the sector label, and only depend on the sequence of three patterns that are separated by these two domain walls. For this, however, all possibilities have been exhausted by considering two and three quasiholes, respectively. We can thus list the following rules, applicable to general n-quasihole states, obtained directly from Eqs. (4.70) and (4.71):

- If the two quasiholes to be exchanged are associated with domain walls between ground-state strings $\ldots 3030|2121|121\ldots$ or $\ldots 2121|1212|030\ldots$, then after exchange the state remains in the same sector and picks up the phase $e^{i\pi(1/2+2a)}$.

- If the two quasiholes are associated with the pattern $\ldots 3030|21212|030\ldots$, then after the exchange the state merely picks up the phase $e^{i\pi(1/2-a)}$.

- If the quasiholes are associated with the pattern $\ldots 212|03030|21\ldots$, after exchange the state will stay in same topological sector with amplitude $e^{i\pi(1/2+a)}\varphi^{-1}$

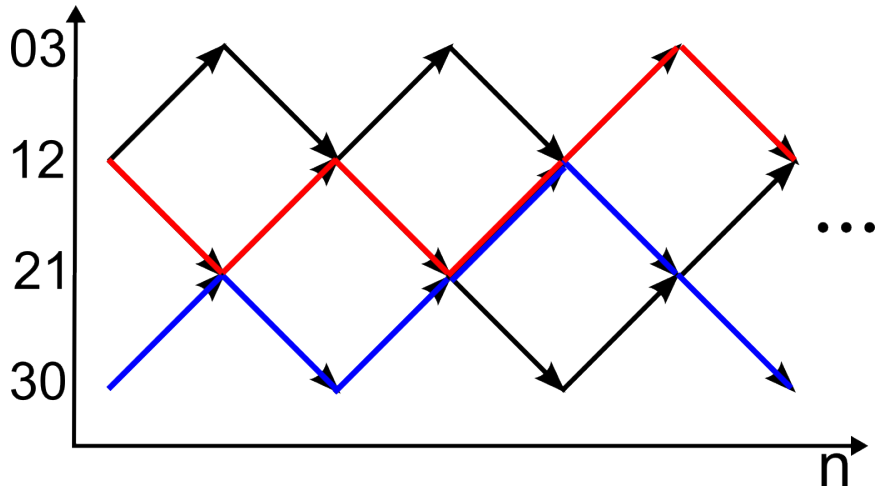

Figure 4.3: Bratteli diagram of the $k = 3$ Read-Rezayi state with two possible paths indicated. The red line corresponds to the sector label 12**11211211211203021**2 and the blue line corresponds to 3**0212030211211203**0.

and transition with amplitude $e^{i\pi(1/2-2a)}\varphi^{-1/2}$ into a sector that has the exchanged quasiholes associated with the pattern $\ldots 2121|121|121\ldots$.

- If the quasiholes are associated with the pattern $\ldots 2121|121|121\ldots$, then after exchange the state will stay in same topological sector with amplitude $e^{i\pi/2}\varphi^{-1}$ and transition with amplitude $e^{i\pi(1/2-2a)}\varphi^{-1/2}$ into a sector that has the exchanged quasiholes associated with the pattern $\ldots 212|03030|21\ldots$.

These rules make it easy to visualize what is going on as a result of braiding in this non-Abelian state, as depicted in Fig. 4.2. It remains to see which of our two solutions, if any, agrees with the representation of the braid group obtained from conformal block monodromies [78]. To make contact between these various representations, let us observe that our representation of topological sectors as patterns separated by domain walls is in natural one-to-one correspondence with the representation given

by paths meandering through a Bratteli diagram, Fig. 4.3. Here, the vertices of the diagram are associated with the various ground-state patterns according to their "height" in the diagram, and the links represent the possible domain walls between them. A left-to-right path along the links of the diagram then represents an allowed sequence of patterns separated by domain walls, hence, a topological sector. The same diagrammatic labeling of sectors also naturally arises through fusion rules in the CFT analysis of the RR states. With this identification, it becomes easy to see that the above rules describing our solution are, for $a = -1/5$, in one-to-one correspondence with the "tensor representation" established in Ref. [78] based on the analysis of conformal blocks.

To make this point, we briefly review the latter. In the tensor representation given by Slingerland and Bais [78], topological sectors, or paths through the Bratteli diagram, are represented by tensor products of vectors $v_{\Lambda_i,\Lambda_{i+1}}$ of the "domino" form $v_{\Lambda_1,\Lambda_2} \otimes v_{\Lambda_2,\Lambda_3} \otimes v_{\Lambda_3,\Lambda_4} \otimes \cdots \otimes v_{\Lambda_{n-1},\Lambda_n}$. Here, Λ_i represents the "height" of the i-th vertex in the path (Fig. 4.3), $\Lambda_{i+1} = \Lambda_i \pm 1$, and $v_{\Lambda_i,\Lambda_{i+1}}$ is a formal vector representing a link between two neighboring vertices at heights Λ_i, Λ_{i+1}, respectively. At general level k, Λ_i takes on values $0, \ldots, k$.

In this tensor product basis, exchange of the quasiholes with indices i and $i+1$ is represented by a matrix $R_{k,i}$ which acts only on the i-th and $(i+1)$-th factors [78]:

$$\begin{aligned} R_{k,i}\, v_{\Lambda_i,\Lambda_i+1} \otimes v_{\Lambda_i+1,\Lambda_i+2} &= \alpha\, v_{\Lambda_i,\Lambda_i+1} \otimes v_{\Lambda_i+1,\Lambda_i+2} \\ R_{k,i}\, v_{\Lambda_i,\Lambda_i-1} \otimes v_{\Lambda_i-1,\Lambda_i-2} &= \alpha\, v_{\Lambda_i,\Lambda_i-1} \otimes v_{\Lambda_i-1,\Lambda_i-2} \end{aligned} \tag{4.72}$$

$$\begin{aligned} R_{k,i}\, v_{\Lambda_i,\Lambda_i+1} \otimes v_{\Lambda_i+1,\Lambda_i} &= -\alpha q^{-1} v_{\Lambda_i,\Lambda_i+1} \otimes v_{\Lambda_i+1,\Lambda_i} \ (\Lambda_i = 0) \\ R_{k,i}\, v_{\Lambda_i,\Lambda_i-1} \otimes v_{\Lambda_i-1,\Lambda_i} &= -\alpha q^{-1} v_{\Lambda_i,\Lambda_i-1} \otimes v_{\Lambda_i-1,\Lambda_i} \ (\Lambda_i = k) \end{aligned} \tag{4.73}$$

$$\begin{aligned} \begin{pmatrix} R_{k,i}\, v_{\Lambda_i,\Lambda_i+1} \otimes v_{\Lambda_i+1,\Lambda_i} \\ R_{k,i}\, v_{\Lambda_i,\Lambda_i-1} \otimes v_{\Lambda_i-1,\Lambda_i} \end{pmatrix} &= \begin{pmatrix} -\alpha q^{-\Lambda_i/2-1} \frac{1}{\lfloor \Lambda_i+1 \rfloor_q} & -\alpha q^{-1/2} \frac{\sqrt{\lfloor \Lambda_i+2 \rfloor_q \lfloor \Lambda_i \rfloor_q}}{\lfloor \Lambda_i+1 \rfloor_q} \\ -\alpha q^{-1/2} \frac{\sqrt{\lfloor \Lambda_i+2 \rfloor_q \lfloor \Lambda_i \rfloor_q}}{\lfloor \Lambda_i+1 \rfloor_q} & \alpha q^{\Lambda_i/2} \frac{1}{\lfloor \Lambda_i+1 \rfloor_q} \end{pmatrix} \\ &\times \begin{pmatrix} v_{\Lambda_i,\Lambda_i+1} \otimes v_{\Lambda_i+1,\Lambda_i} \\ v_{\Lambda_i,\Lambda_i-1} \otimes v_{\Lambda_i-1,\Lambda_i} \end{pmatrix} \ (0 < \Lambda_i < k) \end{aligned} \tag{4.74}$$

where $q = e^{2\pi i/(k+2)}$, $\alpha = q^{(1-M)/(2(kM+2))}$, M is related to the filling factor via $\nu = 3/(3M+2)$, and "q-deformed integers" $\lfloor m \rfloor_q$ are defined as,

$$\lfloor m \rfloor_q = \frac{q^{m/2} - q^{-m/2}}{q^{1/2} - q^{-1/2}} \ . \tag{4.75}$$

In our case $k = 3$ and $M = 0$, so $q = e^{2\pi i/5}$ and $\alpha = e^{i\pi/10}$. In this case, it is not difficult to check that Eqs. (4.72)–(4.74) reduce to the rules established in the beginning of this section, once tensor products are reinterpreted as sequences of patterns via paths in the Bratteli diagram.

To wit, our first rule is equivalent to Eq. (4.72). To see this, observe that the two domain walls defined by the ground-state sequence $\ldots 3030\underset{|}{|}2121\underset{|}{|}121\ldots$ could be represented on the Bratteli diagram Fig. 4.3 by $v_{0,1} \otimes v_{1,2}$ or by $v_{3,2} \otimes v_{2,1}$, both of which follow the form of Eq. (4.72). A similar observation can be made about $\ldots 2121\underset{|}{|}1212\underset{|}{|}030\ldots$. The phase picked up by the states in Eq. (4.72) is $\alpha = e^{i\pi/10}$,

which is equivalent to the phase in our first rule $e^{i\pi(1/2+2a)}$, where we take $a = -1/5$ here and in the following. Similarly, one can observe that the pattern in our second rule is represented by the vectors in Eq. (4.73). The phase in that equation is $-\alpha q^{-1} = e^{7i\pi/10}$, which is equivalent to the phase in the second rule, $e^{i\pi(1/2-a)}$. Finally, our third and fourth rules are together equivalent to Eq. (4.74). The patterns $\ldots 212\underline{|}03030\underline{|}21\ldots$ and $\ldots 2121\underline{|}121\underline{|}121\ldots$ can be written as $v_{1,0}\otimes v_{0,1}$ and $v_{1,2}\otimes v_{2,1}$ or as $v_{2,3}\otimes v_{3,2}$ and $v_{2,1}\otimes v_{1,2}$, which appear in Eq. (4.74) for $\Lambda_i = 1$ and $\Lambda_i = 2$, respectively. Up to a change in the order of the basis states, the matrix in Eq. (4.74) for either value of Λ_i gives the matrix elements stated in the third and fourth rules; this equivalence is shown here for $\Lambda_i = 2$:

$$\begin{aligned}\begin{pmatrix} -\alpha q^{-2}\frac{1}{\lfloor 3\rfloor_q} & -\alpha q^{-1/2}\frac{\sqrt{\lfloor 4\rfloor_q\lfloor 2\rfloor_q}}{\lfloor 3\rfloor_q} \\ -\alpha q^{-1/2}\frac{\sqrt{\lfloor 4\rfloor_q\lfloor 2\rfloor_q}}{\lfloor 3\rfloor_q} & \alpha q\frac{1}{\lfloor 3\rfloor_q} \end{pmatrix} &= \begin{pmatrix} e^{3i\pi/10}\varphi^{-1} & e^{9i\pi/10}\varphi^{-1/2} \\ e^{9i\pi/10}\varphi^{-1/2} & e^{i\pi/2}\varphi^{-1} \end{pmatrix} \\ &= \begin{pmatrix} e^{i\pi(1/2+a)}\varphi^{-1} & e^{i\pi(1/2-2a)}\varphi^{-1/2} \\ e^{i\pi(1/2-2a)}\varphi^{-1/2} & e^{i\pi/2}\varphi^{-1} \end{pmatrix}.\end{aligned} \tag{4.76}$$

We hence see that one of our two solutions does indeed agree with the prediction based on conformal block monodromies, with the other one being closely related.

Furthermore, it appears that the solutions we obtained form a true subset of the solutions that can be derived by imposing the relevant fusion rules, together with the axioms defining general anyon models (see, e.g., Refs. [79, 75, 76]). If, in addition

to the pentagon and hexagon equations, one imposes unitarity and modularity, these admit four solutions [75, 80]. Two of these appear to be identical to ours, with the other two related to the former by complex conjugation. We observe that in our approach, there is no reason to expect that solutions automatically come in complex conjugate pairs. This is so since the coherent state ansatz explicitly assumes a holomorphic dependence on quasihole coordinates (see Sec. 3.1), corresponding to a choice of sign for the magnetic field that renders trial wave functions for the RR state holomorphic (in both electron and quasihole coordinates). Our findings thus seem to imply that for the "missing" two solutions, one cannot construct holomorphic trial wave functions that can be adiabatically deformed (through a continuous family of local Hamiltonians) into the thin torus patterns we work with.

Chapter 5

The Gaffnian State

In addition to the wave functions which arise from unitary CFTs, there is also considerable interest in analytic trial states that are similarly related to nonunitary CFTs [81, 82]. The physical interpretation of such states remains much more subtle. Here, the field theoretic mapping employed in the unitary case does not lead to a topological quantum field theory that can serve as the low energy effective theory of the state in question. In particular, the conformal block monodromies cannot be interpreted to describe adiabatic transport, as they do not result in unitary transformations on states. In contrast, adiabatic transport describes (a limit of) the time evolution governed by a Hermitian Hamiltonian, and is therefore always described by a unitary transformation. For these reasons, it has been argued [82, 28, 29, 83, 31] that states obtained from nonunitary CFTs describe gapless critical points within the phase diagram of quantum Hall states, especially in those cases where a local parent Hamil-

Parts of this chapter originally appeared in Ref. [60].

tonian for the state exists. Examples of the latter kind include the Haldane-Rezayi (HR) state [81], and the state known as Gaffnian, which has surfaced in the literature as early 1993 through a fixed many-body clustering property [84], and which has been thoroughly discussed and was proposed to be critical using a CFT construction [82],

The question arises what hidden orders can be identified in such nonunitary states, whether they be remnants of topological orders or orders of a different kind. Unfortunately, there is currently no efficient and universally applicable method to test for the topologically ordered [67] nature of a state directly through the study of ground state properties. Much progress along these lines has recently been made through the analysis of entanglement spectra [85, 86], which are directly related to edge spectra. It has been argued that the edge spectrum of the Gaffnian is inconsistent with that of any unitary CFT, and that this contradicts the existence of a gap in the bulk spectrum [83], which is required for a topological phase. In principle, topological orders can be detected through nonlocal order parameters [87], though it remains difficult to explicitly construct such objects for general non-Abelian topological orders in microscopic quantum Hall wave functions. The situation is similar in quantum magnetism. There, nonlocal operators detecting a topological phase can be directly constructed for toy models [88] defined on highly constrained Hilbert spaces where a gauge structure is explicit (see Ref. [89] for a general discussion). However, such order parameters generally remain elusive in models where similar physics is emergent within the low energy sector of a larger Hilbert space (e.g., Ref. [90]). The situation is much simpler in one-dimensional systems exhibiting a Haldane or Luttinger liquid

phase. The hidden orders of these phases can be probed through nonlocal objects measuring squeezed particle configurations [91, 92], and their origin is quite manifest, e.g., in certain limits of Luttinger liquids where the wave function assumes a special factorized form [93, 94, 95, 96]. For topological orders, on the other hand, the most direct probe that can, in principle, be implemented at a microscopic wave function level is the study of the braiding statistics of localized elementary excitations.

In this Chapter, we ask the question whether the Gaffnian trial wave functions may define some unitary anyon model through the adiabatic transport of trial state quasiholes in the presence of a finite size gap. Indeed, this question is mathematically well defined. The quasihole trial states can be characterized as the unique zero modes of a local parent Hamiltonian [84, 82]. For given quasihole configuration, the associated conformal block wave functions define a finite-dimensional subspace, which can be interpreted as a fiber over a point in the quasihole configuration space. The question is thus whether the holomomy associated with exchange paths in this configuration space induces well-defined statistics. It is clear from the outset that if this is so, the holonomies must be quite different from the conformal block monodromies, since these holonomies give rise to unitary transformations on fibers. Physically, this is clear from the fact that these holonomies describe the adiabatic transport of quasiholes protected by a finite size gap. Mathematically, it follows from the fact that the connection on our vector bundle is a Wilczek-Zee connection defined in terms of a physical scalar product.

The question defined above can be rigorously addressed only by calculating the

Wilczek-Zee connection from the given analytic wave functions. Unfortunately, we do not know how to do this for the Gaffnian state. Instead, we will use this question as a testbed for the coherent state method. Our motivation to clarify the applicability of this method to a nonunitary state is twofold. A negative result (no consistent anyon model) would further strengthen the case that the TT limit contains information about the gapped or gapless nature of the underlying state. This has been explored recently for the HR state [44], though not with regard to statistics. On the other hand, if a consistent anyon model is obtained, we can argue that this is at least a very plausible scenario for the holonomies defined by the Gaffnian quasihole states, as we will further elaborate below.

Some of the arguments underlying the coherent state method, in particular the justification for the factorized form of the ansatz (see Eq. (5.3) below), also rest on a notion of locality, which is more subtle in a gapless state. We argue however, that the necessary assumptions still apply, as long as there is a finite gap in the *charge* sector of the system, independent of the existence of gapless neutral excitations. The scaling of the charge gap of the Gaffnian state has been discussed in some detail in Ref. [97], but at the moment, the question whether it remains finite in the thermodynamic limit has not been conclusively resolved to the best of our knowledge.

We will proceed in a manner largely the same as the RR case in Chapter 4: We begin by considering properties of n-quasihole states. We then find the braiding matrices for the cases $n = 2$ and $n = 3$, which are together sufficient to construct a representation of the braid group of n quasiholes for any n. Details of these calcula-

tions are presented in Appendices C and D.

5.1 General solution for n quasiholes

The thin torus patterns of the bosonic $\nu = 2/3$ Gaffnian, and their relation to the underlying minimal model CFT, have been thoroughly discussed by Ardonne [98]. For the six degenerate Gaffnian ground states, these patterns read $200200\ldots$, $020020\ldots$, and $002002\ldots$, which we will call "(200)-type", or $011011\ldots$, $101101\ldots$, and $110110\ldots$, which we refer to as "(011)-type". There are three elementary domain wall strings: 100 and 001, which occur between (200)-type and (011)-type ground states, and 010, which occurs between two different (011)-type ground states. These domain walls may link various different combinations of ground state patterns, thus forming charge 1/3 solitons. The number of LLL orbitals is $L = (3N - n)/2$.

To specify the topological sector labels, we follow the convention of Sec. 4.1: α distinguishes classes of sectors that are not related by translation, and $c = -1, 0, 1$ distinguishes the three translationally-related members of each class for a given α. Below, we will also use translational properties to define a unique convention for how the c labels are to be assigned. As usual, the domain wall positions can change only by multiples of a certain "stride" within each topological sector (here, multiples of 3), and are thus of the general form $a_j = 3n_j + f_j(c, \alpha)$, with $f_j(c, \alpha)$ an offset factor. The latter's value for symmetric domain walls is uniquely determined by symmetry. However, for asymmetric domain walls, a certain ambiguity exists *a priori* in how to

α	Thin torus pattern	$f_1(\alpha)$	$f_2(\alpha)$
1	002002**00**$\underline{\mathbf{1}}$101101**10**$\underline{\mathbf{0}}$2002002	$-s$	$-2+s$
2	1101101**1**$\underline{\mathbf{0}}$**0**2002002$\underline{\mathbf{0}}$**01**10110	$-1+s$	$2-s$
3	1101100$\underline{\mathbf{1}}$**01**1011**01**$\underline{\mathbf{1}}$**0**110110	1	0

Table 5.1: $c = 0$ thin torus patterns for a two–quasihole Gaffnian state, and the offset functions of the associated domain walls. The elementary domain wall strings are in bold, and the orbital positions, $3n_j$, are underlined. Patterns for $c = 1$ (resp. -1) can be obtained by shifting each occupancy number one orbital to the right (left), and the shift functions obtained using $f_j(c, \alpha) = f_j(\alpha) + c$.

define the domain wall position precisely with respect to the adjacent orbitals. This is accounted for by the shift—or asymmetry—parameter s. See Table 5.1 for details.

We define the coherent states as in Eqs. (4.1) and (4.2),

$$|\psi_{c,\alpha}(\{h\})\rangle = \mathcal{N} \sum_{a_1<\ldots<a_n} \prod_{j=1}^{n} \phi_{\alpha,j}(h_j, \kappa a_j)\, |a_1, \ldots, a_n; c, \alpha\rangle\,, \tag{5.1}$$

$$\overline{|\psi_{c,\alpha}(\{h\})\rangle} = \mathcal{N}' \sum_{a_1<\ldots<a_n} \prod_{j=1}^{n} \overline{\phi}_{\alpha,j}(h_j, \overline{\kappa} a_j) \overline{|a_1, \ldots, a_n; c, \alpha\rangle}. \tag{5.2}$$

However, here the Gaussian amplitude form factor,

$$\phi_{\alpha,j}(h_j, a_j) = \exp\left[\frac{i}{3}(h_{jy} + \delta(\alpha, j)/\kappa)\kappa a_j - \gamma(h_{jx} - \kappa a_j)^2\right], \tag{5.3}$$

has a coefficient of $1/3$ on the ih_y term. This is because the "stride" of the Gaffnian domain walls is different than the cases studied above. The dual counterpart to Eq. (5.3) is

$$\overline{\phi}_{\alpha,j}(h_j, a_j) = \phi_{\alpha,j}(-ih_j, a_j)|_{\kappa\to\bar{\kappa}}, \tag{5.4}$$

Here, as before, $\kappa = 2\pi/L_y$, $\bar{\kappa} = 2\pi/L_x$, and $\delta(\alpha, j)$ can be shown to be 0 or π, taking

on the same value for symmetry-related (translation or inversion) domain walls. $\mathcal{N}$ and $\mathcal{N}'$ are normalization factors.

Eqs. (5.1) and (5.2) are related by a linear transformation, and we define transition functions $u^{\sigma}_{c,c',\alpha,\alpha'}(\{h\})$ exactly as in Eq. (4.5). The transition functions' dependence on h, (c,c'), and (α,α') separates into the following factorized form:

$$u^{\sigma}_{c,c',\alpha,\alpha'}(\{h\}) = u(\{h\})M_{c,c'}\xi^{\sigma}_{\alpha,\alpha'}, \tag{5.5}$$

with $u(\{h\})$ and $M_{c,c'}$ fully determined by translational symmetry:

$$u(\{h\}) = \exp\left(\frac{i\pi}{3}\sum_j h_{jx}h_{jy}\right), \tag{5.6}$$

$$M = \frac{1}{\sqrt{3}}\begin{pmatrix} e^{2\pi i(L-1)/3} & e^{-2\pi iL/3} & e^{2\pi i/3} \\ e^{-2\pi iL/3} & 1 & e^{2\pi iL/3} \\ e^{2\pi i/3} & e^{2\pi iL/3} & e^{2\pi i(L-1)/3} \end{pmatrix}. \tag{5.7}$$

The matrix M is in the "natural" c basis, defined by,

$$\sum_j n_j = \frac{1}{3}L(L-c) - \frac{1}{3}\sum_j a_j \mod L, \tag{5.8}$$

where n_j is the occupation number of the jth orbital in the pattern labeling the state.

Global paths (shown in in Fig. 2.5 for $n = 2$ quasiholes) constrain the $\xi^{\sigma}_{\alpha,\alpha'}$s as before. For n quasiholes in configuration σ, we first consider moving the rightmost

quasihole around the torus to become the leftmost. After this move the system is in configuration $g_x(\sigma)$ (see Table 4.4), and continuity across the torus boundary dictates,

$$\xi^{g_x(\sigma)} = B^{-1}\mathrm{diag}[e^{-2\pi i L/3 - iL\delta(\alpha,n)/3 - i/3\sum_j \delta(\alpha,j)}]\xi^{\sigma}\mathrm{diag}[e^{-2\pi i f_j(\alpha)/3}], \tag{5.9}$$

in correspondence with Eqs. (4.29) and (4.56). The matrix B is defined as before (see Eq. (4.28) for $n = 2$ and Eq. (4.57) for $n = 3$). Now consider moving the topmost quasihole of a state in configuration σ up, so that it crosses the upper boundary to become the bottommost quasihole in the resulting configuration $g_y(\sigma)$. The continuity condition on the ξ matrices analogous to Eq. (5.9) reads,

$$\xi^{g_y(\sigma)} = \mathrm{diag}[e^{-2\pi i f_j(\alpha)/3}]\xi^{\sigma}\mathrm{diag}[e^{-2\pi i L/3 - iL\delta(\alpha,n)/3 - i/3\sum_j \delta(\alpha,j)}]B. \tag{5.10}$$

In the previous cases, for each n we applied both global path equations in succession to constrain ξ^{σ} for one particular quasihole configuration: $\sigma = +$ for $n = 2$ and $\sigma = +,+$ for $n = 3$. We generalize this be defining a special configuration for each n: $\sigma_I = +,+,\cdots,+$. This is shown in Fig. 5.1. It is easy to see that σ_I is always invariant under the two moves described above performed in succession, i.e., $g_y(g_x(\sigma_I)) = \sigma_I$. Hence, Eqs. (5.9) and (5.10) together constrain the matrix elements of ξ^{σ_I}.

As before (Secs. 4.2.2 and 4.2.2), the system is symmetric under the operators τ_x and τ_y which each induce reflection in their subscripted direction in conjunction with

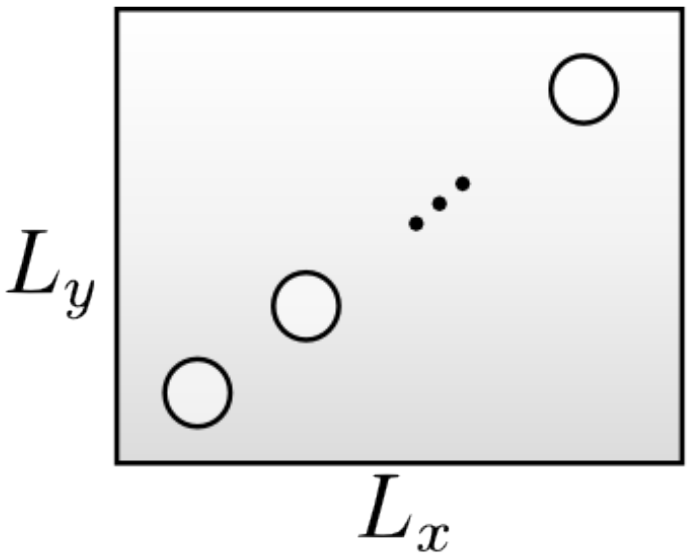

Figure 5.1: We use σ_I as a shorthand for the n-quasihole configuration $\sigma = +, +, \cdots, +$. This is the configuration in which the leftmost (first) quasihole is bottommost, the next to the right (second) is the next above, and so on.

α	Thin torus pattern	$f_1(\alpha)$	$f_2(\alpha)$	$f_3(\alpha)$
1	002**00**$\underline{\mathbf{1}}$101101**1**$\underline{\mathbf{0}}$**1**0110110**1**$\underline{\mathbf{1}}$**00**2002	$-s$	0	s
2	11011$\underline{\mathbf{0}}$**1**0110**1**$\underline{\mathbf{0}}$**0**2002002**0**$\underline{\mathbf{0}}$**1**10110	1	$-2+s$	$1-s$
3	1101**1**$\underline{\mathbf{0}}$**0**2002002$\underline{\mathbf{0}}$**0**1101**1**$\underline{\mathbf{0}}$**1**$\underline{\mathbf{0}}$110110	$-1+s$	$2-s$	-1
4	11011$\underline{\mathbf{0}}$**1**0110**1**$\underline{\mathbf{0}}$**1**0110**1**$\underline{\mathbf{0}}$**1**$\underline{\mathbf{0}}$110110	1	0	-1

Table 5.2: $c = 0$ thin torus patterns for a three-quasihole Gaffnian state, and the offset functions of the associated domain walls. The elementary domain wall strings are in bold, and the orbital positions, $3n_j$, are underlined. Patterns for $c = 1(-1)$ can be obtained by shifting each occupancy number one orbital to the right (left), and the shift functions obtained using $f_j(c, \alpha) = f_j(\alpha) + c$.

time reversal. These symmetries further constrain the ξ^σs.

$$\xi^{g_{\tau_x}(\sigma)} = (B_\tau)^{-1}\mathrm{diag}[e^{iL/3\sum_j \delta(\alpha,j)}](\xi^\sigma)^*\mathrm{diag}[e^{2\pi i/3\sum_j(1+\delta(\alpha,j)/\pi)f_j(\alpha)}], \tag{5.11}$$

$$\xi^{g_{\tau_y}(\sigma)} = \mathrm{diag}[e^{2\pi i/3\sum_j(1+\delta(\alpha,j)/\pi)f_j(\alpha)}](\xi^\sigma)^*\mathrm{diag}[e^{iL/3\sum_j \delta(\alpha,j)}]B_\tau. \tag{5.12}$$

In the above, $g_{\tau_x}(\sigma)$ is the configuration that results from starting with configuration σ and sending $x \to -x$; and similarly $g_{\tau_y}(\sigma)$ results from sending $y \to -y$. The matrix B_τ is defined as in Eq. (4.49) for $n = 3$, and is the identity for $n = 2$. Performing the operations τ_x and τ_y in succession on a system starting in the configuration σ_I gives σ_I again, i.e., $g_{\tau_y}(g_{\tau_x}(\sigma_I)) = \sigma_I$. In this way Eqs. (5.11) and (5.12) allow us to further constrain the elements of ξ^{σ_I}.

We adiabatically transport quasiholes along the same path as before (see Secs. 2.8, 4.2.3, and 4.3.3, as well as Fig. 2.6). In the following expression we do not specify the number of quasiholes, their configuration, or which adjacent pair is braided, though these must all be specified to find a particular braiding matrix. In general, the result of adiabatic transport, expressed as a matrix in the α vector space, is,

$$\begin{pmatrix} |\Psi_1\rangle \\ |\Psi_2\rangle \\ \vdots \\ |\Psi_n\rangle \end{pmatrix} \to e^{i\Phi_{\mathrm{AB}}}\Xi^\sigma(\Xi^{\sigma'})^\dagger \begin{pmatrix} |\Psi_1\rangle \\ |\Psi_2\rangle \\ \vdots \\ |\Psi_n\rangle \end{pmatrix}. \tag{5.13}$$

Here, Φ_{AB} is the Aharonov-Bohm phase, equal to the charge of a quasihole, $-1/3$,

times the area enclosed by the braiding path. The quantities $|\Psi_\alpha\rangle$ are the three-component column vectors with entires $|\psi_{c,\alpha}\rangle$. Ξ^σ is the matrix $\xi^\sigma \otimes M$ (where we identify the states $|\psi_{c,\alpha}\rangle$ with a formal tensor product basis $|\alpha\rangle \otimes |c\rangle$). σ is the initial configuration of the quasiholes, and σ' the other configuration that occurs during braiding (see Fig. 2.6), i.e., the one obtained from σ by crossing the line $h_{jx} = h_{ix}$ or the line $h_{jy} = h_{iy}$.

It turns out that the result of braiding is always block diagonal in the c labels, i.e., the braid matrix $\Xi^\sigma(\Xi^{\sigma'})^\dagger$ is of the form $\chi_i(n) \otimes \mathbb{I}_{c_{\max}\times c_{\max}}$, where we call $\chi_i(n) = \xi^\sigma(\xi^{\sigma'})^\dagger$ the "reduced" braid matrix associated with a counter-clockwise exchange of the i-th and $i+1$-st of n quasiholes. This fact is a direct consequence of translational invariance. Moreover, $\chi_i(n)$ is found to be independent of the initial configuration σ, as one would expect.

As before, a final set of constraint equations comes from the imposition of certain locality constraints on the braid matrix. The constraint equations, combined with the above symmetries, then lead to a discrete set of (usually intimately related) solutions for the statistics. We will discuss the full set of constraint equations and their solutions in App. C for the two-quasihole case, and in App. D for the three-quasihole case. Here we will summarize the results of this calculation by giving the (reduced) braid

matrices obtained from it for both two and three particles:

$$\begin{aligned}\chi_1(2) &= \xi^{+}(\xi^{-})^{\dagger} \\ &= e^{-i\pi/3}\begin{pmatrix} e^{-i\pi a} & & \\ & e^{i\pi a}\varphi^{-1} & e^{-2i\pi a}\varphi^{-1/2} \\ & e^{-2i\pi a}\varphi^{-1/2} & \varphi^{-1} \end{pmatrix},\end{aligned} \tag{5.14}$$

$$\begin{aligned}\chi_1(3) &= \xi^{\{++\}}(\xi^{\{0+\}})^{\dagger} \\ &= e^{-i\pi/3}\begin{pmatrix} e^{2i\pi a} & & & & \\ & e^{2i\pi a} & & & \\ & & & e^{i\pi a}\varphi^{-1} & e^{-2i\pi a}\varphi^{-1/2} \\ & & & e^{-2i\pi a}\varphi^{-1/2} & \varphi^{-1} \end{pmatrix},\end{aligned} \tag{5.15}$$

where $a = \pm 1/5$, and φ is the golden ratio, $\varphi = (1+\sqrt{5})/2$. The parameter s is found to have one of two values: $s = 2 - 3a/2$, one for each sign of a. Just as in the case of the $k = 3$ Read-Rezayi state discussed in Chapter 4 there are two solutions, which are related by an Abelian phase and complex conjugation. In the above, we have also fixed a gauge degree of freedom associated with unitary transformations.

Together with the locality constraint described above, these two matrices imply the result of braiding any adjacent pair in a state of n quasiholes. A "tensor representation" of the statistics just as discussed in Ref. [78] can then immediately be

constructed in complete analogy with Chapter 4.

5.2 Discussion

The two solutions obtained in the preceding section are related to one another simply by complex conjugation and an overall Abelian phase. They describe Fibonacci anyons and are thus closely related to those obtained for the $k = 3$ Read-Rezayi (RR) state in Chapter 4. In essence, the solutions obtained from the RR patterns and those obtained here are the same up to an Abelian phase. This statement excludes global exchange paths on the torus involving processes such as the ones depicted in Fig. 2.5, as we will further explain below. This close correspondence between the solutions found from RR and Gaffnian patterns is a manifestation of rank-level duality between the associated $\mathrm{SU}(2)_3$ and $\mathrm{SU}(3)_2$ fusion rules, respectively. This duality was also discussed by Ardonne [98] in terms of domain walls. It is manifest in the Bratteli diagrams of Fig. 5.2, which in the present context represent the rules for domain wall formation between ground state patterns for the respective states. Note, however, that there is a three-to-two correspondence between the RR and Gaffnian sectors, rather than one-to-one. This is so since each sector, i.e., each path in the Bratteli diagram, is threefold degenerate under translations in the Gaffnian case, but only twofold in the RR case. The correspondence between Gaffnian and RR sectors is perfect if we limit ourselves to the $n-1$ generators of the braid group $\sigma_{i,i+1}$, $i = 1, \ldots, n-1$, which exchange the i-th and $i+1$-st quasihole. These generate the full braid group in the

plane, but not on the torus. On the torus, these generators leave certain subspaces of topological sectors invariant, which all start and end in the same pattern in the topological sector label. These subspaces for the Gaffnian are then in correspondence with similar subspaces for the RR state, in the sense that there are isomorphisms between them that commute with braiding, except for an overall Abelian phase. This correspondence, however, gets spoiled by the inclusion of the remaining generators on the torus, which mix the subspaces. This happens differently for the Gaffnian and the RR case, since there are six such subsectors in the former case, but only four in the latter.

The subtle differences between our solutions for the Gaffnian and the RR case on the torus are of a piece with the difference in overall Abelian phase. It is well known that the overall Abelian phase could in principle assume any value in planar geometry, but on the torus, it is constrained by the topological degeneracies characterizing the state. In the coherent state method, one source of phase differences is the factor $i/3$ in the coherent state ansatz, Eq. (5.3), which is generally related to the "stride" of the domain wall in a given sector, which equals 3 in the present case and 2 in the RR case (compare Eq. (4.3)). This stride is of course identical to the center-of-mass degeneracy. In particular, one may see that the equations obtained from global processes shown in Fig. 2.5 are quite sensitive to this stride and the associated phase (see Eq. (C.1) in App. C). In view of the importance of these processes in our method, and the fact that they spoil the correspondence between Gaffnian and RR topological sectors as explained above, it may not be clear *a priori* that the consistency equations

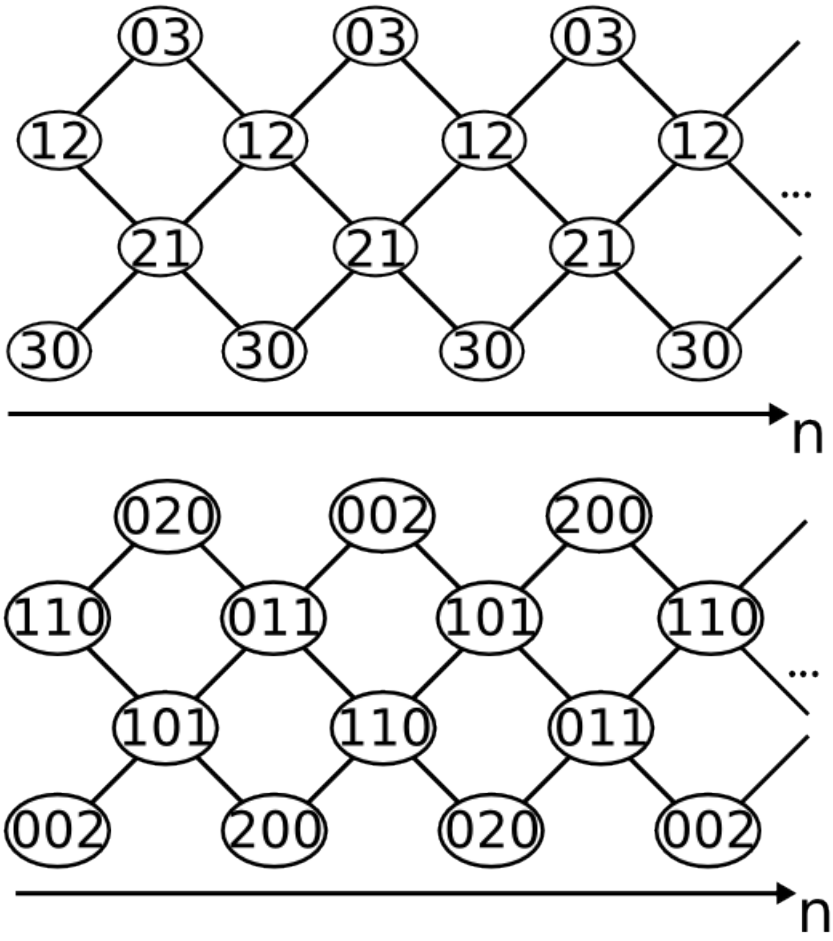

Figure 5.2: Bratteli diagrams depicting the $c = 0$ patterns in the RR state (top) and the Gaffnian (bottom). Valid topological sectors on the torus are represented by paths which start at the left, take one step right (either up or down) for each quasihole in the state, and end on the same type of ground state pattern—(200)-type or (011)-type—as they began, minding periodic boundary conditions. There is a one-to-one correspondence between the paths in the lower diagram and the patterns in Tables 5.1 and 5.2, and also between the valid paths in the upper and lower diagrams. This latter correspondence is how the $SU(2)_3$ and $SU(3)_2$ rank-level duality manifests in terms of patterns. It should be noted that for each sector which corresponds to a path in one of these diagrams, there is for RR an additional sector related to the first by translation, and two additional translated sectors for the Gaffnian.

we obtain in both cases admit closely related solutions, in the sense discussed. That this is so can be traced back to the fact that the translational degree of freedom, c, decouples early on (see below Eq. (5.5)), and the remaining α degree of freedom is fully analogous in both cases. This is how rank-level duality becomes manifest in the present formalism. For similar reasons, our solutions for the Gaffnian and RR states, which were both obtained at the maximum (bosonic) filling factor, could be generalized quite easily to lower filling factors.

As emphasized initially, the Fibonacci-type solutions we obtained are distinct from the anyon model associated with the conformal block monodromies of the Gaffnian state. The latter describes so-called Yang-Lee anyons, whose relation to Fibonacci anyons and the associated Galois duality has enjoyed much interest recently [99, 100]. Yang-Lee anyons are associated with nonunitary F-matrices consistent with the $\mathrm{SU}(3)_2$ fusion rules. It has been known for some time, however, that the same fusion rules admit unitary solutions of the Fibonacci type also; these are realized by the non-Abelian spin singlet (NASS) state of Ref. [101]. Indeed, it is not difficult to perform checks confirming that one of our solutions, that corresponding to $s = 17/10$, agrees exactly with the monodromies of the NASS state (including the overall phase). The dominance patterns of the NASS state have been discussed more recently [102], and it seems clear that the calculation presented here can be carried over to this state without essential changes. In all, this confirms once more for the case of $\mathrm{SU}(3)_2$ that the coherent state ansatz produces a subset of all unitary anyon models consistent with given fusion rules.

In the case of the unitary NASS state, our results support the usual conjecture that the holonomies associated with adiabatic transport agree with conformal block monodromies. In the case of the Gaffnian, things are more subtle. We have argued that in this case, provided that the coherent state ansatz is justified, the holonomies give rise to a well defined Fibonacci anyon statistics, possibly (given the twofold ambiguity of our solution) identical to those of the NASS state. In particular, we believe that our ansatz is indeed well justified if the gap of the Gaffnian parent Hamiltonian does not close in the charge sector. If so, this would presumably remain a formal property of the Gaffnian state that is not robust to perturbations, even ones that do not open a gap in the neutral sector. However, it might shine new light on the formal connections between the Gaffnian and the NASS state, which have been discussed previously [98].

Chapter 6

Zero Mode Counting

Counting the number of zero-mode states has been an integral part of the study of solvable FQH Hamiltonians on the sphere [58, 61, 62, 63, 64], where the counting is aided by the polynomial structure of the underlying wave functions. No such polynomial structure is apparent in the wave functions on the torus, however, so to count states on that topology another source of structure information is needed. Such information is provided by the thin torus patterns.

Using the method of Ref. [44], we will develop formulae to count the zero modes for each state studied in previous chapters. This method makes use of the fact that, by taking the zero-mode wave functions to the thin limit, both the position degeneracy of the quasiholes and the topological sector degeneracy are made manifest through the patterns. However, even though the thin limit is used, the results obtained do not depend in any way on the aspect ratio. Adiabatic continuity between the thin torus patterns and the bulk states ensures that the numbers of states in those two

regimes are identical. Using the patterns from the thin torus limit, we will derive formulae for the numbera of various states on the torus and on the sphere. Since the latter have been derived previously, the sphere results will serve as a useful check on the method.

Once again, we will begin with the simplest state, the $\nu = 1/2$ Laughlin state, and successively count the more complex MR, RR, and Gaffnian states.

6.1 $\nu = 1/2$ Laughlin counting

We will count the number of zero modes of fixed particle number N and number of domain walls n, which we call $\Phi(N, n)$. The number of orbitals in the LLL will be called L; the orbitals are numbered sequentially from 0 to $L - 1$. For the $\nu = 1/2$ Laughlin state [11], $L = 2N + n$ on the torus and $L = 2N + n - 1$ on the sphere.

To count the zero modes on the sphere, we will make use of strings of integers from the "prolate spheroid limit", the limit in which the sphere is stretched along some axis while keeping the surface area fixed. In this limit, integer patterns emerge. These are equivalent to the "dominance patterns" in the Jack polynomial representation of the wave functions on the sphere [51, 52, 53]. The sphere patterns are identical to the patterns in the thin torus limit of the same state, save for one key difference. On the torus, an FQH state has a set of degenerate ground state zero modes, whereas, on the sphere, one zero mode is the unique ground state. Just as quasiholes on the torus correspond, in the thin limit, to domain walls between ground state strings,

Thin torus patterns	Thin sphere patterns
0|01010	0|0101
0|0|0101	10|0|01
10|0|010	1010|0
010|0|01	|01010
1010|0|0	|010|01
|01010|0	10|010
|010|010	
0|010|01	
10|010|0	

Table 6.1: $\nu = 1/2$ Laughlin zero mode patterns on the thin torus and thin sphere, for $N = 2$ particles and $n = 2$ quasiholes. Domain wall positions are marked with |.

so too will quasiholes on the sphere correspond to domain walls between the *exact same* set of strings as on the torus. However, spherical boundary conditions dictate that each thin sphere pattern return to the unique ground state string at the left and right edges. Any pattern which has some non-ground-state string on the left (resp. right) edge is said to have a domain wall located at zero (L). As an example, recall from Chapter 2, the thin torus limits of the Laughlin ground states are 0101... and 1010..., and domain walls appear as additional zeros in ground state strings, e.g. 010|010 .... On the sphere, the ground state is 1010 . . . 1, and boundary conditions dictate that this string must appear at the left and right edges of each pattern. A detailed example is presented in Table 6.1, where, all the patterns for $N = 2$ particles and $n = 2$ domain walls are shown.

To derive the zero-mode counting formulae, we first enumerate the possible positions the n domain walls can take within a pattern, which we call "position degen-

eracy". We first consider the counting on the sphere before considering the torus. Domain walls take positions which are halfway between LLL orbitals—i.e., for the domain wall string $0\vert 0$, the domain wall is not coincident with the left or the right orbital, but is halfway between. A domain wall at the far left of the pattern is to the left of orbital 0 at position $-1/2$, and a domain wall at the far right is at position $L-1+1/2$. To simplify the notation, we will refer to the position of the ith domain wall shifted up by $1/2$ as w_i, for $0 \leq i \leq n-1$. The w_i are then integers characterized by the conditions,

$$\begin{aligned} 0 \leq w_0 < w_1 < \cdots < w_{n-1} \leq L, \\ w_{i+1} - w_i = 1 \mod 2. \end{aligned} \tag{6.1}$$

The enumeration of domain wall positions is implicit in Eq. (6.1). This enumeration can become explicit if we introduce integers $k_i = (w_i - i)/2$. In terms of the k_i, both conditions in Eq. (6.1) together become,

$$0 \leq k_0 \leq k_1 \leq \cdots \leq k_{n-1} \leq (L-n+1)/2 = N, \tag{6.2}$$

where the final equation at the right comes from the definition of L on the sphere. The number of ways to satisfy this constraint is the same as the number of n-item multisets—sets that allow repeated elements—with elements drawn from the integers 0 to N. The number of these is $\left(\!\binom{N+1}{n}\!\right)$, where $\left(\!\binom{m}{k}\!\right) = \binom{m+k-1}{k}$ is read "m multichoose

k". Thus the number of Laughlin states on the sphere is,

$$\Phi_{\substack{\text{Laughlin}\\\text{sphere}}}(N,n) = \left(\!\!\binom{N+1}{n}\!\!\right) = \binom{N+n}{n}. \tag{6.3}$$

This agrees with the formula in [61]. The example in Table 6.1 shows that there are six zero-mode patterns on the sphere for $N = 2$ and $n = 2$, and indeed we see that $\Phi(2,2) = 6$.

The zero-mode counting on the torus is very similar to that on the sphere, save that patterns need not only begin in the 10 ground state, but could also begin in the 01 ground state. To count the position degeneracy of the domain walls, we adopt the following procedure. We first consider a restricted subset of patterns of n domain walls, in which each element is a pattern with a domain wall fixed at the far left. In terms of the positions w_i, this restriction fixes $w_0 = 0$. We call this set S_1, with elements denoted s_1, and $|S_1| = \Phi_0(N,n)$ is the number of patterns in this restricted set. We wish to find the set of all patterns, which we can call S_2, and ultimately find the number of patterns $\Phi(N,n) = |S_2|$. We first construct a new set,

$$S_1 \times \overline{L-1} = \{(s_1, m) : s_1 \in S_1, m \in \{0, L-1\}\}. \tag{6.4}$$

The number of elements in this set is $\left|S_1 \times \overline{L-1}\right| = L\,|S_1|$. We can construct a

mapping from $S_1 \times \overline{L-1}$ onto the full set of patterns using the translation operator,

$$\begin{aligned} g : S_1 \times \overline{L-1} &\to S_2, \\ (s_1, m) &\mapsto T_m s_1. \end{aligned} \tag{6.5}$$

Said differently, the set $S_1 \times \overline{L-1}$ and the mapping allow us to construct all the patterns from those in the restricted set by successively translating each restricted pattern by m orbitals. In this way we generate patterns with domain walls fixed not just at zero but at m for $m \in \{0, L-1\}$. However, the set $S_1 \times \overline{L-1}$ contains multiple copies of each pattern in S_2. It is not difficult to see that,

$$\left|g^{-1}(s_2)\right| = n \forall s_2 \in S_2. \tag{6.6}$$

Thus, the total number of states is $|S_2| = \frac{L}{n}|S_1|$, or,

$$\Phi_{\substack{\text{Laughlin} \\ \text{torus}}}(N, n) = \frac{2N+n}{n}\Phi_0(N, n). \tag{6.7}$$

To find an expression for $\Phi_0(N, n)$, we proceed by enumerating the domain wall positional degeneracy as in the sphere counting. The domain wall positions w_i, $0 \leq i \leq n-1$, follow the conditions,

$$\begin{aligned} 0 = w_0 < w_1 < \cdots < w_{n-1} \leq L-1, \\ w_{i+1} - w_i = 1 \mod 2. \end{aligned} \tag{6.8}$$

As before, we introduce integers $k_i = (w_i - i)/2$, in terms of which Eq. (6.8) becomes,

$$0 = k_0 \leq k_1 \leq \cdots \leq k_{n-1} \leq N. \tag{6.9}$$

The number of these is the number of multisets of $n-1$ elements drawn from the integers 0 to N,

$$\Phi_0(N,n) = \left(\!\!\binom{N+1}{n-1}\!\!\right). \tag{6.10}$$

When we combine Eq. (6.10) with Eq. (6.7), we find the number of $\nu = 1/2$ Laughlin zero modes on the torus,

$$\Phi^{\text{Laughlin}}_{\text{torus}}(N,n) = \frac{2N+n}{N+n}\binom{N+n}{n}. \tag{6.11}$$

We find that $\Phi(2,2) = 9$, which agrees with the explicit enumeration in Table 6.1. We also notice that $\Phi(N,0) = 2$ for any N; this number agrees with the torus ground state degeneracy.

6.2 Moore-Read counting

The strategy for zero-mode counting demonstrated above can be generalized to more complicated states. However, such generalization is not completely straightforward. In the Abelian Laughlin case, the only zero-mode degeneracy that had to be enumerated was domain-wall positional degeneracy. In the non-Abelian cases, there is some

"internal degeneracy", insofar as specifying the positions of all the domain walls does not completely specify the state. We will develop in this section a means for counting the number of such states with domain walls at identical positions by examining the Bratteli diagram.

Recall from Chapter 3 the MR [23] thin torus ground states are $0202\ldots$, $2020\ldots$, and $1111\ldots$. The thin sphere ground state is $2020\ldots2$. We work with the bosonic $\nu = 1$ state with $L = N+n/2$ orbitals on the torus and $L = N+n/2-1$ on the sphere. As in the Laughlin case, the domain wall positions are halfway between orbitals, so we call w_i the position of the ith domain wall shifted up by $1/2$.

On the sphere, the positions of the domain walls follow the general inequality

$$0 \leq w_0 \leq w_1 \leq \cdots \leq w_{n-1} \leq L. \tag{6.12}$$

Equality between two adjacent domain wall positions w_i and w_{i+1} is only possible if the string separating domain walls i and $i+1$ has even length. In that case, $w_{i+1} - w_i = 0 \mod 2$. If the length of the string separating i and $i+1$ is odd, which can occur either for a 020- or a 111-type string, then $w_{i+1} - w_i = 1 \mod 2$ and the two can never coincide. We can, in a certain sense, classify zero modes according to the number of these odd-length strings occurring between all the domain walls in their patterns. Different patterns can still have the same positional degeneracy so long as they have the same number of odd-length strings between domain walls, as we can quickly show. We introduce integers $k_i = (w_i - \ell_i)/2$, where ℓ_i is the number

of odd-length strings left of domain wall i, and $\ell = \ell_{n-1}$ is the total number of odd-length strings in the pattern (since, on the sphere, the final string is always even in length). In terms of the k_is, Ineq. (6.12) and the two constraints that follow can be represented by,

$$0 \leq k_0 \leq k_1 \leq \cdots \leq k_{n-1} \leq (L-1-\ell)/2, \tag{6.13}$$

and the number of these multisets of the k_i is,

$$\left(\!\!\binom{\frac{L-1-\ell}{2}+1}{n}\!\!\right). \tag{6.14}$$

To find the total number of patterns, we need only know the number of patterns with ℓ odd-length strings for each allowed value of ℓ, then,

$$\Phi_{\substack{\text{MR}\\ \text{sphere}}}(N,n) = \sum_{\ell} \binom{\frac{L-1-\ell}{2}+n}{n} \times (\text{number of patterns with } \ell). \tag{6.15}$$

To determine the number of patterns with a certain ℓ, we examine the MR Bratteli diagram (see Fig. 6.1).

Recall that the sequences of ground state strings that define a pattern correspond to a certain path through the Bratteli diagram of a state. The links in the path correspond to the domain walls in the pattern. Each link in the path can be represented as a vector pointing either up-and-right or down-and-right. A "kink" occurs between any two successive links that differ in their up/down direction. Two domain walls in a pattern are separated by an odd-length string if and only if the corresponding links

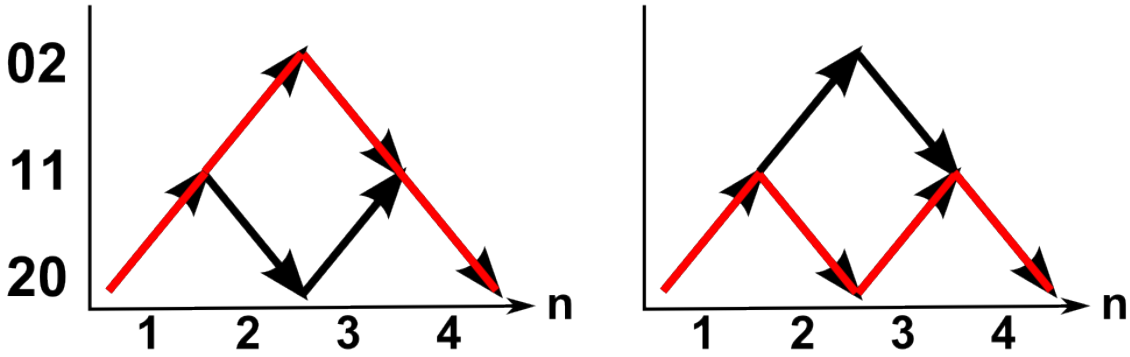

Figure 6.1: The Moore-Read state Bratteli diagram, with the paths for $n = 4$ links shown in red. The left path has one kink, and thus $\ell = 1$; the right path has $\ell = 3$ kinks. These paths correspond to patterns with even N

in that pattern's path have a kink between them. The number of patterns with ℓ odd-length strings is thus equal to the number of paths through the Bratteli diagram with ℓ kinks.

To find a formula for the number of paths with ℓ kinks, we will first introduce another integer F as follows. Every pattern of n domain walls must have at least $n/2 - 1 + \eta$ odd-length strings, where $\eta = 1$ when N is odd and 0 when N is even. This is so because, in the path corresponding to a pattern, every second link will come to an edge and must turn away, which produces a kink. The path with this minimum number of kinks will begin at the bottom row and always proceed from bottom to top and back, except for η (0 or 1) kinks in the middle row. A pattern with more odd-length strings will have "extra" kinks in the middle row. These always come in pairs, as adding an odd number of kinks to the middle would prevent the path from

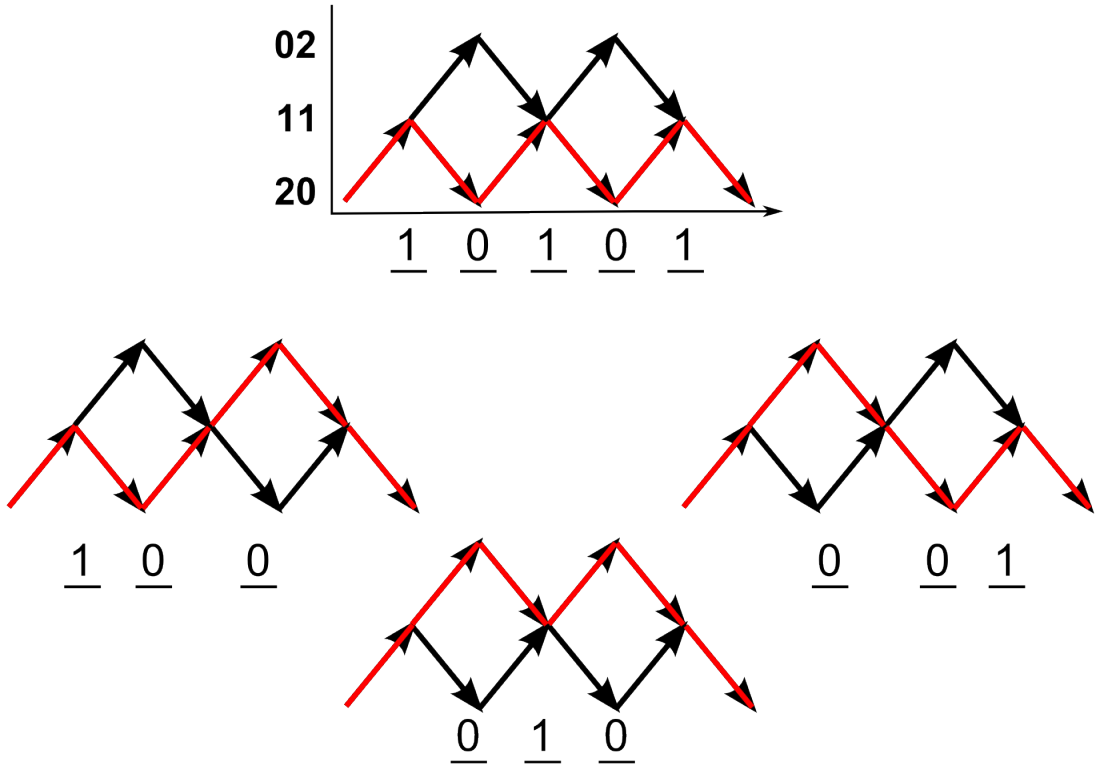

Figure 6.2: MR Bratteli diagram where paths with $n = 6$ links are shown in red. These correspond to patterns with n domain walls and N particles with N odd, which must be so because the number of kinks in the middle of each path is odd. The top path has $\ell = 5$, $F = 3$. Under the analogy it can be mapped to the Laughlin sphere ground state pattern. The bottom three paths have $\ell = 3$, $F = 1$. They can be mapped to Laughlin patterns with two domain walls.

ending at the proper edge. We call the number of kinks in the middle row F, where

$$F = \ell + 1 - n/2. \tag{6.16}$$

Now we have distinguished two different kinds of kinks: Those at the edges of the path, and those in the middle. This distinction will allow us to count the paths. We represent each path as a string of integers as follows. Each kink in the top or bottom row corresponds to a 0, and each kink in the middle corresponds to a 1 (see Fig. 6.2).

When we label the paths in this way, the numbers thus generated satisfy the $\nu = 1/2$ Laughlin generalized Pauli principle [103], in that there is no more than one particle in any two adjacent sites. We make an analogy in which the kinks represent "lattice sites" and the kinks in the middle are "occupied". Then the number of paths for a given n and ℓ (or, equivalently, n and F) is given by the number of Laughlin states with $L' = \ell$, $N' = F$, and $n' = L' - 2N' = n/2 - F$, where primed quantities are properties of the analog state. Plugging these into Eq. (6.3), we find that,

$$\Phi_{\substack{\text{Laughlin} \\ \text{sphere}}}(N' = F, n' = n/2 - F) = \binom{n/2}{F}. \tag{6.17}$$

With Eq. (6.17) and the appropriate substitution of F into Eq. (6.15), we find that the number of MR zero modes on the sphere is,

$$\Phi_{\substack{\text{MR} \\ \text{sphere}}}(N, n) = \sum_{F=N \mod 2} \binom{\frac{N-F}{2} + n}{n} \binom{n/2}{F}. \tag{6.18}$$

This agrees with the results derived in Ref. [61], in which a similar hierarchy approach—enumerating the internal degeneracy of a state using the full counting of a simpler state—was taken. In that reference, the author used the notation "n" for the number of quasihole pairs, which is $n/2$ here.

The number of MR zero modes on the torus can be found in a similar fashion to the MR zero modes on the sphere. As we did in the Laughlin case on the torus, we will first consider a restricted set of patterns. In this case, we only include those

patterns which have a domain wall fixed at zero as before, but also an odd-length string at the end of the pattern. The number of such patterns can be found by fixing the number of odd-length strings, ℓ, or equivalently fixing the number of kinks in the Bratteli diagram path. Then the number of patterns in the restricted set with a given number of kinks is the position degeneracy of the domain walls times the internal degeneracy, or,

$$\binom{\frac{L-\ell}{2}+n-1}{n-1} \times (\text{number of patterns with } \ell). \tag{6.19}$$

The number of patterns with ℓ odd-length strings can again be found from the Bratteli diagram paths with ℓ kinks. However, the paths with ℓ kinks on the torus will be superficially equivalent to the paths with $\ell - 1$ kinks on the sphere. On the torus, the two ends of each path must be joined together to enforce periodic boundary conditions[1]. All paths in the restricted subset will have a kink at the "zero" location where the ends of the path are joined. The definition of this set, including only those patterns with a domain wall at zero and an odd-length string at the end, is equivalent to including only those patterns with a domain wall at zero and which correspond to paths with a kink at zero. When such a path is shown as in our diagrams here, this kink will not be readily apparent, and so such a path will appear to have $\ell - 1$ kinks if the boundary conditions are not taken into account.

[1]When N is odd, a path which begins on the bottom row must end at the top row. To obey periodic boundary conditions, then, one must connect the two ends of the path with a twist when N is odd, equivalent to joining the Bratteli diagram not on an ordinary 2D strip but on a Möbius strip.

We again make an analogy to Laughlin patterns by marking 0s on all kinks in the top and bottom rows (including the kink at "zero"), and a 1 on all kinks in the middle row. The patterns thus generated are the Laughlin patterns on the torus, with $L' = \ell$, $N' = F$, (where $F = \ell - n/2$ is again the number of kinks in the middle row) and $n' = L' - 2N' = n/2 - F$.

To generate the full set of patterns from the restricted set, we follow a similar procedure as in the Laughlin torus case. We create a new set, in which we include each pattern in the restricted set translated $0, 1, \ldots, L-1$ times. Thus this set has L times as many patterns as the restricted set. But there will be ℓ preimages of each pattern under g. In the set language of Sec. 6.1,

$$\left|g^{-1}(s_2)\right| = \ell \forall s_2 \in S_2. \tag{6.20}$$

In Eq. (6.6), we found that $|g^{-1}(s_2)| = n \forall s_2 \in S_2$, which is not identical to Eq. (6.20). The behavior of Eq. (6.6) is actually special to the Laughlin case, in which an odd string follows every domain wall in the pattern and thus a kink follows every link in the path. For a given n in the Laughlin case, there is only a single ℓ, $\ell = n$, so Eq. (6.6) is a special case of Eq. (6.20).

Then the number of unique patterns is,

$$\Phi_{\substack{\text{MR}\\ \text{torus}}}(L, n) = \sum_{\ell} \frac{L}{\ell} \binom{\frac{L-\ell}{2} + n - 1}{n-1} \times \Phi_{\substack{\text{Laughlin}\\ \text{torus}}}(L' = \ell, N' = F, n' = n/2 - F), \tag{6.21}$$

or, equivalently,

$$\Phi_{\substack{\text{MR}\\\text{torus}}}(N,n) = \sum_{F=N \mod 2} \frac{2N+n}{\frac{N-F}{2}+n}\binom{\frac{N-F}{2}+n}{n}\binom{n/2}{F}. \tag{6.22}$$

This is equivalent to the result in Ref. [44], where the authors work with the fermionic $\nu = 1/2$ MR state rather than the bosonic $\nu = 1$ state. Eq. (6.22) gives the correct state counting for every case except $n = 0$. There, we expect the formula to give the ground state degeneracy, but instead $\Phi_{\text{MR,torus}}(N, n = 0) = 4$. In the next section we will need to use this formula when $n = 0$, so we will multiply the formula by a corrective factor. When N is even, the ground states are the three familiar $20\ldots$, $02\ldots$, and $11\ldots$ patterns; when N is odd, only $111\ldots$ is possible. So our corrective factor takes the form,

$$\left(\frac{3^{1-\eta}}{4}\right)^{\delta_{n,0}}, \tag{6.23}$$

where, again, $\eta = N \mod 2$.

6.3 $k = 3$ Read-Rezayi counting

The counting of the Read-Rezayi [58] zero modes will continue the trend started in previous sections. The patterns can be broken into groups with a certain number of odd-length strings, and the number in each group will be factorizable into a positional degeneracy term times an internal degeneracy term. The latter will be found by making an analogy to the MR patterns and using the formulae from the previous

section.

In Chapter 4 we saw that the RR thin torus ground state patterns are $3030\ldots$, $0303\ldots$, $2121\ldots$, and $1212\ldots$. The sphere ground state is $3030\ldots3$. There are $L = (2N+n)/3$ LLL orbitals on the torus, and $L = (2N+n)/3 - 1$ on the sphere. Domain walls occur halfway between orbitals, so w_i for $0 \leq i \leq n-1$ denotes the ith domain wall position shifted up by $1/2$.

To count the position degeneracy on the sphere, we follow the same procedure as in the MR case. Again, we define ℓ as the number of odd-length strings. For such states with a certain fixed ℓ, the number of patterns that are equivalent up to changes in domain wall positions is

$$\binom{\frac{L-1-\ell}{3}+n}{n}. \tag{6.24}$$

The number of such patterns will given by an analogy to the MR counting.

Here, we define $F = [3(\ell+1)-n]/2$. As in the MR case, F encodes the locations of kinks in the Bratteli diagram, but the encoding scheme is now different. If a link which leads into a kink is directed up (respectively, down), we label the kink by the number of rows between the kink and the top (bottom) row. See the top right of Fig. 6.3. Kinks that occur at the top or bottom edge rows are always labeled 0. Kinks in the two middle rows are labeled 2 or 1 depending on whether the incoming link points away from or towards the nearest edge row. The value of F for a given path is the sum over the integer labels on the kinks.

Again, we notice that the sequences of integers on the kinks form recognizable

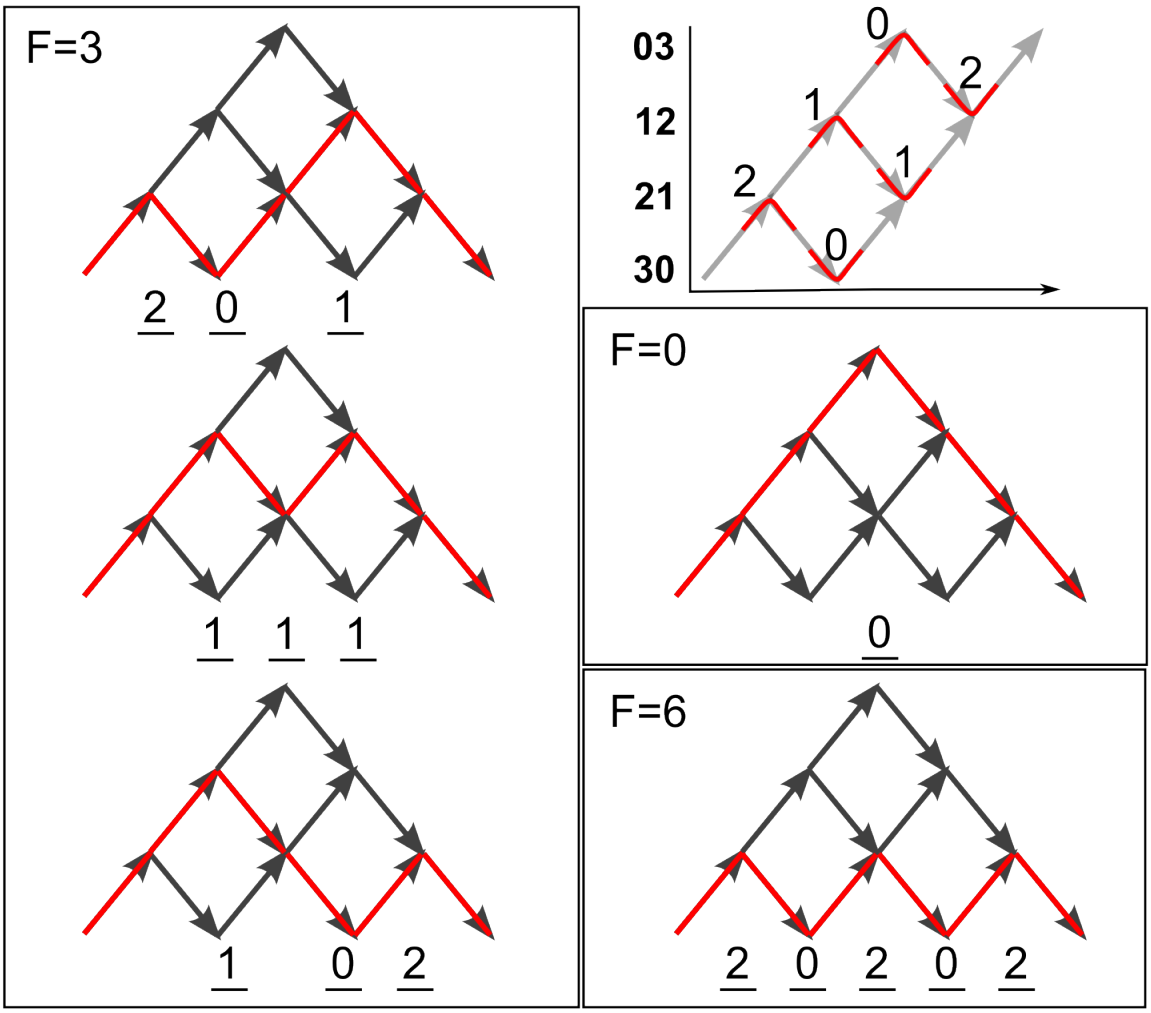

Figure 6.3: Boxed: The RR $n = 6$ paths for all the allowed values of F. Top right: A depiction of the labeling scheme for the kinks. A kink that occurs at some position with some orientation will be assigned an integer. Shown here are each possible position and orientation of kinks and the integers assigned to them.

patterns. In this case, the patterns thus formed satisfy the generalized Pauli principle for the MR states: no more than two particles in two sites. The number of paths with given n and F is then equal to $\Phi_{\substack{\text{MR}\\\text{sphere}}}$ with $L' = \ell$, $N' = F$, and $n' = 2(L' - N' + 1) = 2(n - F)/3$,

$$\Phi_{\substack{\text{MR}\\\text{sphere}}}(N' = F, n' = 2\frac{n-F}{3}) = \sum_{F'=F \mod 3} \binom{\frac{F-F'}{2} + 2\frac{n-F}{3}}{2\frac{n-F}{3}} \binom{\frac{n-F}{3}}{F'}. \tag{6.25}$$

When Eq. (6.25) is combined with Eq. (6.24), we can find the total number of zero modes,

$$\Phi_{\substack{\text{RR}\\\text{sphere}}}(N, n) = \sum_{F=N \mod 3} \binom{\frac{N-F}{3} + n}{n} \sum_{F'=F \mod 2} \binom{\frac{F-F'}{2} + 2\frac{n-F}{3}}{2\frac{n-F}{3}} \binom{\frac{n-F}{3}}{F'}. \tag{6.26}$$

This agrees with the formula in Ref. [61].

To count RR zero modes on the torus, we will once again need to first count a restricted subset of patterns which have a domain wall at zero and an odd-length final string. The paths corresponding to these patterns will again have a "hidden" kink at zero which comes from joining the two ends. If we follow the same general procedure as before, we claim that for a fixed value of ℓ, the number of zero modes is,

$$\Phi_{\substack{\text{RR}\\\text{torus}}}(L, n, \ell) = \frac{L}{\ell} \binom{\frac{L-\ell}{3} + n - 1}{n - 1} \times \Phi_{\substack{\text{MR}\\\text{torus}}}(L' = \ell, N' = F, n' = 2\frac{n-F}{3}). \tag{6.27}$$

where, on the torus, $F = (3\ell - n)/2$. Making the appropriate substitutions,

$$\Phi_{\substack{\text{RR}\\\text{torus}}}(N,n) = \frac{2N+n}{3} \sum_{F=N \mod 3} \binom{\frac{N-F}{3}+n-1}{n-1} \tag{6.28}$$

$$\times \sum_{F'=F \mod 2} \frac{2c}{\frac{F-F'}{2}+2\frac{n-F}{3}} \binom{\frac{F-F'}{2}+2\frac{n-F}{3}}{2\frac{n-F}{3}} \binom{\frac{n-F}{3}}{F'}, \tag{6.29}$$

where c is the correction factor from the end of Sec. 6.2,

$$c = \left(\frac{3^{1-\eta}}{4}\right)^{\delta_{n,F}}, \tag{6.30}$$

with $\eta = F \mod 2$. As in the MR case, the above formula does not give the correct result for $n = 0$. In fact, Eq. (6.28) with $n = 0$ has binomial coefficients with negative arguments, which cannot be easily remedied with a constant correction factor. But for every other value of $n > 0$ it produces the correct zero mode counting.

6.4 Gaffnian counting

The general strategy we have employed in each example thus far has been the following. We parametrize the zero modes by some ℓ, or equivalently some F, and each zero mode with the same F has the same positional degeneracy. Then we find the number of zero modes with a certain F via an analogy to another state lower down a "hierarchy" [61]. In our previous examples, this has been exactly the Read-Rezayi hierarchy [58]; the Laughlin state is $k = 1$ on the hierarchy, the Pfaffian is $k = 2$,

and the state we have just counted in Sec. 6.3 is $k = 3$. In terms of patterns, the analogy can be made manifest by labeling the Bratteli diagram paths of each zero mode with integers on the kinks; those integers form the patterns of the state lower in the hierarchy, for which we already have a counting formula.

A similar hierarchy approach will be employed to count the Gaffnian [59] zero modes. We will see that the position degeneracy of the zero modes can again be parametrized by some F, which can be used to find some labeling of the Bratteli diagram paths, and those in turn give rise to patterns in another state. However, the labeling strategy will not be the same as in previous cases.

The Gaffnian ground state patterns on the torus are the $200200\ldots$-type patterns, and the $011011\ldots$-type patterns. The ground state on the sphere is $200200\ldots2$. The number of orbitals in the LLL is $L = (3N-n)/2$ on the torus and $L = (3N-n)/2-2$ on the sphere. We adopt the convention that domain wall positions are located in the middle orbital of the three-orbital-wide domain wall string, e.g., $1\overset{\downarrow}{0}\overset{\uparrow}{0}$ and $0\overset{\downarrow}{1}\overset{\uparrow}{0}$. The Gaffnian domain wall positions are coincident with orbitals, unlike previous cases where the domain walls were halfway between orbitals. For this reason we change the labeling of the orbitals from $[0, L-1]$ to $[1, L]$. Then the domain wall positions w_i for $0 \leq i \leq n-1$ take values in the range $[0, L+1]$.

In the MR and RR cases, the positions w_i and w_{i-1} of two adjacent domain walls were, at minimum, separated by 1 or 0 orbitals if the string separating them was odd or even in length. In the Gaffnian case, different pairs of adjacent domain walls can at minimum be separated by 0, 1, or 2 orbitals, and this separation constant depends

not on properties of the adjoining string but only on the types of the two domain walls. Example patterns for each separation are $\ldots 20\overset{\downarrow}{1}1\overset{\downarrow}{0}020\ldots$, $\ldots 20\overset{\downarrow}{1}10\overset{\downarrow}{1}01\ldots$, and $\ldots 10\overset{\downarrow}{1}011\overset{\downarrow}{0}10\ldots$, respectively. We define the minimum separation between w_i and w_{i-1} as $g_i = w_i - w_{i-1} \mod 3$ for $1 \leq i \leq n-1$, and $g_0 = 0$. We define the cumulative separation $\ell_i = \sum_{j=0}^{i} g_j$, and $\ell = \ell_{n-1}$ (on the sphere). As before, regardless of any differences in the sequence of ground state strings that make up the pattern, two zero modes with the same ℓ will have the same degeneracy in domain wall position. The domain wall positions on the sphere obey the constraints,

$$\begin{gathered} 0 \leq w_0 \leq w_1 \leq \cdots \leq w_{n-1} \leq L+1 \\ w_i - w_{i-1} = g_i \mod 3. \end{gathered} \tag{6.31}$$

In terms of sequential integers $k_i = (w_i - \ell_i)/3$, Eq. (6.31) becomes the single constraint,

$$0 \leq k_0 \leq k_1 \leq \cdots \leq k_{n-1} \leq (L+1-\ell)/3. \tag{6.32}$$

Introducing the integer $F = [2(\ell+1) - n]/3$, the upper bound in (6.32) becomes $(N-F)/2$. The number of choices for the k_is is $\left(\!\!\binom{(N-F)/2+1}{n}\!\!\right) = \binom{(N-F)/2+n}{n}$.

Now we know the position degeneracy of each zero mode, parametrized by the integer F, but we need to know how many zero modes there are with that F. As before, we can find this by examining the paths through the Bratteli diagram. F corresponds to a certain labeling of each path, which is not in this case a labeling of integers on kinks. For the Gaffnian paths, F corresponds to the number of times the

path crosses the "center line" of the Bratteli diagram (see Fig. 6.4). On the sphere, since each path must begin at the bottom row and end either at the bottom row (if n is even) or top row (if n is odd), the maximum value of F is $F_{\max} = n-2$. (In fact, for $N < n$, the zero modes cannot make a pattern that corresponds to the maximally crossed path. The actual maximum value of F is $F_{\max} = \min(N, n-2)$.)

We will enumerate the paths with an analogy, which can be found as follows. For a given path, each kink that occurs in either of the the middle two rows is viewed as an empty "lattice site", whereas a kink at the top or bottom row is an "occupied" site. For instance, the "maximally crossed" state will have $F_{\max} - 1$ kinks, all in the middle two rows of the diagram. This path is analogous to a fully empty lattice. The paths for some other F, less than $F_{\max}$, are generated by "occupying" $(F_{\max} - F)/2$ kinks. Occupying a formerly unoccupied kink is equivalent to flipping a kink from row 1 to row 3 or from row 2 to row 0. Any kinks adjacent to the occupied one have now become straightened, and are no longer occupiable. The equivalent statement in terms of the analog pattern is that a 1 must be surrounded by 0s, and we see that the patterns formed in this way are Laughlin patterns. The analogous quantities are $L' = n-3$, $N' = (n-F)/2 - 1$, and $n' = F$. Note that in all analogies considered in previous Secs., F was a particle analog, i.e., $N' = F$. In this case F is a domain wall analog, i.e., $n' = F$. The internal degeneracy of the Gaffnian zero modes is thus given by the Laughlin formula in Eq. (6.3),

$$\Phi^{\text{Laughlin}}_{\text{sphere}}(N' = \frac{F_{\max} - F}{2}, n' = F) = \binom{\frac{n+F}{2} - 1}{F}. \tag{6.33}$$

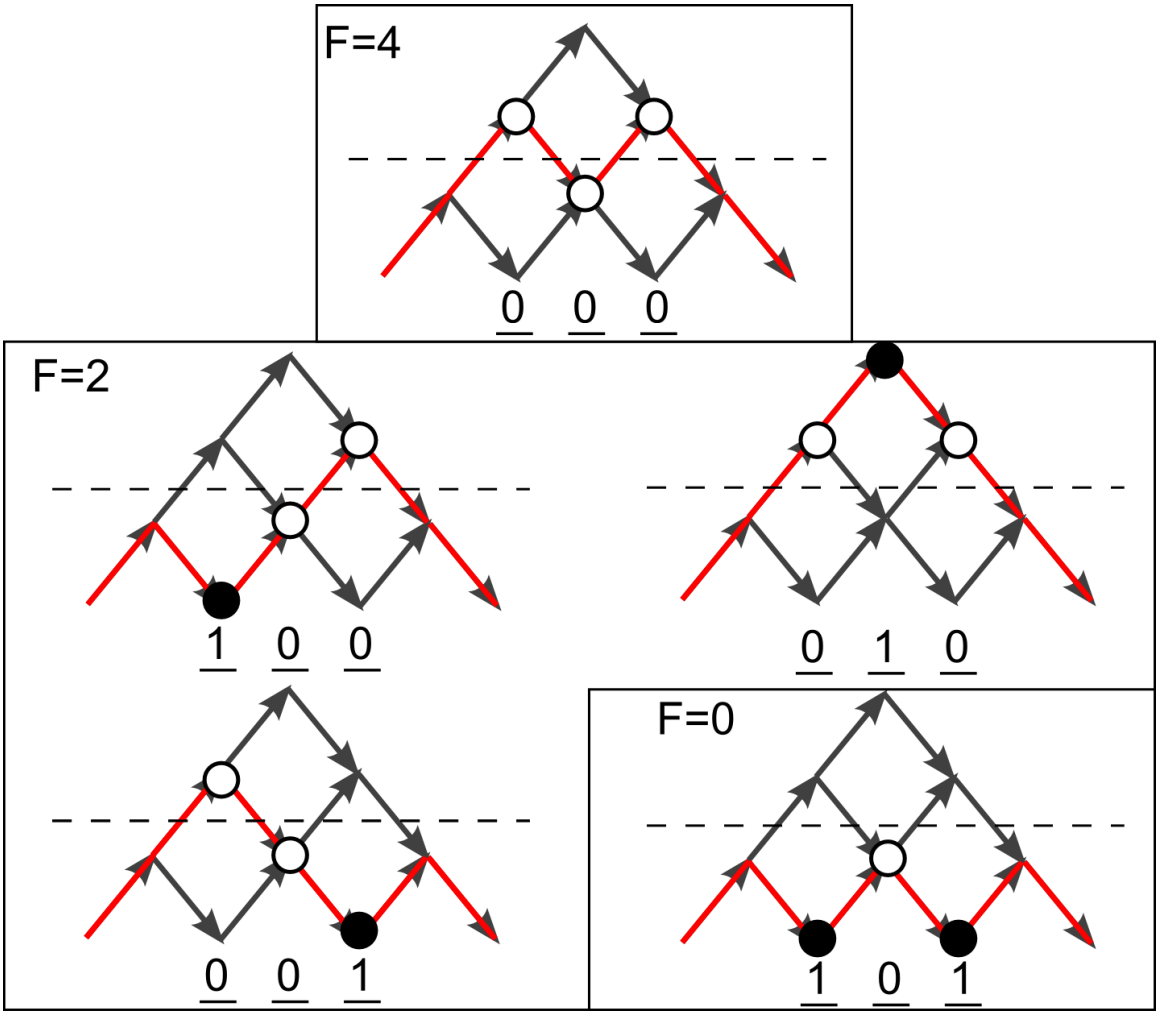

Figure 6.4: The $n = 6$ Gaffnian paths on the sphere. The paths are organized into groups with the same number of "center line" crossings, F. The $F = 4$, maximal crossing, path is shown with unfilled circles on its kinks, representing unoccupied "lattice sites" in a Laughlin analogy pattern. The lower values of F will "occupy" successively more of these sites, with occupied sites shown as filled circles. If one interprets the filled and unfilled circles as 0s and 1s respectively, the resulting patterns, shown below each path, are $\nu = 1/2$ Laughlin patterns on the sphere with F domain walls.

The number of Gaffnian states on the sphere is then,

$$\Phi^{\text{Gaffnian}}_{\text{sphere}}(N,n) = \sum_{F=n \mod 3} \binom{\frac{N-F}{2}+n}{n} \binom{\frac{n+F}{2}-1}{F}. \tag{6.34}$$

This result agrees with the formula in Ref. [59][2].

To find the Gaffnian formula on the torus, we make use of the the familiar procedure of previous Sections. We initially restrict ourselves to a set containing the patterns with a domain wall at zero which follows a kink in the path; we can enumerate these using a straightforward extension of the Gaffnian sphere counting method. To generate the full set of patterns, we translate each pattern in the restricted set all possible ways, which generates a set with L times the number of patterns as the restricted set. But this new set contains ℓ copies of each pattern having cumulative separation ℓ, so we divide by that number to correct the overcounting and sum over the allowed values of ℓ (or, equivalently, F). Some of the parameters on the torus are different, namely $F_{\max} = \min(N,n)$ since paths need not only begin and end at the edges of the diagram, and $\ell = \ell_n$ which accounts for the separation across the torus boundary between the "last" domain wall and the "first".

In the end, it can be shown that the number of Gaffnian states on the torus is given by,

$$\Phi^{\text{Gaffnian}}_{\text{torus}}(N,n) = \sum_{F=n \mod 3} \frac{3N+n}{\frac{N-F}{2}+n} \binom{\frac{N-F}{2}+n}{n} \frac{n}{n+F} \binom{\frac{n+F}{2}}{F}. \tag{6.35}$$

[2] In that reference, the author uses n to refer to the number of quasihole pairs, so our n is his $2n$.

This formula has the advantage that it can be made to give the correct state counting for $n = 0$. If we regard the term under the sum as an analytic function of n and take the limit $n \to 0$, then we find that $\Phi(N, n \to 0) = 6$, which agrees with the ground state degeneracy.

Appendix A

$k = 3$ Read-Rezayi solution: Two quasiholes

We begin with Eqs. (4.42) and (4.43), the locality and unitarity conditions, respectively, and seek to constrain the $\xi^{\sigma}_{\alpha,\alpha'}$ coefficients. As written, Eq. (4.43) does not provide information about the overall phase of ξ^{σ}, which is the overall phase relation between the two mutually dual bases. This phase is, *a priori*, arbitrary. We have, however, chosen a phase convention by defining the action of the antilinear operator τ for both bases (in agreement with the phase relation chosen in Eq. (2.4)). The symmetry under τ gave rise to Eq. (4.37), which we can use together with Eq. (4.30) (from the "global path" along x) to replace $(\xi^{+})^{\dagger}$ in favor of ξ^{+}, rewriting Eq. (4.43)

This appendix originally appeared in Ref. [7].

as

$$\xi^{+}\begin{pmatrix} p & 0 & 0 \\ 0 & p^{-1} & 0 \\ 0 & 0 & -1 \end{pmatrix}(\xi^{+})^{T}\begin{pmatrix} 0 & \Delta & 0 \\ \Delta & 0 & 0 \\ 0 & 0 & 1 \end{pmatrix}e^{-i\frac{\pi}{2}} = \mathbb{I}_{3\times 3}\ . \tag{A.1}$$

We will expand this matrix product by plugging the form Eq. (4.33) for ξ^{+} derived from global path constraints. This gives four independent constraint equations for the $\xi_{\alpha,\alpha'}$s:

$$\Delta p^{3}{\xi_{11}}^{2} + \Delta p{\xi_{12}}^{2} - \Delta p^{2}{\xi_{13}}^{2} = 0 \tag{A.2a}$$

$$\xi_{31}\left(-p^{2}\xi_{11} + \Delta p\xi_{12}\right) + p\xi_{13}\xi_{33} = 0 \tag{A.2b}$$

$$2\Delta p\xi_{11}\xi_{12} + p{\xi_{13}}^{2} = e^{i\frac{\pi}{2}} \tag{A.2c}$$

$$2p{\xi_{31}}^{2} - {\xi_{33}}^{2} = e^{i\frac{\pi}{2}} \tag{A.2d}$$

Recall $p = -\exp\left[i\pi(s+\frac{1}{2})\right]$ and $\Delta^{2} = 1$. Similarly, we may use Eq. (4.37) in the definition of the reduced braid matrix χ, Eq. (4.41), writing χ as $\xi^{+}(\xi^{+})^{T}$. Expanding the latter again with Eq. (4.33) and comparing the result to the locality constraint Eq. (4.42), we find two additional independent constraint equations:

$$(1+p^{2})\xi_{11}\xi_{12} - \Delta p{\xi_{13}}^{2} = 0 \tag{A.2e}$$

$$\xi_{31}\left(\xi_{11} - \Delta p\xi_{12}\right) + \xi_{13}\xi_{33} = 0\ . \tag{A.2f}$$

We will use the constraint equations (A.2) to solve for the unknown elements of χ, the dots in Eq. (4.42), which can be found from the expansion of the product $\xi^+(\xi^+)^T$ to be:

$$\xi_{11}{}^2 + \xi_{12}{}^2 + \xi_{13}{}^2 = \chi_{11} \tag{A.3a}$$

$$p^4\xi_{11}{}^2 + \xi_{12}{}^2 + p^2\xi_{13}{}^2 = \chi_{22} \tag{A.3b}$$

$$2p\xi_{31}{}^2 + \xi_{33}{}^2 = \chi_{33} \tag{A.3c}$$

$$\Delta\xi_{31}\left(-p^3\xi_{11} + \Delta\xi_{12}\right) - \Delta p\xi_{13}\xi_{33} = \chi_{23} = \chi_{32} \tag{A.3d}$$

We can break the solution of Eqs. (A.2) into two major sections, which are based on the two ways to satisfy the equation we obtain by combining Eqs. (A.2e) and (A.2a):

$$p^2\xi_{11}{}^2 + \xi_{12}{}^2 - \Delta\xi_{11}\xi_{12} - \Delta p^2\xi_{11}\xi_{12} = 0 \tag{A.4}$$

There are two solutions to this equation:

$$\xi_{12} = \Delta p^2\xi_{11} \tag{A.5a}$$

$$\text{or } \xi_{12} = \Delta\xi_{11}\,. \tag{A.5b}$$

We will now show that the first of the above equations never leads to consistent independent solutions, except in the special case $\xi_{13} = 0$. To see this, we feed Eqs.

(A.5) back into Eq. (A.2e), and find, respectively, that

$$\xi_{13}{}^2 = p^2(p+p^{-1})\xi_{11}{}^2 \tag{A.6a}$$

$$\text{or } \xi_{13}{}^2 = (p+p^{-1})\xi_{11}{}^2\,. \tag{A.6b}$$

We first utilize the above to study all cases with $\xi_{13} = 0$. This implies either $\xi_{11} = 0$, or $p \in \{i, -i\}$. The former leads to a contradiction in Eq. (A.2c). It is then straightforward to show that for $p \in \{i, -i\}$, the solutions of the system (A.2) produce the braid matrix

$$\chi = e^{-i\frac{\pi}{2}} \begin{pmatrix} \mp p & 0 & 0 \\ 0 & \mp p & 0 \\ 0 & 0 & 1 \end{pmatrix}, \tag{A.7}$$

with the upper (lower) sign corresponding to Eq. (A.5a) (Eq. (A.5b)). Equation (A.7) corresponds to a consistent solution to the constraint equations (A.2). However, when Eq. (A.7) is generalized to an n-quasihole system using the locality arguments of Sec. 3.5, it is not difficult to see that the resulting braid matrix violates the Yang-Baxter equation. While this might suffice to rule out this solution, we have emphasized in the beginning that our approach requires no *a priori* assumption that any aspect of quasiparticle exchange is topological. We will thus show more directly in App. B that Eq. (A.2) leads to contradictions in the present framework when three quasiholes are considered. Since we can rule out the special solution leading to the upper sign in Eq. (A.7), this case has not been mentioned in the main text.

We now proceed by exploring solutions with $\xi_{13} \neq 0$. We first show that Eq. (A.5a) does not lead to further independent solutions. To this end, we plug Eqs. (A.5) first into Eq. (A.2f),

$$\xi_{13}\xi_{33} = -(1-p^3)\xi_{31}\xi_{11} \tag{A.8a}$$

$$\text{or } \xi_{13}\xi_{33} = -(1-p)\xi_{31}\xi_{11}\,, \tag{A.8b}$$

and similarly into Eq. (A.2b):

$$\xi_{13}\xi_{33} = -(p^2-p)\xi_{31}\xi_{11} \tag{A.9a}$$

$$\text{or } \xi_{13}\xi_{33} = -(1-p)\xi_{31}\xi_{11}\,. \tag{A.9b}$$

While Eqs. (A.8b) and (A.9b) are identical, Eqs. (A.8a) and (A.9a) turn out to be consistent with one another only in cases where both sides vanish on both equations. We have already discussed all cases with $\xi_{13} = 0$. To satisfy Eqs. (A.8a) and (A.9a), we may thus focus on the case $\xi_{33} = 0$. On the right-hand side, we can rule out $\xi_{31} = 0$ because, with $\xi_{33} = 0$, it contradicts Eq. (A.2d). We can similarly rule out $\xi_{11} = 0$ because, with Eq. (A.5) and Eq. (A.6), it violates Eq. (A.2c). The only other way to solve both Eqs. (A.8a) and (A.9a) is to have $p = \pm 1$. In this case, however, both equations (A.5) are identical. Thus, Eq. (A.5a) does not produce independent valid solutions, except for $p \in \{i, -i\}$, leading to the braid matrix Eq. (A.7) (upper sign). As mentioned, the latter leads to inconsistencies in the case of three quasiholes.

To find the solution to the constraints (A.2) that will be consistent with the three-quasihole case, we now discard Eq. (A.5a) and proceed to work from Eq. (A.5b), and the equations (A.6b), (A.8b) derived from it. First, we plug Eqs. (A.5b) and (A.6b) into Eq. (A.2c), which will give us an explicit form for ${\xi_{11}}^2$:

$$ {\xi_{11}}^2 = \frac{e^{i\pi/2}}{(1+p)^2} \,. \tag{A.10} $$

In particular $\xi_{11} \neq 0$. From Eq. (A.8b) we thus obtain

$$ \begin{aligned} (1-p)^2 {\xi_{31}}^2 &= \frac{{\xi_{13}}^2}{{\xi_{11}}^2} {\xi_{33}}^2 \\ &= (p+p^{-1}) {\xi_{33}}^2 \,, \end{aligned} \tag{A.11} $$

where we have used Eq. (A.6b). Elimination of ξ_{33} by means of Eq. (A.2d) then gives

$$ \begin{aligned} {\xi_{31}}^2 &= (p+p^{-1}) \frac{e^{i\pi/2}}{(1+p)^2} \\ &= (p+p^{-1}) {\xi_{11}}^2 \end{aligned} \tag{A.12} $$

We can now revisit the unknown elements of χ. We rewrite Eq. (A.3) using the

equations we have developed above.

$$p^{-1}(1+p)^2{\xi_{11}}^2 = \chi_{11} \tag{A.13a}$$

$$p(p+p^{-1}-1)(1+p)^2{\xi_{11}}^2 = \chi_{22} \tag{A.13b}$$

$$(p+p^{-1}-1)(1+p)^2{\xi_{11}}^2 = \chi_{33} \tag{A.13c}$$

$$\Delta(1-p)(1+p)^2\xi_{31}\xi_{11} = \chi_{23} = \chi_{32} \tag{A.13d}$$

We need only plug into Eq. (A.13d) the square root of Eq. (A.12) to write each element of χ in terms of ${\xi_{11}}^2$, for which we have the expression in Eq. (A.10). We can also absorb the Δ factor in Eq. (A.13d) into the $\pm$ induced by taking this square root. Thus we reach the following form of the braid matrix

$$\chi = e^{i\frac{\pi}{2}} \begin{pmatrix} p^{-1} & 0 & 0 \\ 0 & p(p+p^{-1}-1) & \pm\sqrt{p+p^{-1}}(1-p) \\ 0 & \pm\sqrt{p+p^{-1}}(1-p) & p+p^{-1}-1 \end{pmatrix}, \tag{A.14}$$

which was presented in the main text as Eq. (4.44).

Appendix B

$k = 3$ Read-Rezayi solution: Three quasiholes

Here we will solve a system of equations for the elements of the three-quasihole transition matrix elements $\xi_{\alpha,\alpha'}$ and the resulting braid matrix. The procedure is the same as that employed for two quasiholes: Using various constraints on ξ^{σ} already derived in the main text, we write out the matrix elements of the unitarity equation, $\xi^{++}(\xi^{++})^{\dagger} = \mathbb{I}_{4\times 4}$, and the locality constraint Eq. (4.45). This gives a system for the remaining unknown elements of ξ^{++}. However, we must recall that the form in Eq. (4.45) was based, in part, on the two-quasihole braid matrix Eq. (4.44). In App. A we found one other "special" solution for this matrix, namely Eq. (A.7) (upper sign), that was not presented in the main text. Here we will consider this special solution also, giving rise to a modified version of Eq. (4.45), and show that this solution

This appendix originally appeared in Ref. [7].

leads to inconsistencies with three-quasihole braiding.

Just as we did in App. A, we first use the (antilinear) mirror symmetry to eliminate complex conjugation from the definition of the reduced braid matrix, $\chi = \xi^{++}(\xi^{-+})^\dagger$. This is achieved by using Eqs. (4.50) and (4.58). The result is

$$\chi = \xi^{++} \begin{pmatrix} \tilde{\Delta}^2 p & & & \\ & p^{-1} & & \\ & & -1 & \\ & & & -1 \end{pmatrix} (\xi^{++})^T \begin{pmatrix} & \tilde{\Delta}^{-1} & & \\ \tilde{\Delta}^{-1} & 0 & & \\ & & 1 & \\ & & & 1 \end{pmatrix} e^{-i\pi\lambda + i\pi}. \quad \text{(B.1)}$$

We will expand this matrix product using the constrained form of ξ^{++} in Eq. (4.62), reproduced here:

$$\xi^{++} = \begin{pmatrix} \xi_{11} & \tilde{\Delta}^2\xi_{13} & \xi_{13} & \xi_{14} \\ \tilde{\Delta}^2\xi_{13} & \tilde{\Delta}^2 p^2 \xi_{11} & -\tilde{\Delta}^{-1} p \xi_{13} & -\tilde{\Delta}^{-1} p \xi_{14} \\ \xi_{13} & -\tilde{\Delta}^{-1} p \xi_{13} & \tilde{\Delta}^2 p^2 \xi_{11} & -\tilde{\Delta} p \xi_{14} \\ \xi_{41} & -\tilde{\Delta}^{-1} p \xi_{41} & -\tilde{\Delta} p \xi_{41} & \xi_{44} \end{pmatrix}, \quad \text{(B.2)}$$

where we recall $\tilde{\Delta}^4 = 1$, and p is defined in terms of the shift parameter s as before. We gain a system of constraint equations for the $\xi_{\alpha,\alpha'}$s by plugging Eq. (B.2) into Eq. (B.1) and equating the product to one of the following expressions for χ that have been derived from locality and from consistency with the two-quasihole solution. For generic parameter p, we found that the latter must be of the form Eq. (4.45), which

we reproduce here as

$$\chi_{\text{loc}} = e^{i\frac{\pi}{2}} \begin{pmatrix} . & & & \\ & . & & \\ & & p(p+p^{-1}-1) & \pm\sqrt{p+p^{-1}}(1-p) \\ & & \pm\sqrt{p+p^{-1}}(1-p) & p+p^{-1}-1 \end{pmatrix}, \tag{B.3}$$

with blanks denoting zeros. The 2x2 block in the above was taken directly from the two-quasihole solution, Eq. (A.14), as explained in the main text. For $p \in \{i, -i\}$, however, we found an additional solution to the two-quasihole system of equations, leading to the form of the braid matrix Eq. (A.7). Using this form and the same reasoning that lead to Eq. (B.3), for $p \in \{i, -i\}$ the reduced braid matrix must be of the form

$$\chi_{\text{loc}} = e^{-i\frac{\pi}{2}} \begin{pmatrix} . & & & \\ & . & & \\ & & \mp p & \\ & & & 1 \end{pmatrix}, \tag{B.4}$$

where the lower sign is just a special case of Eq. (B.3), but the upper sign corresponds to the "special" solution.

We equate χ_{loc} to Eq. (B.1). We first focus on those matrix elements for which χ_{loc} is identically zero in all cases. By means of Eq. (B.2), this gives rise to the following three equations:

$$\tilde{\Delta}(p-p^2){\xi_{13}}^2+\tilde{\Delta}^{-1}p^3{\xi_{11}}^2-\tilde{\Delta}p^2{\xi_{14}}^2=0 \tag{B.5a}$$

$$\tilde{\Delta}^{-1}p{\xi_{13}}^2+(p^3-p^2)\xi_{11}\xi_{13}-\tilde{\Delta}^{-1}p^2{\xi_{14}}^2=0 \tag{B.5b}$$

$$\xi_{41}\left(-p^2\xi_{11}+\tilde{\Delta}^{-1}(p-p^2)\xi_{13}\right)+\tilde{\Delta}^2p\xi_{14}\xi_{44}=0. \tag{B.5c}$$

We will also use equations gained from enforcing the unitarity of ξ^{++}. If we expand $\xi^{++}(\xi^{++})^\dagger=\mathbb{I}_{4\times4}$ using Eq. (B.2) we find the following independent equations:

$$|\xi_{11}|^2+2\,|\xi_{13}|^2+|\xi_{14}|^2=1 \tag{B.5d}$$

$$3\,|\xi_{41}|^2+|\xi_{44}|^2=1 \tag{B.5e}$$

$$\xi_{41}\left({\xi_{11}}^*-2\tilde{\Delta}p{\xi_{13}}^*\right)+{\xi_{14}}^*\xi_{44}=0 \tag{B.5f}$$

$$\tilde{\Delta}^2\xi_{13}{\xi_{11}}^*+p^2\xi_{11}{\xi_{13}}^*-\tilde{\Delta}^{-1}p\,|\xi_{13}|^2-\tilde{\Delta}^{-1}p\,|\xi_{14}|^2=0 \tag{B.5g}$$

For convenience, we may also write the unitarity condition in the form $(\xi^{++})^\dagger\xi^{++}=\mathbb{I}_{4\times4}$, yielding a similar (and equivalent) set of equations, one of them being $3\,|\xi_{14}|^2+|\xi_{44}|^2=1$. By comparison with Eq. (B.5e), this implies

$$|\xi_{14}|^2=|\xi_{41}|^2\ . \tag{B.6}$$

Once the $\xi_{\alpha,\alpha'}$ are known, Eq. (B.1) allows us to obtain the following expressions for

the unknown elements of χ:

$$\chi_{11} = \chi_{22} = \left(2\tilde{\Delta}^{-1} p\xi_{11}\xi_{13} + \tilde{\Delta}^2 p{\xi_{13}}^2 + \tilde{\Delta}^2 p{\xi_{14}}^2\right) e^{-i\pi\lambda + i\pi} \tag{B.7a}$$

$$\chi_{33} = \left(-p^4{\xi_{11}}^2 + 2\tilde{\Delta}^2 p{\xi_{13}}^2 - \tilde{\Delta}^2 p^2{\xi_{14}}^2\right) e^{-i\pi\lambda + i\pi} \tag{B.7b}$$

$$\chi_{44} = \left[\tilde{\Delta}^2(2p - p^2){\xi_{41}}^2 - {\xi_{44}}^2\right] e^{-i\pi\lambda + i\pi} \tag{B.7c}$$

$$\chi_{34} = \chi_{43} = \left[\xi_{41}\left(\tilde{\Delta}^{-1} p^3\xi_{11} + 2\tilde{\Delta}^2 p\xi_{13}\right) + \tilde{\Delta} p\xi_{14}\xi_{44}\right] e^{-i\pi\lambda + i\pi}. \tag{B.7d}$$

If we subtract Eq. (B.5b) (times $\tilde{\Delta}^2$) from Eq. (B.5a), the resultant equation can be solved two ways.

$$\xi_{13} = -\tilde{\Delta} p\xi_{11} \tag{B.8a}$$

$$\text{or } \xi_{13} = \tilde{\Delta}\xi_{11} \tag{B.8b}$$

We can quickly eliminate one of these possibilities by comparing to the equations from unitarity. When Eqs. (B.8) are put into Eq. (B.5g), they respectively produce the equations

$$|\xi_{14}|^2 = -3\,|\xi_{11}|^2 \tag{B.9a}$$

$$\text{or } |\xi_{14}|^2 = |\xi_{11}|^2\left(p + p^{-1} - 1\right). \tag{B.9b}$$

Whereas we can put Eqs. (B.8) into Eq. (B.5d) and get the same equation for both

cases:

$$|\xi_{14}|^2 = -3\,|\xi_{11}|^2 + 1\,, \tag{B.10}$$

which clearly contradicts Eq. (B.9a). Thus Eqs. (B.8a) and (B.9a) are not true. Eliminating $|\xi_{14}|^2$ from Eqs. (B.9b) and (B.10) gives us an expression for $|\xi_{11}|^2$, which we can turn into an expression for ${\xi_{11}}^2$ with the inclusion of some phase θ_1.

$${\xi_{11}}^2 = \frac{e^{i\theta_1}p}{(1+p)^2}\,. \tag{B.11}$$

Furthermore, putting Eq. (B.8b) into either Eq. (B.5a) or Eq. (B.5b) gives:

$${\xi_{14}}^2 = \tilde{\Delta}^2(p + p^{-1} - 1)\,{\xi_{11}}^2 \tag{B.12}$$

which fixes the phase between ${\xi_{14}}^2$ and ${\xi_{11}}^2$. Together with Eq. (B.6), this also implies

$${\xi_{41}}^2 = e^{2i\theta_2}\tilde{\Delta}^2(p + p^{-1} - 1)\,{\xi_{11}}^2\,, \tag{B.13}$$

where we introduced another phase θ_2. Assuming first that $\xi_{14} \neq 0$, we define $e^{i\theta_2} = \xi_{41}/\xi_{14}$ (cf. Eq. (B.6)), we may solve Eq. (B.5c) for ξ_{44}:

$$\xi_{44} = (2p-1)\tilde{\Delta}^2 e^{i\theta_2}\xi_{11}\,. \tag{B.14}$$

It is easy to see that the last equation also holds in cases where $\xi_{14} = \xi_{41} = 0$.[1] With

[1] In this case, Eqs. (B.5d), (B.8b) imply $|\xi_{11}| = 1/\sqrt{3}$, and $|\xi_{44}| = 1$ from Eq. (B.5e). From Eq. (B.12), we must then have $p + p^{-1} - 1 = 0$, hence $(2p-1)^3 = -3$. The absolute values in

Eqs. (B.8b), (B.12), (B.13), and (B.14) we can rewrite the unknown elements of χ in terms of ${\xi_{11}}^2$, and Eqs. (B.7) become

$$\chi_{11} = \chi_{22} = (1+p)^2 {\xi_{11}}^2 e^{-i\pi\lambda + i\pi} \tag{B.15a}$$

$$\chi_{33} = p(1-p)(1+p)^2 {\xi_{11}}^2 e^{-i\pi\lambda + i\pi} \tag{B.15b}$$

$$\chi_{44} = e^{2i\theta_2}(1-p)(1+p)^2 {\xi_{11}}^2 e^{-i\pi\lambda + i\pi} \tag{B.15c}$$

$$\chi_{34} = \chi_{43} = e^{i\theta_2}\sqrt{p+p^{-1}-1}(1+p)^2 {\xi_{11}}^2 e^{-i\pi\lambda + i\pi} \tag{B.15d}$$

Or, using Eq. (B.11),

$$\chi = e^{i\theta} \begin{pmatrix} p & & & \\ & p & & \\ & & p^2(1-p) & e^{i\theta_2}p^2\sqrt{p+p^{-1}-1} \\ & & e^{i\theta_2}p^2\sqrt{p+p^{-1}-1} & e^{2i\theta_2}p(1-p) \end{pmatrix} \tag{B.16}$$

where we have defined $e^{i\theta} = e^{i\theta_1 - i\pi\lambda + i\pi}$. This is the result quoted in the main text as Eq. (4.63). It is worth noting that once again, the δ parameters have dropped out. The derivation of Eq. (B.11) is valid irrespective of the value of p, since we have thus far not used the diagonal matrix elements of χ_{loc}, which may take on special values for $p \in \{i, -i\}$. We are now able to rule out $p \in \{i, -i\}$, and thus the "special" solution obtained in App. A. For in this case, Eq. (B.16) has non-zero off-diagonal matrix

Eq. (B.14) therefore work out, and Eq. (B.14) must thus hold for some phase θ_2, which is then defined through this equation.

elements, whereas Eq. (B.4) does not. This justifies Eqs. (4.44) and (4.45) in the main text, which ignore the "special" solution. Requiring consistency between the non-zero matrix elements of Eqs. (4.45) and (4.63), which we have not done in this Appendix, finally provides information about the phase p, relating it to the golden mean. This short argument is presented in the main text.

Appendix C

Gaffnian solution: Two quasiholes

The set of constraint equations to solve for the reduced braid matrix come from enforcing the unitarity of the ξ matrices, the locality condition discussed in the main text, and the global path relations Eqs. (5.9) and (5.10). We will begin by enforcing the latter. As discussed above, we can apply Eqs. (5.9) and (5.10) in succession to constrain ξ^{σ_I} because $\sigma_I = g_y(g_x(\sigma_I))$. Applying these two equations, with the data from Table 5.1, results in the constraint equation

$$\xi^{\sigma_I} = \begin{pmatrix} & \Delta p^{-1} & \\ \Delta p & 0 & \\ & & -1 \end{pmatrix} \xi^{\sigma_I} \begin{pmatrix} & \Delta p & \\ \Delta p^{-1} & 0 & \\ & & -1 \end{pmatrix}, \tag{C.1}$$

where $p = -\exp[-2\pi i(1+s)/3]$, $\Delta = \exp[-2\pi i(L/2+1)D/3]$, and $D = 0$ or 1 if the δ parameter for the 100-type domain walls is 0 or π, respectively. Equation (C.1)

This appendix originally appeared in Ref. [60].

is satisfied when

$$\xi^{\sigma_I} = \begin{pmatrix} \xi_{11} & \xi_{12} & \xi_{13} \\ \xi_{12} & p^2\xi_{11} & -\Delta p\xi_{13} \\ \xi_{31} & -\Delta p\xi_{31} & \xi_{33} \end{pmatrix}. \tag{C.2}$$

Mirror symmetry, Eqs. (5.11) and (5.12), can also produce a constraint equation because $g_{\tau_y}(g_{\tau_x}(\sigma_I)) = \sigma_I$. However, in the case of two quasiholes, applying Eqs. (5.11) and (5.12) in succession results in the trivial equation, $\xi^{\sigma_I} = \xi^{\sigma_I}$.

The process of solving for the reduced braid matrix is similar to the solution given for $n = 2$ in Ref. [7]. We gain the following equations by demanding that ξ^{σ_I} is unitary,

$$e^{i\pi/3} = 2\Delta\eta^{-D}p\xi_{11}\xi_{12} + \eta^D p{\xi_{13}}^2, \tag{C.3a}$$

$$e^{i\pi/3} = 2\eta^D p{\xi_{31}}^2 - {\xi_{33}}^2, \tag{C.3b}$$

$$0 = \Delta\eta^{-D}p^3{\xi_{11}}^2 + \Delta\eta^{-D}p{\xi_{12}}^2 - \Delta\eta^D p^2{\xi_{13}}^2, \tag{C.3c}$$

$$0 = \eta^{-D}\xi_{31}\left(-p^2\xi_{11} + \Delta p\xi_{12}\right) + \eta^D p\xi_{13}\xi_{33}, \tag{C.3d}$$

where $\eta = \exp(-2\pi i/3)$. Two additional equations come from the requirement that braiding is local; as said above, this means that the result of braiding should only depend on the sequence of three ground-state patterns forming the two domain walls associated with the braided quasiholes, and that only the pattern in the middle may change as a result of braiding. Imposing these locality considerations tells us that

$\chi_1(2)$ must be of the form

$$\chi_1(2) = \begin{pmatrix} \cdot & 0 & 0 \\ 0 & \cdot & \cdot \\ 0 & \cdot & \cdot \end{pmatrix}, \tag{C.4}$$

where "$\cdot$"s are unknown, potentially nonzero, matrix elements for which we will solve. By applying the form in Eq. (C.4) to the matrix $\chi_1(2) = \xi^{\sigma_I}(\xi^{\sigma_I\prime})^\dagger$ derived from adiabatic transport, the zero elements give two more independent constraint equations,

$$0 = \eta^{-D}(1+p^2)\xi_{11}\xi_{12} - \Delta\eta^D {\xi_{13}}^2, \tag{C.5a}$$

$$0 = \eta^{-D}\xi_{31}\left(\xi_{11} - \Delta p\xi_{12}\right) + \eta^D\xi_{13}\xi_{33}. \tag{C.5b}$$

Solving this system of six equations, (C.3) and (C.5), is formally similar to the solution in the Appendices of Ref. [7], so the details will not be repeated here. Just as in that reference, there are two solutions: A special solution in which $p = \pm i$,

$${\xi_{11}}^2 = \frac{1}{2}\eta^D e^{i\pi/3}p^{-1}, \tag{C.6a}$$

$$\xi_{12} = \Delta\xi_{11}, \tag{C.6b}$$

$$\xi_{13} = \xi_{31} = 0, \tag{C.6c}$$

$${\xi_{33}}^2 = -e^{i\pi/3}, \tag{C.6d}$$

which produces the reduced braid matrix

$$\chi_1(2) = e^{2\pi i/3} \begin{pmatrix} p & 0 & 0 \\ 0 & p & 0 \\ 0 & 0 & e^{-i\pi/3} \end{pmatrix} \tag{C.7}$$

(but we will show in Appendix D that this solution is inconsistent with the equations from three-quasihole braiding), and the consistent solution,

$$\xi_{11}{}^2 = \frac{\eta^D e^{i\pi/3}}{(1+p)^2}, \tag{C.8a}$$

$$\xi_{12} = \Delta\xi_{11}, \tag{C.8b}$$

$$\xi_{13}{}^2 = \eta^D(p+p^{-1})\xi_{11}{}^2, \tag{C.8c}$$

$$\xi_{31}{}^2 = \eta^D(p+p^{-1})\xi_{11}{}^2, \tag{C.8d}$$

$$\xi_{33}{}^2 = \eta^{-D}(1-p)^2\xi_{11}{}^2, \tag{C.8e}$$

which produces the reduced braid matrix

$$\chi_1(2) = e^{-i\pi/3}\times$$
$$\begin{pmatrix} p^{-1} & 0 & 0 \\ 0 & p(p+p^{-1}-1) & \pm e^{i\pi D/3}(1-p)\sqrt{p+p^{-1}} \\ 0 & \pm e^{-i\pi D/3}(1-p)\sqrt{p+p^{-1}} & p+p^{-1}-1 \end{pmatrix}. \tag{C.9}$$

This two-quasihole reduced braid matrix is the same as that in Ref. [7] except for two

features: The D-dependent phase on the off-diagonal elements (though this will later be removed with a unitary transformation), and the overall Abelian phase, which here is $e^{-i\pi/3}$ and in Ref. [7] was $e^{i\pi/2}$.

Appendix D

Gaffnian solution: Three quasiholes

The solution for the reduced braid matrix of three quasiholes begins similarly to that for two quasiholes. We first constrain ξ^{σ_I} using global path relations, Eqs. (5.9) and (5.10), and mirror symmetry, Eqs. (5.11) and (5.12). Applying the former two in succession and filling in the data from Table 5.2 gives the constraint

$$\xi^{\sigma_I} = \begin{pmatrix} & \tilde{\Delta}p^{-1} & \\ & 0 & -\eta^D \\ \tilde{\Delta}p & & \\ & & -1 \end{pmatrix} \xi^{\sigma_I} \begin{pmatrix} & & \tilde{\Delta}p & \\ \tilde{\Delta}p^{-1} & 0 & & \\ & -\eta^D & & \\ & & & -1 \end{pmatrix}, \tag{D.1}$$

where p is defined as in Appendix C, and $\tilde{\Delta} = \exp\left[-2\pi i(L/2+1)D/3\right]$. This definition for $\tilde{\Delta}$ is seemingly the same as that for Δ in Appendix C, but in the case of two quasiholes $L = 1$ modulo 3, and here $L = 0$ modulo 3.

This appendix originally appeared in Ref. [60].

The two mirror symmetry equations, (5.11) and (5.12), can be applied in succession to ξ^{σ_I} to give

$$\xi^{\sigma_I} = \begin{pmatrix} 1 & & & \\ & 0 & \eta^D & \\ & \eta^{-D} & 0 & \\ & & & 1 \end{pmatrix} \xi^{\sigma_I} \begin{pmatrix} 1 & & & \\ & 0 & \eta^{-D} & \\ & \eta^D & 0 & \\ & & & 1 \end{pmatrix}. \tag{D.2}$$

Equations (D.1) and (D.2) together constrain ξ^{σ_I} to be of the form

$$\xi^{\sigma_I} = \begin{pmatrix} \xi_{11} & \xi_{12} & \eta^{-D}\xi_{12} & \xi_{14} \\ \xi_{12} & \eta^D p^2 \xi_{11} & -\tilde{\Delta} p \xi_{12} & -\tilde{\Delta}^{-1} p \xi_{14} \\ \eta^{-D}\xi_{12} & \tilde{\Delta} p \xi_{12} & \eta^{-D} p^2 \xi_{11} & -\tilde{\Delta} p \xi_{14} \\ \xi_{41} & -\tilde{\Delta}^{-1} p \xi_{41} & -\tilde{\Delta} p \xi_{41} & \xi_{44} \end{pmatrix}. \tag{D.3}$$

The structure of this matrix is almost identical to the corresponding matrix ξ^{++} in Ref. [7], save that the D-dependent phases η^D and $\tilde{\Delta}$ are different. There, $\tilde{\Delta}$ was defined such that $\tilde{\Delta}^2 = e^{i\pi D}$, whereas here $\tilde{\Delta}^2 = e^{2i\pi D/3} = \eta^{-D}$. We might then find a braid matrix with a non-trivial dependence on D. However, the symmetry relations in Eqs. (5.9), (5.10), (5.11), and (5.12) also have additional D-dependent phases compared to their corresponding forms in Ref. [7], and we will see that by following the same steps as in that reference to find the braid matrix solution, all the D-dependent phases will conspire to cancel save for those on the off-diagonal elements

which can be removed via a unitary transformation.

By requiring that ξ^{σ_I} be unitary, we find the following constraint equations,

$$1 = |\xi_{11}|^2 + 2\,|\xi_{12}|^2 + |\xi_{14}|^2\,, \tag{D.4a}$$

$$0 = \tilde{\Delta}\xi_{12}{\xi_{11}}^* + \tilde{\Delta}^{-1}p^2\xi_{11}{\xi_{12}}^* - p\,|\xi_{12}|^2 - p\,|\xi_{14}|^2\,, \tag{D.4b}$$

$$0 = \xi_{41}\left({\xi_{11}}^* - 2\tilde{\Delta}^{-1}p{\xi_{12}}^*\right) + {\xi_{14}}^*\xi_{44}, \tag{D.4c}$$

$$1 = 3\,|\xi_{41}|^2 + |\xi_{44}|^2\,. \tag{D.4d}$$

The locality of braiding tells us not only that some elements of $\chi_1(3)$ must be zero, as was the case for two quasiholes, but also that the 2×2 block with off-diagonal elements must be equal to the equivalent 2×2 block in $\chi_1(2)$. This is because the sequences of ground state patterns of the domain walls associated with the quasiholes to be braided are the same for those two supersectors in the two- and three-quasihole cases. In other words, $\chi_1(3)$ must be of the form

$$\chi_1(3) = e^{-i\pi/3}\times$$
$$\begin{pmatrix} . & & & \\ & . & & \\ & & p(p+p^{-1}+1) & \pm e^{i\pi D/3}(1-p)\sqrt{p+p^{-1}} \\ & & \pm e^{-i\pi D/3}(1-p)\sqrt{p+p^{-1}} & p+p^{-1}+1 \end{pmatrix}, \tag{D.5}$$

if Eq. (C.9) is the correct reduced braid matrix for two-quasiholes, and of the form

$$\chi_1(3) = e^{2\pi i/3} \begin{pmatrix} . & & & \\ & . & & \\ & & p & 0 \\ & & 0 & e^{-i\pi/3} \end{pmatrix}, \tag{D.6}$$

with $p = \pm i$, if Eq. (C.7) is the correct matrix (which we will show is not the case). We find our constraint equations by equating the product $\chi_1(3) = \xi^{\sigma_I}(\xi^{\sigma_I{}'})^\dagger$, obtained from adiabatic transport, with the forms above. We can perform the two solutions in parallel by using only the elements of Eqs. (D.5) and (D.6) that are zero in both. This produces the constraint equations

$$0 = p^3 {\xi_{11}}^2 - \tilde{\Delta}^2(p-1)p{\xi_{12}}^2 - p^2{\xi_{14}}^2, \tag{D.7a}$$

$$0 = \tilde{\Delta}(p-1)p^2\xi_{11}\xi_{12} + \tilde{\Delta}^2 p{\xi_{12}}^2 - p^2{\xi_{14}}^2, \tag{D.7b}$$

$$0 = -\xi_{41}\left[p\xi_{11} + \tilde{\Delta}(p-1)\xi_{12}\right] + \xi_{14}\xi_{44}. \tag{D.7c}$$

The set of constraint equations, (D.4) and (D.7), is solved when

$$\xi_{11}{}^2 = \frac{e^{i\theta_1}}{(1+p)^2}, \tag{D.8a}$$

$$\xi_{12} = \tilde{\Delta}^{-1}\xi_{11}, \tag{D.8b}$$

$$\xi_{14}{}^2 = (p + p^{-1} - 1)\xi_{11}{}^2, \tag{D.8c}$$

$$\xi_{41}{}^2 = e^{2i\theta_2}(p + p^{-1} - 1)\xi_{11}{}^2, \tag{D.8d}$$

$$\tag{D.8e}$$

which produces the reduced braid matrix

$$\chi_1(3) = e^{-i\pi/3 + i\theta_1} \times$$
$$\begin{pmatrix} 1 & & & \\ & 1 & & \\ & & p(1-p) & \pm e^{i\theta_2 + i\pi D/3} p\sqrt{p+p^{-1}-1} \\ & & \pm e^{i\theta_2 - i\pi D/3} p\sqrt{p+p^{-1}-1} & e^{2i\theta_2}(1-p) \end{pmatrix}. \tag{D.9}$$

Just as in Appendix C, Eq. (D.9) is the same reduced braid matrix as was found in Ref. [7] for three quasiholes, except that here the off-diagonal elements have an additional D-dependent phase and the overall Abelian phase is different.

We have yet to enforce consistency between the 2×2 blocks in the two- and three-quasihole braid matrices; to do so we equate Eq. (D.9) to Eqs. (D.5) and (D.6) in turn. The latter produces a contradiction, because the off-diagonal elements of

Eq. (D.9) are not zero for $p = \pm i$. Thus Eq. (C.6) is not a consistent solution for two quasiholes, and Eqs. (C.7) and (D.6) are not consistent braid matrices. Enforcing consistency between Eqs. (D.5) and (D.9) implies that

$$p + p^{-1} = \varphi, \tag{D.10}$$

where φ is the golden ratio, $\varphi = (1 + \sqrt{5})/2$. In other words,

$$p = \exp\left(\pm\frac{i\pi}{5}\right), \tag{D.11}$$

or, if we define $a = \pm 1/5$, $p = \exp(i\pi a)$. This is all the same as in Ref. [7]. However, here the s parameter is defined differently in terms of p than in Ref. [7]; we have defined $p = -\exp[-2\pi i(1+s)/3]$, so the s parameter is also constrained to be

$$s = 2 - \frac{3a}{2}. \tag{D.12}$$

Consistency also implies

$$e^{i\theta_1} = p^2, \tag{D.13}$$

$$e^{2i\theta_2} = 1. \tag{D.14}$$

The expressions for $\chi_1(2)$ and $\chi_1(3)$ in Eqs. (5.14) and (5.15), respectively, have been simplified with respect to Eqs. (C.9) and (D.9) and have undergone a unitary

transformation in which each state is multiplied by $(-e^{i\pi D/3})^{\#200}$, where #200 is the number of $200200\ldots$ strings in the thin torus pattern associated with that state. This unitary transformation removes the dependence on the unkonwn parameter D.

Bibliography

[1] D. C. Tsui, H. L. Stormer, and A. C. Gossard, Phys. Rev. Lett. **48**, 1559 (1982).

[2] R. E. Prange and S. M. Girvin, *The Quantum Hall Effect: Second Edition* (Springer-Verlag, 1990).

[3] K. v. Klitzing, G. Dorda, and M. Pepper, Phys. Rev. Lett. **45**, 494 (1980).

[4] R. Willett, J. P. Eisenstein, H. L. Stormer, D. C. Tsui, A. C. Gossard, and J. H. English, Phys. Rev. Lett. **59**, 1776 (1987).

[5] A. R. Hamilton, M. Y. Simmons, F. M. Bolton, N. K. Patel, I. S. Millard, J. T. Nicholls, D. A. Ritchie, and M. Pepper, Phys. Rev. B **54**, R5259 (1996).

[6] H. Stormer, Physica B **177**, 401 (1992).

[7] J. Flavin and A. Seidel, Phys. Rev. X **1**, 021015 (2011), Copyright (2011) by the American Physical Society.

[8] A. Stern, Ann. Phys. **323**, 204 (2008).

[9] R. B. Laughlin, Phys. Rev. B **23**, 5632 (1981).

[10] B. I. Halperin, Phys. Rev. B **25**, 2185 (1982).

[11] R. B. Laughlin, Phys. Rev. Lett. **50**, 1395 (1983).

[12] V. J. Goldman and B. Su, Science **267**, 1010 (1995).

[13] R. de Picciotto, M. Reznikov, M. Heiblum, V. Umansky, G. Bunin, and D. Mahalu, Nature **389**, 162 (1997).

[14] L. Saminadayar, D. C. Glattli, Y. Jin, and B. Etienne, Phys. Rev. Lett. **79**, 2526 (1997).

[15] J. Martin, S. Ilani, B. Verdene, J. Smet, V. Umansky, D. Mahalu, D. Schuh, G. Abstreiter, and A. Yacoby, Science **305**, 980 (2004).

[16] F. Wilczek and A. Zee, Phys. Rev. Lett. **52**, 2111 (1984).

[17] B. I. Halperin, Helv. Phys. Acta. **56**, 75 (1983).

[18] F. D. M. Haldane, Phys. Rev. Lett. **67**, 937 (1991).

[19] E. Artin, Ann. Math. **48**, 101 (1947).

[20] J. Leinaas and J. Myrheim, Il Nuovo Cimento B **37**, 1 (1977).

[21] M. V. Berry, Proc. R. Soc. Lond. A **392**, 45 (1984).

[22] D. Arovas, J. R. Schrieffer, and F. Wilczek, Phys. Rev. Lett. **53**, 722 (1984).

[23] G. Moore and N. Read, Nucl. Phys. B **360**, 362 (1991).

[24] W. Bishara, P. Bonderson, C. Nayak, K. Shtengel, and J. K. Slingerland, Phys. Rev. B **80** (2009).

[25] A. Y. Kitaev, Ann. Phys. **303**, 2 (2003).

[26] S. Das Sarma, M. Freedman, and C. Nayak, Phys. Rev. Lett. **94**, 166802 (2005).

[27] C. Nayak and F. Wilczek, Nucl. Phys. B. **479**, 529 (1996).

[28] N. Read, Phys. Rev. B **79**, 045308 (2009).

[29] Read, N., arXiv:0807.3107 (2008).

[30] P. Bonderson, V. Gurarie, and C. Nayak, Phys. Rev. B **83**, 075303 (2011).

[31] N. Read and D. Green, Phys. Rev. B **61**, 10267 (2000).

[32] D. A. Ivanov, Phys. Rev. Lett. **86**, 268 (2001).

[33] A. Stern, F. von Oppen, and E. Mariani, Phys. Rev. B **70**, 205338 (2004).

[34] M. Stone and S.-B. Chung, Phys. Rev. B **73**, 014505 (2006).

[35] M. Oshikawa, Y. B. Kim, K. Shtengel, C. Nayak, and S. Tewari, Ann. Phys. **322**, 1477 (2007).

[36] J. K. Jain, Phys. Rev. Lett. **63**, 199 (1989).

[37] F. D. M. Haldane and E. H. Rezayi, Phys. Rev. Lett. **54**, 237 (1985).

[38] A. Seidel, H. Fu, D.-H. Lee, J. M. Leinaas, and J. E. Moore, Phys. Rev. Lett. **95**, 266405 (2005).

[39] A. Seidel and D.-H. Lee, Phys. Rev. Lett. **97**, 56804 (2006).

[40] Seidel, A. and Lee, D.-H., Phys. Rev. B **76**, 155101 (2007).

[41] A. Seidel and K. Yang, Phys. Rev. Lett. **101**, 036804 (2008).

[42] A. Seidel, Phys. Rev. Lett. **101**, 196802 (2008).

[43] Seidel, A., Phys. Rev. Lett. **105**, 026802 (2010).

[44] A. Seidel and K. Yang, Phys. Rev. B **84**, 085122 (2011).

[45] E. J. Bergholtz and A. Karlhede, Phys. Rev. Lett. **94**, 26802 (2005).

[46] Bergholtz, E. J. and Karlhede, A., J. Stat. Mech. **L04001** (2006).

[47] E. J. Bergholtz, J. Kailasvuori, E. Wikberg, T. H. Hansson, and A. Karlhede, Phys. Rev. B **74**, 081308 (2006).

[48] E. J. Bergholtz, T. H. Hansson, M. Hermanns, and A. Karlhede, Phys. Rev. Lett. **99**, 256803 (2007).

[49] E. J. Bergholtz and A. Karlhede, Phys. Rev. B **77**, 155308 (2008).

[50] E. Wikberg, E. J. Bergholtz, and A. Karlhede, J. Stat. Mech.: Theor. Exp. **2009**, P07038 (2009).

[51] B. A. Bernevig and F. D. M. Haldane, Phys. Rev. Lett. **100**, 246802 (2008).

[52] Bernevig, B. A. and Haldane, F. D. M., Phys. Rev. B **77**, 184502 (2008).

[53] Bernevig, B. A. and Haldane, F. D. M., Phys. Rev. Lett. **101**, 246806 (2008).

[54] X.-G. Wen and Z. Wang, Phys. Rev. B **77**, 235108 (2008).

[55] X.-G. Wen and Z. Wang, Phys. Rev. B **78**, 155109 (2008).

[56] M. Barkeshli and X.-G. Wen, Phys. Rev. B **82**, 233301 (2010).

[57] Barkeshli, M. and Wen, X.-G., Phys. Rev. B **82**, 245301 (2010).

[58] N. Read and E. H. Rezayi, Phys. Rev. B **59**, 8084 (1999).

[59] B. Simon, Phys. Rev. Lett. **51**, 2167 (1983).

[60] J. Flavin, R. Thomale, and A. Seidel, arXiv:1201.3355v1 (2012).

[61] N. Read, Phys. Rev. B **73**, 245334 (2006).

[62] E. Ardonne, N. Read, E. H. Rezayi, and K. Schoutens, Nucl. Phys. B **607**, 549 (2001).

[63] E. Ardonne, J. Phys. A **35**, 447 (2002).

[64] E. Ardonne, R. Kedem, and M. Stone, J. Phys. A **38**, 617 (2005).

[65] F. D. M. Haldane, Phys. Rev. Lett. **51**, 605 (1983).

[66] F. D. M. Haldane, Phys. Rev. Lett. **55**, 2095 (1985).

[67] X.-G. Wen and Q. Niu, Phys. Rev. B **41**, 9377 (1990).

[68] T. Einarsson, Phys. Rev. Lett. **64**, 1995 (1990).

[69] E. H. Rezayi and F. D. M. Haldane, Phys. Rev. B **50**, 17199 (1994).

[70] S. A. Trugman and S. Kivelson, Phys. Rev. B **31**, 5280 (1985).

[71] R. Tao and D. J. Thouless, Phys. Rev. B **28**, 1142 (1983).

[72] S. Jansen, E. H. Lieb, and R. Seiler, Comm. Math. Phys. **285**, 503 (2008).

[73] W. P. Su, J. R. Schrieffer, and A. J. Heeger, Phys. Rev. B **22**, 2099 (1980).

[74] M. Greiter, X.-G. Wen, and F. Wilczek, Nucl. Phys. B **374**, 567 (1992).

[75] P. Bonderson, Ph.D. thesis, California Institute of Technology (2007).

[76] A. Y. Kitaev, Ann. Phys. **321** (2006).

[77] E. Ardonne, E. J. Bergholtz, J. Kailasvuori, and E. Wikberg, J. Stat. Mech. **2008**, P04016 (2008).

[78] J. K. Slingerland and F. A. Bais, Nucl. Phys. B. **612**, 229 (2001).

[79] J. Preskill, *Lecture Notes for Physics 219: Quantum Computation* (2004), URL `http://www.theory.caltech.edu/ preskill/ph219/topological.pdf`.

[80] P. Bonderson (2011), private communication.

[81] F. D. M. Haldane and E. H. Rezayi, Phys. Rev. Lett. **60**, 956 (1988).

[82] S. H. Simon, E. H. Rezayi, N. R. Cooper, and I. Berdnikov, Phys. Rev. B **75**, 75317 (2007).

[83] N. Read, Phys. Rev. B **79**, 245304 (2009).

[84] M. Greiter, Bull. Am. Phys. Soc. **38**, 137 (1993).

[85] H. Li and F. D. M. Haldane, Phys. Rev. Lett. **101**, 010504 (2008).

[86] R. Thomale, A. Sterdyniak, N. Regnault, and B. A. Bernevig, Phys. Rev. Lett. **104**, 180502 (2010).

[87] N. Read, Phys. Rev. Lett. **62**, 86 (1989).

[88] G. Misguich, D. Serban, and V. Pasquier, Phys. Rev. Lett. **89**, 137202 (2002).

[89] K. Gregor, D. A. Huse, R. Moessner, and S. L. Sondhi, New J. Phys. **13**, 025009 (2011).

[90] A. Seidel, Phys. Rev. B **80**, 165131 (2009).

[91] M. den Nijs and K. Rommelse, Phys. Rev. B **40**, 4709 (1989).

[92] H. V. Kruis, I. P. McCulloch, Z. Nussinov, and J. Zaanen, Phys. Rev. B **70**, 075109 (2004).

[93] M. Ogata and H. Shiba, Phys. Rev. B **41**, 2326 (1990).

[94] M. Ogata, M. U. Luchini, and T. M. Rice, Phys. Rev. B **44**, 12083 (1991).

[95] A. Seidel and D.-H. Lee, Phys. Rev. Lett. **93**, 046401 (2004).

[96] T. C. Ribeiro, A. Seidel, J. H. Han, and D.-H. Lee, Europhys. Lett. **76**, 891 (2006), ISSN 0295-5075.

[97] Tőke, C. and Jain, J. K., Phys. Rev. B **80**, 205301 (2009).

[98] E. Ardonne, Phys. Rev. Lett. **102**, 180401 (2009).

[99] E. Ardonne, J. Gukelberger, A. W. W. Ludwig, A. Trebst, and M. Troyer, New J. Phys. **13**, 045006 (2011).

[100] M. H. Freedman, J. Gukelberger, M. B. Hastings, S. Trebst, M. Troyer, and Z. Wang, Phys. Rev. B **85**, 045414 (2012).

[101] E. Ardonne and K. Schoutens, Phys. Rev. Lett. **82**, 5096 (1999).

[102] E. Ardonne and N. Regnault, Phys. Rev. B **84**, 205134 (2011).

[103] F. D. M. Haldane (2006).